

DISS. ETH NO. 28395

**THE ROLE OF MIR-379-410 CLUSTER-MEDIATED PRR7  
INHIBITION IN HOMEOSTATIC SYNAPTIC DEPRESSION**

A thesis submitted to attain the degree of  
DOCTOR OF SCIENCES of ETH ZURICH  
(Dr. sc. ETH Zurich)

presented by

*MICHIKO O. INOUE*

Master of Philosophy in Biological Science (Biochemistry), University of Cambridge

born on 08.01.1992

accepted on the recommendation of

Prof. Dr. Gerhard Schratt

Prof. Dr. Isabelle Mansuy

Prof. Dr. Theofanis Karayannis

2022

## SUMMARY

Homeostatic plasticity is a neuroprotective process that allows neurons and neural circuits to maintain stable activity in the face of destabilizing stimuli. This self-regulation is carried out through modulation of excitatory synapses at the neuronal level and excitation-inhibition balance at the circuit level. Many neuropsychiatric and neurodegenerative diseases exhibit abnormal excitation and inhibition, therefore suggesting an aberrancy in homeostatic plasticity and highlighting the importance of studying the molecular mechanisms governing this ability. In my thesis, I focused on Homeostatic Synaptic Depression (HSD), a type of homeostatic plasticity. HSD is characterized by dendritic spine elimination and decreased excitatory transmission in response to chronically elevated network activity in a cell-autonomous manner. Recent findings (Fiore et al., 2014; Cohen et al., 2011) suggested that members of the miRNA cluster miR379-410 are important regulators of HSD through inhibiting translation of synaptic proteins locally. Therefore, I sought to explore the role of cluster miRNAs in HSD in more detail. Here, I studied the synaptic protein Proline-rich protein 7 (Prr7), a candidate predicted to be a highly specific target of the miRNA cluster, with the aim of elucidating a novel molecular pathway underlying HSD.

Through qPCR, western blot, and immunostaining analyses, I found that Prr7 was downregulated at both RNA and protein levels in dendrites of hippocampal neurons treated with picrotoxin (PTX) for 48h, a stimulus that induces HSD. Furthermore, Prr7 knockdown led to a reduction in dendritic spine numbers to levels comparable to that induced by 48h PTX, as well as a downregulation of the GluA1 subunit of AMPA-type glutamate receptors. These findings suggested that Prr7 loss in dendrites is necessary and sufficient for spine elimination during HSD. Next, through luciferase assays and immunostaining, I found that Prr7 reduction by PTX was robustly prevented through transfection of a cocktail of inhibitors against cluster members miR-329-3p and miR-495-3p. The PTX-induced spine elimination was also prevented with this miRNA inhibitor cocktail. Moreover, through a dual sensor assay I found that both miRNAs are activated during HSD. These results indicated that miR-329-3p and miR-495-3p are induced and required for Prr7 downregulation and spine elimination by PTX. Finally, I found that Prr7 knockdown reduces expression of the synaptic scaffolding protein SPAR, an effect that was prevented via CDK5 inhibition, thereby tying Prr7 protein reduction together with a previously established HSD mechanism.

In summary, these results indicate a novel pathway wherein cluster members miR-329-3p and miR-495-3p target Prr7 locally, which leads to SPAR destabilization and spine elimination in HSD. Future experiments may be directed to explore the pathophysiological significance of the miR-329/495/Prr7 regulation in neuropsychiatric and neurodegenerative disorders, as well as seizure development and sleep disturbances often comorbid with these conditions.

## ZUSAMMENFASSUNG

Die homöostatische Plastizität ist ein neuroprotektiver Prozess, der es Neuronen und neuronalen Schaltkreisen ermöglicht, angesichts destabilisierender Reize eine stabile Aktivität aufrechtzuerhalten. Diese Selbstregulierung erfolgt durch Modulation der erregenden Synapsen auf neuronaler Ebene und Erregungs-Hemmungs-Gleichgewicht (E-I balance) auf Schaltkreisebene. Viele neuropsychiatrische und neurodegenerative Erkrankungen weisen eine abnormale Erregung auf, was auf eine Abweichung in der homöostatischen Plastizität hindeutet und die Bedeutung der Untersuchung der molekularen Mechanismen hervorhebt, die diese Fähigkeit steuern. In meiner Doktorarbeit habe ich mich auf die homöostatische synaptische Depression (HSD) konzentriert, eine Form der homöostatischen Plastizität. HSD ist gekennzeichnet durch Eliminierung dendritischer Dornen und verringerte exzitatorische Übertragung als Reaktion auf chronisch erhöhte Netzwerkaktivität auf zellautonome Weise. Neuere Erkenntnisse (Fiore et al., 2014; Cohen et al., 2011) legen nahe, dass Mitglieder des miRNA-Clusters miR379-410 wichtige Regulatoren von HSD sind, indem sie die Translation synaptischer Proteine lokal hemmen. Daher habe ich versucht, die Rolle von Cluster-miRNAs bei HSD genauer zu untersuchen. Hier konzentrierte ich mich auf das synaptische Protein Proline-rich protein 7 (Prr7), von dem vorhergesagt wird, dass es ein hochspezifisches Ziel des miRNA-Clusters ist, in dem Bestreben, einen neuen molekularen Weg zu beschreiben, der HSD zugrunde liegt.

Durch qPCR, Western Blot und Immunfärbungsanalysen fand ich heraus, dass Prr7 sowohl auf RNA- als auch auf Proteinebene in Dendriten von Hippocampus-Neuronen herunterreguliert war, die 48 Stunden lang mit PicROTOXIN (PTX) behandelt wurden, einem Stimulus, der HSD induziert. Darüber hinaus führte der Prr7-Knockdown zu einer Verringerung der dendritischen Dornen-Zahlen auf ein Niveau, das mit dem durch 48h-PTX induzierten vergleichbar war, sowie zu einer Herunterregulierung der GluA1-Untereinheit von Glutamatrezeptoren vom AMPA-Typ. Diese Ergebnisse legten nahe, dass der Prr7-Verlust in Dendriten notwendig und ausreichend für die Dornen-Eliminierung während HSD ist. Als nächstes fand ich durch Luciferase-Assays und Immunfärbung heraus, dass die Prr7-Reduktion nach 48 Stunden PTX durch die Transfektion eines Cocktails von Inhibitoren gegen die Clustermitglieder miR-329-3p und miR-495-3p verhindert wurde. Auch die PTX-induzierte Dornen-Eliminierung wurde mit diesem miRNA-Inhibitor-Cocktail verhindert. Darüber hinaus fand ich durch einen Dual-Sensor-Assay heraus, dass beide miRNAs während HSD aktiviert werden. Diese Ergebnisse zeigten, dass miR-329-3p und miR-495-3p induziert werden und für die Prr7-Herunterregulierung und Dornen-Eliminierung durch PTX erforderlich sind. Schliesslich fand ich heraus, dass der Prr7-Knockdown die Expression des synaptischen Gerüstproteins SPAR reduziert, ein Effekt, der durch CDK5-Hemmung verhindert wurde. Diese Beobachtung bringt die Reduktion des Prr7-Proteins mit einem zuvor etablierten HSD-Mechanismus in Verbindung.

Zusammenfassend deuten diese Ergebnisse auf einen neuen Weg hin, bei dem die Clustermitglieder miR-329-3p und miR-495-3p lokal auf Prr7 abzielen, was zu SPAR-Destabilisierung und Dornen-Eliminierung bei HSD führt. Zukünftige Experimente könnten darauf ausgerichtet sein, die pathophysiologische Bedeutung der miR-329/495/Prr7-Regulation bei neuropsychiatrischen und neurodegenerativen Erkrankungen sowie die Entwicklung von Anfällen und Schlafstörungen zu untersuchen, die häufig mit diesen Erkrankungen einhergehen.

## ACKNOWLEDGEMENTS

First of all, I sincerely thank Prof. Dr. Gerhard Schratt for the wonderful opportunity to work on such an interesting project in his laboratory. Not only was I able to learn many new experimental techniques and explore an entirely new field, but also I believe I grew as a scientist thanks to his constant encouragement, constructive feedback, and patience. He continuously helped me to become a more independent worker while also being an invaluable source of advice when needed. I have really enjoyed my time here.

Thank you very much to the members of my thesis advisory committee, Prof. Dr. Isabelle Mansuy, and Prof. Dr. Theofanis Karayannis for their thoughtful comments, and helping me to see the project from creative and fresh perspectives. I also thank Prof. Dr. Michael Siegrist for being the chairperson for my doctoral examination.

I would like to give special thanks to Dr. Roberto Fiore for his continuous and honest feedback, many of which were pivotal for the direction of the project. I am very grateful to him for always being an open ear for scientific discussion throughout my PhD. My lab mates (both past and present) have made my stay in Zurich and time in the lab amazing. Thank you to David Colameo and Irina Ammann for contributing to the project, as well as Michael Soutschek for helping me to get started. Thank you to everyone in the lab for providing such a warm, positive, and stimulating environment to work in, for being always helpful and for your comments at the data meetings: Darren Kelly, Carlotta Gilardi, Dr. Jochen Winterer, Emanuel Sonder, Dr. Pierre-Luc Germain, Prakruti Nanda, Cristina Furler, Tati Wüst, Dr. Helena Martins, Dr. Reetu Daswani, Dr. Ram Narayanan, Dr. Silvia Bicker, and Dr. Fridolin Gross. Thank you also to Sonja Bamert, and to all of the members of the Bohacek Lab. I feel honored to be surrounded by such wonderful people.

Lastly, I am grateful as always to my close family, friends, past mentors and teachers.

## TABLE OF CONTENTS

<b>LIST OF ABBREVIATIONS</b> .....	<b>6</b>
<b>INTRODUCTION</b> .....	<b>9</b>
<i>Homeostatic plasticity is a neuroprotective mechanism triggered by chronic activity or inactivity and is driven by changes in postsynaptic AMPAR expression</i> .....	9
<i>Homeostatic plasticity is morphologically reflected by dendritic spine changes</i> .....	10
<i>Homeostatic plasticity is fundamentally different from other forms of plasticity</i> .....	11
<i>Homeostatic plasticity is a cell-autonomous mechanism</i> .....	13
<i>Homeostatic Synaptic Depression (HSD) is a type of homeostatic plasticity triggered in response to chronic excitation</i> .....	14
<i>The role of miRNAs in HSD is suggested but elusive</i> .....	16
<i>miR-379-410 cluster members are brain-enriched miRNAs with known roles in synaptic plasticity</i> . ....	17
<i>Prr7 is a potentially highly specific target of cluster miRNAs and is a synaptic protein</i> .....	18
<i>Prr7 is enriched in the hippocampus</i> .....	19
<i>Aims</i> .....	21
<b>MANUSCRIPT</b> .....	<b>22</b>
<i>Title and abstract</i> .....	22
<i>Introduction</i> .....	22
<i>Results</i> .....	24
<i>Discussion</i> .....	43
<i>Materials and Methods</i> .....	48
<i>Acknowledgements, Conflicts of Interest, Author Contributions</i> .....	53
<i>Supplemental Methods and Data</i> .....	54
<b>DISCUSSION</b> .....	<b>60</b>
<i>miR-329-3p and miR-495-3p target Prr7 locally in dendrites</i> .....	60
<i>Prr7 loss leads to SPAR degradation in a CDK5-dependent manner</i> .....	62
<i>Prr7 loss leads to GluA1 reduction</i> .....	62
<i>miRNA regulation in the context of NF-<math>\kappa</math>B-mediated HSD endpoint</i> .....	63
<i>HSD in proximal vs. distal dendrites</i> .....	63
<i>Prr7 as a switch governing excitotoxicity</i> .....	64
<i>Exosome-mediated Prr7 signaling in homeostatic plasticity</i> .....	65
<i>Further considerations to apply findings to circuit, regional, behavioral-levels</i> .....	66
<b>REFERENCES</b> .....	<b>69</b>

## LIST OF ABBREVIATIONS

°C degrees Celsius

μ micro

**AAV** Adeno-associated virus

**AMPA** α-amino-3-hydroxy-5-methyl-4-isoxazolepropionic acid receptor

**ANOVA** analysis of variance

**BDNF** Brain-derived neurotrophic factor

**BME** 2-Mercaptoethanol/β-mercaptoethanol

**CaMK** Calcium/calmodulin-dependent protein kinase

**CaMK4** Calcium/calmodulin-dependent protein kinase type IV

**CaMKK** Calcium/calmodulin-dependent protein kinase Kinase

**CDK5** Cyclin-dependent-like kinase 5

**ChR2** Channel rhodopsin 2

**c-Jun** Jun proto-oncogene, AP-1 transcription factor subunit, p39

**CMV** Cytomegalovirus

**Ctr** control

**Ctrsh** control short hairpin RNA

**DIV** Days in vitro

**DMEM** Dulbecco's Modified Eagle Medium

**DMSO** Dimethylsulfoxide

**DNA** Deoxyribonucleic acid

**dsRed** *Discosoma* sp-derived basic red fluorescent protein

**ECL** Enhanced chemiluminescent substrate

**EDTA** Ethylenediaminetetraacetic acid

**eGFP** Enhanced green fluorescent protein

**EGTA** Ethylene glycol-bis(β-aminoethyl ether)-N,N,N',N'-tetraacetic acid

**EtOH** Ethanol

**FBW7** F-box and WD repeat domain-containing 7 ubiquitin ligase component

**Fig** Figure

**GABA-A** gamma-Aminobutyric acid type A receptor

**GAPDH** Glyceraldehyde-3-phosphate dehydrogenase

**GDB** Gelatin dilution buffer

**GluA1 (alternative name: Gria1)** Glutamate receptor 1

**GluA2 (alternative name: Gria2)** Glutamate receptor 2

**h** hours

**HA** Human influenza hemagglutinin

**HA-Cav1.2** Human influenza hemagglutinin-tagged calcium channel voltage-dependent L-type alpha 1C subunit

**HCl** Hydrochloric acid

**HEK293T** Human Embryonic Kidney 293T

**HEPES** 4-(2-hydroxyethyl)-1-piperazineethanesulfonic acid

**hp** hairpin

**HRP** Horseradish peroxidase enzyme

**HSD** Homeostatic Synaptic Depression

**hSyn** Human synapsin 1

**KCl** potassium chloride

**kD** kilodalton

**LTP** Long-term potentiation

**Map2** microtubule-associated protein 2

**MeOH** Methanol

**mEPSC** miniature excitatory postsynaptic currents

**min** minutes

**miR-329-3p** 3p strand (originating from 3' arm of precursor) of microRNA-329

**miR-495-3p** 3p strand (originating from 3' arm of precursor) of microRNA-495

**miRNA** MicroRNA

**mM** millimolar

**mRNA** messenger ribonucleic acid

**Mut** mutant

**N-cadherin** neural cadherin, cadherin-2

**Nedd4-1** Neural precursor cell expressed developmentally downregulated protein 4-1

**Ng** nanogram

**ng/ml** nanograms per milliliter

**NMDAR** N-methyl-D-aspartate receptor

**ns** not significant

**NSF** N-ethylmaleimide-sensitive fusion protein

**PBS** Phosphate-buffered saline

**pcDNA3** Plasmid cloning DNA 3

**PEI** Polyethylenimine

**PET** Polyethylene Terephthalate

**Plk2 (alternative name: SNK)** Serine/threonine-protein kinase/Polo-like kinase 2/Serum-inducible kinase

**pLNA** Locked nucleic acid-enhanced antisense miRNA inhibitor

**pmol** picomoles

**Prr7** Proline-rich protein 7

**Prr7sh** Proline-rich protein 7 short hairpin RNA

**PSD** postsynaptic density

**PSD-95 (alternative names: Dlg4, SAP-90)** Postsynaptic density protein 95/Disks large homolog 4/Synapse-associated protein 90

**PTX** picrotoxin

**Pum2** Pumilio homolog 2

**qPCR** Real time polymerase chain reaction, quantitative polymerase chain reaction

**RBP** RNA binding protein

**RIPA** Radioimmunoprecipitation assay buffer

**RISC** RNA-induced silencing complex

**RNA** Ribonucleic acid

**RNAi** RNA interference

**RNA-seq** RNA sequencing

**Ros** Roscovitine

**RT-qPCR** Quantitative reverse transcription polymerase chain reaction

**S.D.** standard deviation

**SDS** Sodium dodecyl sulfate

**SDS-PAGE** Sodium dodecyl sulfate-polyacrylamide gel electrophoresis

**SEM** standard error of the mean

**shRNA** Small/short hairpin RNA

**SPAR (Sipa1-1)** Spine-associated Rap GTPase-activating protein/Signal-induced proliferation-associated 1-like protein 1

**TBST** Tris-buffered saline

**Tris** Tris(hydroxymethyl)aminomethane

**TTX** Tetrodotoxin

**Tukey's post-hoc HSD test** Tukey's post hoc Honest Significant Difference test

**U6** Type III RNA polymerase III promoter

**UTR** Untranslated region

**WT** wild type

## INTRODUCTION

*Homeostatic plasticity is a neuroprotective mechanism triggered by chronic activity or inactivity and is driven by changes in postsynaptic AMPAR expression*

Homeostasis (derived from the Greek words *homeo* meaning “similar”, and *stasis* meaning “standing still”) is a central physiological phenomenon observed in numerous organ systems, and broadly describes the tendency to resist change in order to maintain a steady internal environment (Cannon, 1929). Thus, in the context of the nervous system, homeostatic plasticity refers to the compensatory return to a defined “set point” of firing rate by a neuron in the face of destabilizing influences (Turrigiano, 2007). This inherent ability to resist change is critical for the function, as well as survival (in severe cases such as exposure to excitotoxic stimuli) of neurons.

This capacity for compensatory self-regulation works bidirectionally, and is facilitated mainly through regulation of postsynaptic AMPA-type glutamate receptor (AMPA) abundance. The bidirectionality was demonstrated in an *in vitro* context in dissociated primary cortical cultures (Turrigiano et al., 1998). Namely, chronic blockade of cortical cultures by 48h treatment of Na<sup>+</sup> channel blocker tetrodotoxin (TTX) led to an increase in miniature postsynaptic current (mEPSC) amplitude of pyramidal neurons without changing kinetics. Conversely, blocking GABA-mediated inhibition through 48h bath application of bicuculline led to a decrease in mEPSC amplitude and return of firing rates comparable to the control condition. The bidirectionality of homeostatic plasticity and the particular contribution of AMPARs were corroborated in another study (O’Brien et al., 1998), where chronic inhibition of excitatory synaptic transmission of cultured spine neurons by 72h AMPAR and NMDA-type glutamate receptor (NMDAR) blockade led to increased EPSC amplitude, while chronic activity via picrotoxin (PTX)/strychnine treatment led to reduced mEPSC amplitude.

Moreover, both studies showed that mEPSC amplitude changes could be attributed to alteration in specifically postsynaptic glutamate receptor number or function, more so than presynaptic changes. Namely, pulses of glutamate to pyramidal neurons, in the presence of TTX and NMDAR blocker AP5 led to increased glutamate current amplitude at the soma and apical dendrite while no differences in the rise or peak times were observed, indicating mEPSC amplitude changes were not due to differences in rate of glutamate diffusion or removal (Turrigiano et al. 1998). Additionally, in O’Brien et al. the authors found that excitatory activity correlated with AMPAR subunit GluA1 accumulation through immunostaining studies, which occurred in the absence of any changes in synaptophysin fluorescence intensity, pointing specifically towards modulation of GluA1-containing AMPARs at the postsynaptic membrane.

Although the focus of the present thesis is on homeostatic plasticity of pyramidal (excitatory) neurons as investigated in the above-mentioned studies, it is nevertheless important to recognize that homeostatic plasticity applies also to inhibitory neurons. Accordingly, homeostatic plasticity in both neuronal types

allows adjustment of excitation-inhibition balance, and thereby homeostatic maintenance more broadly in neural circuits. Although the “rules” of compensatory response in inhibitory neurons are distinct from excitatory neurons, they are nevertheless also governed by postsynaptic modulation of AMPAR number or function. This was demonstrated in visual cortical cultures from P4-6 rat pups (Rutherford et al., 1998). Here, the presence of exogenous brain-derived neurotrophic factor (BDNF) upon chronic activity blockade induced by 48h TTX treatment led to opposite changes in mEPSC amplitude between pyramidal neurons and bipolar interneurons in the same culture. The presence of BDNF prevented the compensatory increase in quantal amplitude by pyramidal neurons upon chronic inactivity, whereas BDNF promoted an increase in quantal amplitude by interneurons (with minimal effect on mEPSCs by TTX alone). Furthermore, the EPSC amplitude trends in excitatory vs. inhibitory neurons were consistent with firing rate measurements of these two neuron subtypes with TTX bath application in the presence of BDNF.

As mentioned above, homeostatic mechanisms are understood to be principally governed by changes in AMPA-type glutamatergic synapses. It is, however, important to briefly acknowledge the reported influence of chronic network activity changes on GABAergic synapses. Global blockade of spike activity through 9-day TTX treatment in developing rat hippocampal neurons led to reduced density of GABAergic terminals, and lowered amplitude and frequency of inhibitory postsynaptic currents (IPSCs) (Hartman et al., 2006). This homeostatic response in GABAergic synapses was further supported by another study (Swanwick et al., 2006), in which 48h TTX treatment of cultured hippocampal neurons resulted in decreased IPSC amplitude and reduced sizes of Gad65 (postsynaptic inhibitory) puncta and gamma2 (subunit of GABA-A receptor) clusters.

Put together, homeostatic plasticity acts bidirectionally and involves regulation of postsynaptic AMPAR expression and function. This process has been largely studied and reproduced in pyramidal neurons, although it is necessary to note that homeostatic plasticity also occurs in inhibitory neurons and can involve GABAergic synapse regulation. However, the present thesis will focus on building upon the well-established phenomenon of AMPAR-regulation underlying homeostatic plasticity in pyramidal neurons.

### *Homeostatic plasticity is morphologically reflected by dendritic spine changes*

The majority of excitatory neurotransmitter receptors such as AMPARs, of a pyramidal neuron are presented on protrusions from the dendrite known as dendritic spines (reviewed in Runge et al., 2020). Additionally, dendritic spines serve as the major postsynaptic sites at which most excitatory inputs terminate, whereas inhibitory inputs target the dendritic shafts (Megías et al., 2001). Thus, changes in AMPAR abundance and excitatory transmission in homeostatic plasticity are reflected by alterations in spine morphology, such as spine number. For example, by chronic excitation, reproducible decreases in

dendritic spine density have been demonstrated in cortical and hippocampal neurons (Moulin et al., 2012; Goold and Nicoll, 2010; Fiore et al., 2014). Conversely, increases in dendritic spine density have been found in response to chronic inactivation (Wierenga et al., 2005; Quinn et al., 2019; Nakamura et al., 2018).

The dynamicity of spines is directly determined by their cytoskeleton, which consists primarily of filamentous actin (F-actin), and actin is influenced by glutamate receptor activity (reviewed in Groc and Choquet, 2020). F-actin is controlled by actin regulators, such as the Ras, Rho, and Rap families of small GTPases (Pak et al., 2001; Nakayama et al., 2000). Taken together, spine morphology changes are directly facilitated by actin regulators and are tightly associated with AMPAR function and expression. Therefore, molecular study of homeostatic plasticity requires an understanding of the interplay between actin cytoskeleton and AMPAR dynamics, and the ways in which this interaction is influenced by chronic excitation or inhibition.

#### *Homeostatic plasticity is fundamentally different from other forms of plasticity*

Before discussing the molecular mechanisms that govern homeostatic plasticity, it would perhaps be important to clarify how homeostatic plasticity differs from other known forms of synaptic plasticity, namely Hebbian plasticity and synaptic pruning. Indeed, all of these forms of plasticity could in some cases outwardly share the same final “result” (e.g. spine elimination can be observed in all three forms).

One major distinguishing feature of homeostatic plasticity from other forms is the directionality of the response with respect to the stimulus. Specifically, homeostatic plasticity represents a compensatory response that counters the stimulus and acts as a negative feedback mechanism. Therefore, as mentioned previously, in response to chronic excitation, homeostatic plasticity would work to weaken or eliminate excitatory synapses. In contrast, Hebbian forms of plasticity (such as long-term potentiation (LTP) and long-term depression (LTD)) are considered to operate in a positive feedback manner. For example, in LTP, high frequency stimulation to presynaptic fibers leads to increased potentiation and strengthening of the postsynaptic response (Bliss and Lomo, 1973). In other words, in Hebbian plasticity, the postsynaptic response serves to reinforce the direction of the stimulus received from the presynaptic membrane. Thus, homeostatic plasticity and Hebbian plasticity work in direct opposition to one another. In fact, the opposing directionality of Hebbian and homeostatic plasticity has led to the general understanding that these two mechanisms work in a complementary fashion. For example, the positive feedback of LTP could potentially destabilize and overexcite the neural circuit if not controlled, and thus homeostatic plasticity serves to prevent this “runaway excitation” (Abbot and Nelson, 2000; Turrigiano and Nelson, 2004).

Likewise, synaptic pruning also operates in the positive feedback direction. This is evidenced for example by the fact that synaptic pruning facilitates selective elimination or weakening of synapses that

remain unstimulated during development. In a study of ocular dominance plasticity (Hubel and Wiesel, 1963), experience-dependent synaptic pruning serves as the explanation for selective weakening of synapses associated with the inactive eye, whereas synapses associated with the open eye are maintained and strengthened.

An important difference between homeostatic plasticity and pruning is also the fact that there is a very defined developmental time point specificity in the occurrence of pruning, which is not the case for homeostatic plasticity. Specifically, synaptic pruning is known to primarily occur at two particular points in development: 1) the first two years of birth, and 2) during adolescence into early adulthood in human (Riccomagno et al., 2015). The developmental time point restriction of synaptic pruning in early life and then in adolescence has been demonstrated in rats as well. Namely, the occurrence of early-life pruning in the first postnatal week (P1) until postnatal day 9-10 (P9/P10) has been observed in the context of retinogeniculate pruning (Schafer et al., 2012). Additionally, pruning of synapses during adolescence has been demonstrated in pyramidal neurons of the medial prefrontal cortex in rats from ~P35 (adolescence) to P90 (adulthood), with particular importance of the timing of puberty on this mechanism (Koss et al., 2014; Juraska and Drzewiecki, 2020). Thus, given the developmental specificity, synaptic pruning is likely inactivated in late adulthood, or in fully mature neurons.

In contrast, homeostatic plasticity has been demonstrated to occur in both developing neurons and in fully mature neurons. Hence, the understanding is that neurons are capable of exhibiting homeostatic plasticity regardless of age (Turrigiano et al., 2012). However, this is not to say that the mechanism of homeostatic plasticity remains unchanged throughout life, as there is some evidence of subtle changes in homeostatic mechanism dependent on neuron age. For example, older visual cortical neurons (>18 days *in vitro* (DIV)) respond to 48h TTX treatment by increasing mEPSC frequency and amplitude (Turrigiano et al., 1998; Wierenga et al., 2006), as well as excitatory synapse density, whereas the same manipulation in younger cultures (<14 DIV) yield effects in only mEPSC amplitude without frequency changes (Wierenga et al., 2006). Age-dependency in the homeostatic mechanism has also been suggested in GABAergic synapses, in that chronic activity blockade in developing rat hippocampal neurons by TTX led to reduced density of GABAergic terminals and mIPSC frequency and amplitude, whereas in mature neurons there was a reduction in mIPSC amplitude without any changes in GABAergic synapse density (Hartman et al., 2006).

The mechanisms of homeostatic plasticity and pruning are also fundamentally different. The mechanism of homeostatic plasticity is principally understood to be cell-autonomous (Ibata et al., 2008; Goold and Nicoll, 2010), although there are exceptions (e.g. involvement of TNF $\alpha$  (Beattie et al., 2002 and BDNF secretion (Rutherford et al., 1998)). The cell-autonomous nature of homeostatic plasticity will be discussed in the next section. On the other hand, pruning is largely mediated by non-cell-autonomous mechanisms, with strong participation on the part of glial cells (e.g. microglia, astrocytes). Moreover, immune and apoptosis-associated pathways underlie synaptic pruning, which is not the case for

homeostatic plasticity. For example, complement system activation via pentraxin and major histocompatibility complex (MHC) class I molecules, as well as mitochondrial caspase CASP3 activation have been implicated in synaptic pruning (Kovács et al., 2020; Glynn et al., 2011).

In terms of the comparison between Hebbian plasticity and homeostatic plasticity other than directionality, there is a major difference in temporal and spatial scales in the respective forms. Homeostatic mechanisms operate over a longer time scale (on the scale of hours) (Burrone et al., 2002) compared to Hebbian pathways, which can be extremely rapid (within 10 seconds) (Petersen et al., 1998). In addition, homeostatic plasticity is observed both on a global, cell-wide level (Turrigiano et al., 1998) as well as a more local scale (at the level of individual synapses (Hou et al., 2008) or dendritic segments (Yu and Goda 2009, Rabinowitch and Segev, 2006)). On the other hand, Hebbian plasticity is an exclusively local mechanism, which relies on very precise and specific alignment of presynaptic and postsynaptic activity (Bi and Poo, 1998). Furthermore, there is evidence of the molecular mechanisms being fundamentally different between Hebbian and homeostatic plasticity. This difference is demonstrated for example by the fact that homeostatic plasticity-driven synaptic depression does not depend on the PICK1 protein, whereas LTD does (Anggono et al., 2011).

#### *Homeostatic plasticity is a cell-autonomous mechanism*

The standard paradigms used for study of homeostatic plasticity have been through bath application of inhibitors against GABA receptors, AMPARs, NMDARs, and Na<sup>+</sup> channels, altering the entirety of network activity. Homeostatic plasticity is observed in individual pyramidal neurons in response to these network-wide changes in activity; thus, an important question to ask when probing the molecular pathways of homeostatic plasticity is, what exactly is the identity of “activity” upon network-wide changes that triggers homeostatic plasticity in individual neurons? For instance, is homeostatic plasticity induced principally by changes in the presynaptic inputs from contacting neighboring neurons? Or rather, is it a sensing of changes in one’s own presynaptic glutamate release, or postsynaptic firing activity within individual cells, irrespective of neighboring cells? Alternatively, is homeostatic plasticity only triggered under conditions of large-scale changes in the neural network?

This question was addressed in the context of chronic activity blockade where researchers asked if blocking postsynaptic firing via somatic perfusion of TTX in individual cortical neurons would yield the same compensatory AMPAR accumulation as bath application of TTX (Ibata et al., 2008). They found that, indeed, AMPAR accumulation occurred in the cell that received the local TTX perfusion, which was similar in both magnitude and time course to that induced by bath-applied TTX. Furthermore, they found that the AMPAR accumulation upon local TTX perfusion was dependent on changes in somatic calcium levels in the perfused cell. These results served as first evidence that homeostatic plasticity is a cell-autonomous mechanism; specifically, individual cells detect a change in their own

somatic membrane potential (or postsynaptic firing) by means of somatic calcium sensors, which thereby drives compensatory AMPAR trafficking.

The cell-autonomous nature of homeostatic plasticity driven through intrinsic calcium sensors was further supported for the opposite direction, namely the compensatory loss of AMPARs in response to chronic elevation of network activity (Goold and Nicoll, 2010). Here, channel rhodopsin 2 (ChR2)-expressing neurons were individually photostimulated through optogenetic methods, and spine morphology measurements in addition to voltage clamp recordings of the photostimulated cells obtained. The results revealed that the 24h photostimulation led to reduction of mEPSC frequency and spine density in the stimulated cells specifically, and that these effects were dependent on L-type voltage gated calcium channel opening and subsequent Calcium/Calmodulin Dependent Protein Kinase Kinase (CaMKK) and Calcium/Calmodulin Dependent Protein Kinase 4 (CaMKIV) activation.

Thus, from these two studies, one can gain an understanding that (perhaps counterintuitively), in the face of network-wide activity alterations, it is in fact the sensing of changes in somatic membrane potential by means of intracellular calcium sensors on an individual basis by pyramidal cells, that triggers homeostatic plasticity. Specifically, once calcium sensors CaMKK and CaMKIV are activated, an internal homeostatic mechanism is initiated, for which solely endogenous factors of the given cell are sufficient to drive AMPAR trafficking and cytoskeleton changes.

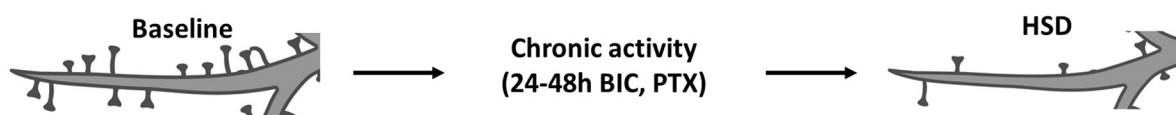
It is necessary to acknowledge, however, that there are in fact known mechanisms of homeostatic plasticity that are non-cell-autonomous (e.g. contribution of secreted factors TNF $\alpha$  and BDNF). Nevertheless, the current understanding is that such extracellular signaling mechanisms occur downstream of somatic calcium influx in individual neurons (Turrigiano, 2008).

*Homeostatic Synaptic Depression (HSD) is a type of homeostatic plasticity triggered in response to chronic excitation*

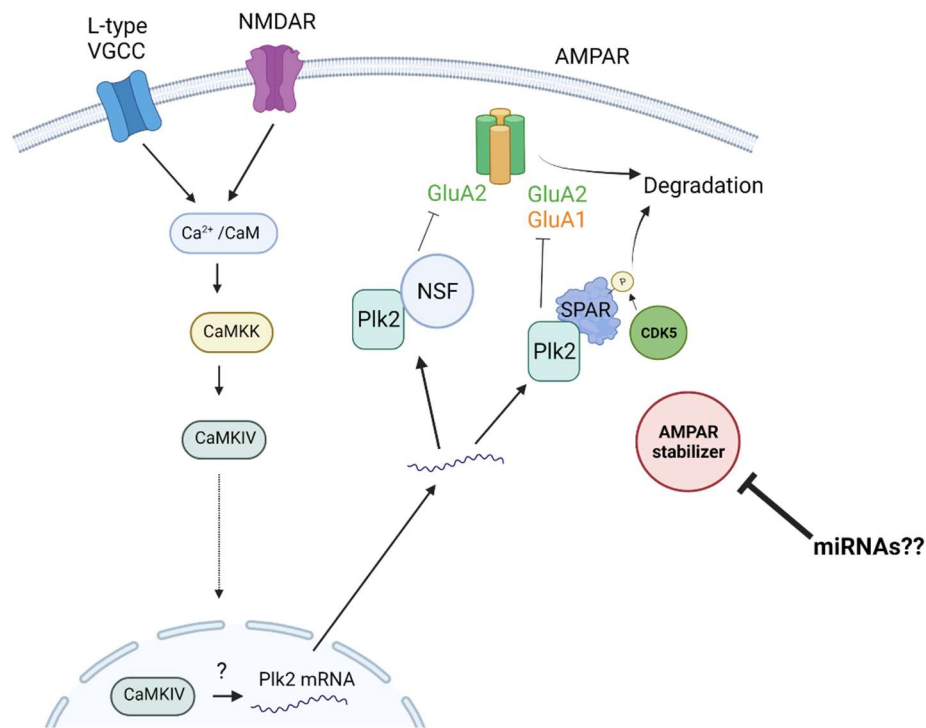
In the present thesis, I examine the molecular mechanism underlying a type of homeostatic plasticity termed Homeostatic Synaptic Depression (HSD). HSD refers to the compensatory response to chronically elevated network activity. In HSD, chronic excitation leads to a compensatory response of AMPAR degradation and actin remodeling resulting in dendritic spine elimination in pyramidal cells (Intro Figure 1). As previously described, the molecular pathway is cell-autonomous and involves the activation of calcium sensors in individual cells, leading to AMPAR degradation and actin remodeling, ultimately resulting in spine collapse. This means that intrinsic mechanisms within individual pyramidal cells underlie AMPAR and cytoskeletal changes. A more detailed picture of this cell-autonomous pathway of HSD has emerged in recent years (with the major pathway summarized in Intro Figure 2).

First, the activation of voltage-gated calcium channels and NMDA-type glutamate receptors leads to calcium influx (Goold and Nicoll, 2010; Wayman et al., 2008; Pak and Sheng, 2003). Calcium binds calmodulin, which triggers a cascade of events, involving activation of calcium/calmodulin-sensitive protein phosphatase (PP2B) (Pak and Sheng, 2003), CaMKK and CaMKIV (Goold and Nicoll, 2010), and transcriptional activation of Polo-like Kinase 2 (Plk2) over a time scale of hours (Kauselmann et al., 1999; Pak and Sheng, 2003). Moreover, following Plk2 transcription, Plk2 mRNA is transported to dendrites, where local translation of Plk2 occurs (this is normally inhibited by Pumilio-2 RNA binding protein under unstimulated conditions (Fiore et al., 2014)). Plk2 promotes the degradation of the spine-associated Rap GTPase-activating protein (SPAR) via CDK5 activity, which subsequently activates the Rap family of small GTPases, causing F-actin remodeling towards spine collapse. SPAR degradation also leads to the internalization and degradation of GluA1 and GluA2-containing AMPARs (Seeburg et al., 2008). In a separate kinase-independent pathway, Plk2 binds to N-ethylmaleimide sensitive factor (NSF) to facilitate the internalization of specifically GluA2-containing AMPARs (Evers et al., 2010).

For clarification, the terms “HSD” and “homeostatic downscaling” both fall under types of homeostatic plasticity in response to chronic excitation. However, HSD refers to spine elimination and EPSC frequency reduction, whereas homeostatic downscaling refers to spine volume reduction and EPSC amplitude decrease. Whether HSD is mechanistically distinct from downscaling is unclear, although the literature at present would suggest that the two forms involve the same pathways and the discrepancy in morphological and electrophysiological analyses is due to the time point studied. In other words, synapse weakening and elimination may actually occur in a sequential manner as part of the same pathway (Fiore et al., 2014).



**Intro Figure 1. Paradigm of Homeostatic Synaptic Depression.**



**Intro Figure 2. Molecular pathway of Homeostatic Synaptic Depression.**

*The role of miRNAs in HSD is suggested but elusive*

As described above, the pathway connecting calcium signaling to AMPARs and actin remodeling factors underlying HSD have been explored. However, knowledge is lacking on how the genes encoding for the important molecular players of this mechanism are coordinately regulated. Furthermore, given the identified presence of over 2500 proteins in synapses (Pielot et al., 2012), it is likely there exist other AMPAR-stabilizing proteins (similar to SPAR), whose regulation are required for HSD. In light of evidence of local homeostatic plasticity mechanisms (e.g. GluA1 accumulation occurring specifically at postsynaptic membranes where presynaptic firing is lowered by an inwardly rectifying K<sup>+</sup> channel (Hou et al., 2008), GluA1 accumulation upon blockade of NMDARs in the dendritic compartment (Sutton et al., 2006), it would be reasonable to consider mechanisms of gene regulation occurring outside of the nucleus, namely post-transcriptional regulation of synaptic protein-encoding genes, in the context of HSD.

microRNAs (miRNAs) are attractive candidates for such a study of post-transcriptional regulation of synaptic protein-encoding genes in HSD. miRNAs are non-coding RNAs that are ~19-23 nucleotides long, and act to silence messenger RNAs (mRNAs) through base-pair interactions with the 3' untranslated regions (3' UTR) (Filipowicz et al., 2008).

As a short introduction to miRNAs, I will briefly review the steps of miRNA biogenesis, processing and the mechanism of mRNA silencing. The miRNA-encoding DNA is first transcribed by RNA Polymerase II, which gives rise to a primary miRNA transcript (pri-miRNA). Still in the nucleus, the 3' and 5' ends of the pri-miRNA are cleaved by the microprocessor complex, whose main components are Drosha and DGCR8 (Winter et al., 2009). The resultant cleaved transcript is called precursor miRNA (pre-miRNA), which has a stem-loop structure and is subsequently exported from the nucleus (Yi et al., 2003; Bohnsack et al., 2004; Lund et al., 2004). The pre-miRNAs are then cleaved by the endoribonuclease Dicer to produce a ~22 nucleotide long miRNA duplex, of which the individual strands are termed either 5p or 3p (Hutvagner et al., 2001). One of the strands is loaded onto the miRNA-induced silencing complex (RISC) (Meister 2013; Kawamata and Tomari 2010), which consists of a member of the Argonaute family of proteins (which acts as the main catalyst of RISC), along with Dicer, TRBP (HIV1-TAR RNA Binding Protein) and/or PACT (Protein Activator of the interferon-induced protein kinase) (Wang HW et al., 2009; Chendrimada et al., 2005; Haase et al., 2005; Lee et al., 2006; Heyam et al., 2015). Based on the 6-8 nucleotide sequence (called the “seed sequence”) at the 5' end of the miRNA strand (Pillai et al., 2005), a target mRNA complementary to this sequence binds to the RISC. This mRNA targeting by the miRNA RISC complex either inhibits mRNA translation or leads to mRNA degradation (Jonas and Iyaurralde, 2015; Bartel 2009).

The ability of a single miRNA to regulate hundreds of genes (Farh et al., 2005) brings forth the idea that they may serve as “master regulators” upstream of mRNAs encoding for synaptic proteins to facilitate synaptic plasticity. Importantly, miRNAs have been demonstrated to regulate translation locally at synapses in activity-dependent processes that involve dendritic cytoskeletal remodeling such as dendritic arborization and dendritic spine morphogenesis (Schratt et al., 2006; Siegel et al., 2009).

Despite the strong existing evidence for miRNA involvement in synaptic plasticity, support for the requirement of individual miRNAs in homeostatic plasticity, and specifically HSD, is rather limited. To date, miR-92a (Letellier et al., 2014) and miR-124 (Hou et al., 2015) have been implicated in the mechanisms of homeostatic upscaling in response to activity blockade. For HSD, miR-485 has been found to be involved in a presynaptic mechanism (Cohen et al., 2011). Moreover, miR-134 (Fiore et al., 2014) acts at the postsynaptic membrane to facilitate HSD, and miR-129 engages in crosstalk with Rbfox RNA binding proteins during HSD (Rajman et al., 2017). Other miRNAs required for HSD are yet to be identified. Additionally, a clear molecular pathway following the role of a specific miRNA in local regulation of a synaptic protein-encoding gene in HSD has not been clarified.

#### *miR-379-410 cluster members are brain-enriched miRNAs with known roles in synaptic plasticity*

A particular group of 38 miRNAs, the miR379-410 cluster, is a large genomic cluster found only in eutherians, and is located within the DLK1-DIO3 region which corresponds to chromosome 14q32 in

human and 12qF1 in mice (Seitz et al., 2003; summarized in da Rocha et al., 2008). Interestingly, this chromosomal region is imprinted, which results in the miRNA cluster being exclusively expressed from the maternal allele (Cattanach and Rasberry, 1993). During development, it is widely expressed in the embryo and placenta, however as development progresses, expression of this miRNA cluster increases in the brain (Labielle et al., 2014). Perhaps owing to this brain enrichment, in the recent years, a number of miR379-410 cluster members have emerged as important regulators in various activity-dependent neuronal processes, such as dendritogenesis (Fiore et al., 2009), neuronal differentiation and migration (Rago et al., 2014) and synaptic plasticity (Cohen et al., 2011).

Regarding the expression of miR379-410 cluster, it is generally hypothesized that all of the miRNAs of the cluster are transcribed as one large polycistronic transcript (Tierling et al., 2006). Despite being transcribed together, however, individual cluster members show considerable variation in expression patterns, which also shift in an activity-dependent manner (Fiore et al., 2009). The variation may be attributed to separate processing pathways (Tierling et al., 2006) or separate mechanisms for miRNA stability, such as target-directed miRNA degradation (TDMD) (Ameres et al., 2010), for individual members.

So far two members of the cluster have been tied to HSD, namely miR-134 (Fiore et al., 2014) and miR-485 (Cohen et al., 2011). Moreover, mice with a functional deletion of the miR379-410 cluster exhibited increased mEPSC frequency and dendritic spine number in hippocampal excitatory neurons, as well as global upregulation of ionotropic glutamate receptor-associated proteins (Lackinger et al., 2019), supporting the idea of miRNA-mediated targeting of AMPAR-associated synaptic proteins. Although the cluster knockout study did not specifically address the role of the miR-379-410 members in homeostatic regulation, the AMPAR-associated synaptic protein and spine morphology changes in the knockout mice, together with the fact that two cluster members have already been implicated in HSD, lead to the strong possibility that additional cluster members play a role in HSD.

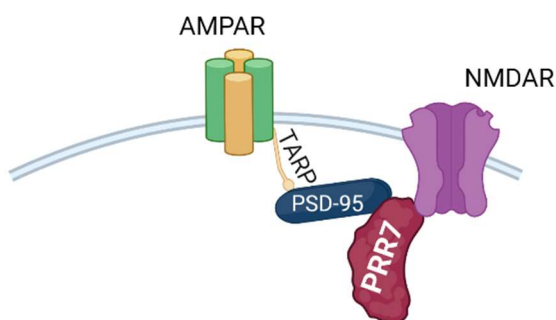
*Prr7 is a potentially highly specific target of cluster miRNAs, and is a synaptic protein*

A particular synaptic target of interest potentially downstream of miR-379-410 cluster regulation is Proline-rich protein 7 (Prr7). Prr7 was significantly upregulated at both RNA and protein levels in the miR379-410-deficient mice, which leads to consideration of Prr7 as an important candidate that is directly controlled by cluster miRNAs (Lackinger et al., 2019). Intriguingly, Targetscan analysis of the Prr7 mRNA 3' UTR indicate predicted binding sites for four miRNAs (miR-377, miR-329, miR-495, miR-411), all of which are members of the miR379-410 cluster, further giving support to the idea that Prr7 expression is regulated by cluster miRNAs.

In addition, Prr7 has been shown to localize at dendrites in multiple studies (Murata et al., 2005; Kravchick et al., 2016; Lee et al., 2018), and has been identified in mass spectrometry-based screens of

postsynaptic densities in rodent brains (Murata et al., 2005; Jordan et al., 2004; Yoshimura et al., 2004), giving reason to believe that it may regulate excitatory synapses during HSD. Prr7 has also been found to associate directly with a major synaptic scaffolding protein, postsynaptic density protein 95 (PSD95) (Murata et al., 2005). Prr7 binds directly to NMDARs as well, but independently of PSD95 binding (Murata et al., 2005; Kravchick et al., 2016). The Prr7-PSD95 association independent of NMDAR binding is intriguing, as it raises the question of what the purpose of the PSD95 interaction is. AMPARs are stabilized at dendritic spines via transmembrane AMPA receptor regulatory protein (TARP) binding to PSD95 (Bats et al., 2007). Thus, the possibility exists that Prr7 serves to stabilize AMPARs indirectly via PSD95 association under basal conditions, and that dissociation occurs during HSD (Intro Figure 3).

Despite the characterization of Prr7 as a synaptic protein, to date the function of synapse-localized Prr7, and its expression regulation in the context of HSD, are unknown. Existing functional studies of Prr7 together suggest that it is a protein with a rather multifaceted and complex function. Namely, Prr7 has been reported to act as a synaptonuclear messenger in neurons, promoting the transcription of apoptotic genes through interfering with c-Jun ubiquitination in the nucleus in the context of excitotoxicity (Kravchick et al., 2016). Additionally, Prr7 secretion via exosomes to facilitate degradation of excitatory synapses has been reported (Lee et al., 2018). However, Prr7's role in HSD in response to chronic excitation has not been addressed.



**Intro Figure 3. Model of Prr7 interactions at the post-synaptic density.**

#### *Prr7 is enriched in the hippocampus*

From Prr7 protein expression analyses in various dissected brain regions from adult mice, Prr7 was found to be particularly enriched in the hippocampus (as well as in the cortex) (Lee et al., 2018). This observation gives reason to investigate miR379-410 cluster-mediated Prr7 regulation in the hippocampus. Accordingly, upregulation of Prr7 mRNA and protein in the miR379-410 cluster knockout mice was observed from RNA and protein lysate isolated from the hippocampus (Lackinger et al., 2019).

Furthermore, much of the literature on homeostatic plasticity have repeatedly been conducted on hippocampal dissociated cultures or hippocampal organotypic slices, which thereby definitively establishes the existence of homeostatic plasticity in the hippocampus. The fact that the hippocampus is comprised primarily of pyramidal cells, drastically outnumbering GABAergic interneurons (Pelkey et al., 2017), also allows one to specifically study homeostatic plasticity mechanisms in excitatory neurons using hippocampal dissociated cultures given the rather homogenous neuronal population. Therefore, studying miRNA-Prr7 interactions in the context of HSD in hippocampal pyramidal neurons would serve to expand upon the existing literature on cell-autonomous HSD molecular pathway, which has already been well-established in this neuronal subtype.

In a general sense, one can imagine that changes in homeostatic plasticity of individual pyramidal cells will exert broader influence at a network-wide level in the hippocampus, thereby regulating homeostasis of hippocampal neural circuits. The regulation of excitability in the hippocampus has strong physiological implications, especially given the known roles of this region principally in learning and memory, but also in emotion regulation, stress response, as well as in sensory and spatial information processing. Indeed, many of the excitation-inhibition (E-I) and excitatory synaptic aberrancies tied to neurological disease are found in the hippocampus or apply to hippocampus-associated neural circuits. For example, there is evidence of hippocampal excitation-inhibition dysregulation in the context of neurodegenerative conditions such as Huntington's (Kamble et al., 2018) and Alzheimer's (AD) (Maestú et al., 2021). Furthermore, dendritic spine loss and AMPAR removal in hippocampal pyramidal neurons has been reported in the context of AD (Hsieh et al., 2007). Altered E-I balance and abnormal synaptic phenotypes have been tied to neuropsychiatric disorders such as autism (ASD) (Sohal and Rubenstein, 2019), Fragile-X (Bagni and Zukin, 2019), and Rett Syndrome (Baj et al., 2014). Glutamatergic mechanism alterations leading to network hyperexcitability have been associated with seizures and epilepsy (Barker-Maliski and White, 2015; Chen et al., 1999; Leite et al. 2005). Moreover, there are correlations between sleep disturbances (e.g. sleep deprivation, lowered sleep quality) and excitatory synaptic alterations (de Vivo et al., 2017; Spano et al., 2019).

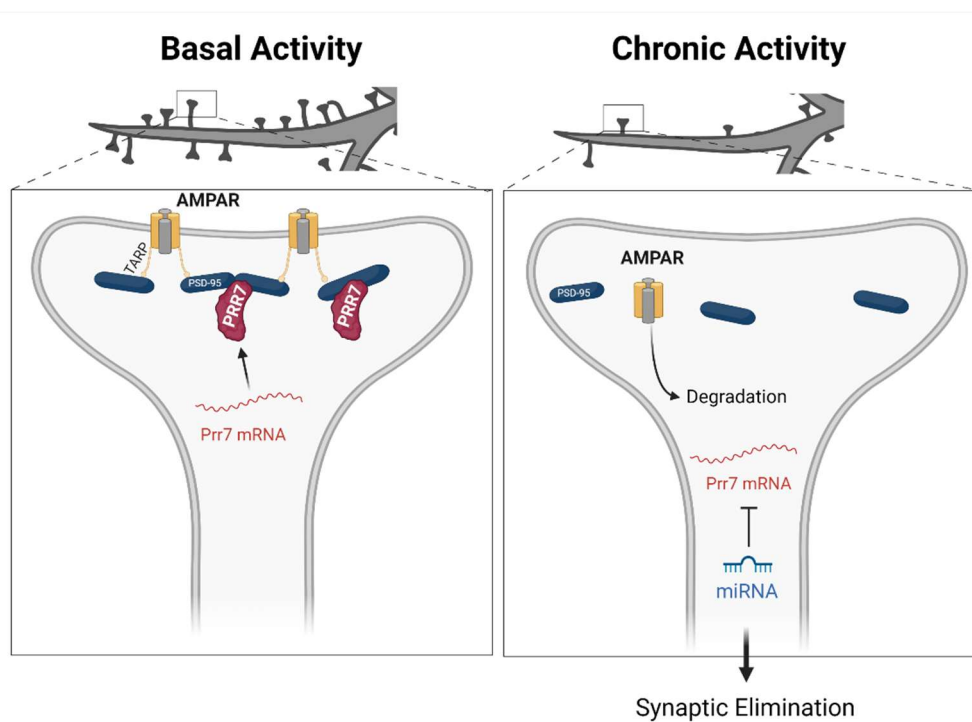
The convergence of excitability dysregulation at the hippocampus may explain the interconnected nature of many of the above-mentioned disorders to one another (e.g. sleep disturbance is association with epilepsy (Malow, 2004); sleep is necessary for consolidation of memory and memory is affected in Alzheimer's disease (Rothschild et al., 2017); epilepsy is comorbid with neuropsychiatric disorders (Besag, 2017). Thus, investigation of the molecular mechanisms of HSD, particularly in hippocampal excitatory neurons, may prove useful in deepening our understanding of the biological basis for these overlapping symptoms.

## Aims

The aims of my thesis project were: 1) to determine which members of the miR379-410 cluster regulate Prr7 expression; 2) determine if miRNA-mediated regulation of Prr7 occurs locally and is necessary for HSD; 3) study the function of synaptic Prr7 in the context of HSD.

My starting model is illustrated below (Intro Figure 4). I wished to test whether heightened network activity induced by 48h GABA receptor blockade by picrotoxin treatment, leads to activation of specific members of the miR379-410 cluster, thereby facilitating inhibition of Prr7 expression. I further wished to ask whether Prr7 expression reduction is necessary for the decrease in excitatory synapses and AMPAR expression implicated in HSD.

The main results of the project are presented in the enclosed manuscript, which is currently a pre-print that has been submitted for publication.



**Intro Figure 4. Starting model of miRNA-mediated Prr7 regulation in the context of HSD.**

## **miR-329 and miR-495-mediated Prr7 downregulation is required for homeostatic synaptic depression in rat hippocampal neurons**

Michiko O. Inouye<sup>1</sup>, David Colameo<sup>1</sup>, Irina Ammann<sup>1</sup>, Gerhard Schratt<sup>1\*</sup>

<sup>1</sup>Laboratory of Systems Neuroscience, Institute for Neuroscience, Department of Health Science and Technology, Swiss Federal Institute of Technology ETH, 8057 Zürich, Switzerland

\*Corresponding author: gerhard.schratt@hest.ethz.ch

Keywords: miRNA, proline-rich protein 7, transmembrane adapter protein 3, homeostatic synaptic depression, synaptic plasticity, AMPAR, SPAR, neurons, hippocampus

### **Abstract**

Homeostatic synaptic depression (HSD) in excitatory neurons is a cell autonomous mechanism which protects excitatory neurons from over-excitation as a consequence of chronic increases in network activity. In this process, excitatory synapses are weakened and eventually eliminated, as evidenced by a reduction in synaptic AMPA receptor expression and dendritic spine loss. Originally considered as a global, cell-wide mechanism, local forms of regulation, such as the local control of mRNA translation in dendrites, are being increasingly recognized in HSD. Yet, identification of excitatory proteins whose local regulation is required for HSD is still limited. Here, we show that Proline-rich protein 7/Transmembrane Adapter Protein 3 (Prr7) downregulation in dendrites of rat hippocampal neurons is necessary for HSD induced by chronic increase in network activity resulting from a blockade of inhibitory synaptic transmission by picrotoxin (PTX). We further identify two activity-regulated miRNAs, miR-329-3p and miR-495-3p, which inhibit Prr7 mRNA translation and are required for HSD. Moreover, we found that Prr7 knockdown reduces expression of the synaptic scaffolding protein SPAR, which is rescued by pharmacological inhibition of CDK5, indicating a role of Prr7 protein in the maintenance of excitatory synapses via protection of SPAR from degradation. Together, our findings highlight a novel HSD mechanism in which chronic activity leads to miR-329 and miR-495-mediated local Prr7 reduction upstream of the CDK5-SPAR pathway.

### **Introduction**

*Evidence of homeostatic synaptic depression (HSD) aberrancy underlying neurological disease*

Homeostatic synaptic depression (HSD) is a type of homeostatic plasticity by which excitatory neurons compensate for increased network activity to maintain a physiological range of excitatory transmission

(reviewed in Turrigiano, 2008; Yu & Goda, 2009; Turrigiano, 2012). Adaptive mechanisms to maintain neuronal homeostasis include changes in synaptic AMPA receptors (Seeburg et al., 2008), and spine number (Kirov et al., 1999; Wierenga et al., 2006). Abnormal dendritic spine density and altered AMPAR internalization have been suggested in epilepsy (Isokawa et al., 1997), schizophrenia (Glantz et al., 2000), and autism spectrum disorder (Hutsler and Zhang, 2010), as well as in disease models of Fragile X (Fmr1-knockout) (Jawaid et al., 2018) and Rett Syndrome (Mecp2-mutant) (Chao et al., 2007), highlighting the importance of HSD regulation for neuronal homeostasis.

Although the majority of studies on HSD have utilized GABA-receptor antagonists (e.g. Picrotoxin (PTX), Bicuculline) to investigate HSD in response to network-wide stimulation, a study employing optogenetic methods of stimulation demonstrated that the mechanism of HSD is cell-autonomous (Goold and Nicoll, 2010). Namely, upon 24h photostimulation of channel rhodopsin-2 (ChR2)-expressing CA1 pyramidal neurons, lowered mEPSC frequency and dendritic spine number were observed onto the cells themselves, indicating that individual neurons possess intrinsic mechanisms to regulate their synapse number in response to chronic activity. The spine loss in HSD is supported by a number of other studies using either optogenetics (Mendez et al., 2018) or pharmacological stimulation (Pak and Sheng, 2003; Fiore et al., 2014; Chowdhury et al., 2018).

Pathways underlying HSD have been examined in detail. In a well-studied mechanism, elevated synaptic activity first causes L-type voltage-gated calcium channel opening and NMDAR activation, which results in calcium influx (Goold and Nicoll, 2010, Pak and Sheng 2003). Calcium binds calmodulin, which initiates a cascade of CaM kinases (Wayman et al., 2008), of which CaMKK and CaMK4 are required for HSD (Goold and Nicoll, 2010). The cascade transcriptionally activates Polo-like kinase (Plk2/SNK), a member of the polo family of serine/threonine protein kinases, over a time scale of hours (Kauselmann et al., 1999; Pak and Sheng, 2003). The induced Plk2 is targeted to dendritic spines and binds to a PSD-95 interacting factor, spine-associated Rap guanosine triphosphatase (GTPase) activating protein (GAP) (SPAR), which has been “primed” for Plk2 binding by CDK5, a proline-directed kinase (Seeburg et al., 2008). The Plk2-SPAR binding results in proteasome-directed SPAR degradation, which has downstream effects on actin dynamics and Rap signaling, eventually leading to AMPAR and NMDAR removal and loss of spines. Whereas the Plk2-SPAR association is linked to synaptic AMPAR reduction without any reported preference to GluA1 or GluA2 subunits, a separate kinase-independent pathway in which Plk2 binds to N-ethylmaleimide-sensitive fusion protein (NSF) which is selective to GluA2 subunit removal has been observed (Evers et al., 2010).

Although there is evidence that excitatory synapses scale in a cell-wide, uniform manner during HSD, theoretical considerations invoke the existence of additional local dendritic mechanisms to assure proper information processing (Rabinowitch and Segev, 2006a,b). In fact, several local dendritic mechanisms which are engaged during homeostatic plasticity have been recently described. For example, chronic inactivity with NMDAR inhibition leads to retinoic acid signaling and stimulation of local GluA1

synthesis (Aoto et al., 2008; Poon and Chen 2008). Similarly, homeostatic upscaling via TTX and AMPAR/NMDAR blockade has also been shown to stimulate local protein synthesis (Sutton et al., 2007), including GluA1 accumulation (Sutton et al., 2006). In the context of HSD, miR-134-mediated local translation of Pumilio-2 (Pum2) mRNA upstream of Plk2 activation was reported (Fiore et al., 2014). The involvement of other miRNAs, namely miR-129 (Rajman et al., 2017) and miR-485 (Cohen et al., 2011) in HSD further suggest the importance of local translation in this process. Additionally, dendrite-specific regulation of excitatory proteins in the context of HSD has been demonstrated on a multi-omics scale (Colameo et al., 2021). Indeed, such local translational mechanisms could explain the spatial specificity of HSD, as demonstrated by homeostatic regulation in individual dendritic compartments (Rabinowitch and Segev, 2006a). The spatial specificity further extends to the synapse level, as scaling depends on the spatial patterns of synaptic potentiation (Rabinowitch and Segev, 2006b). Considering the mounting evidence for local regulation of proteins in plasticity mechanisms such as long-term potentiation (LTP) in both in vitro and in vivo contexts (Miller et al., 2002; Lyles et al., 2006), there is a need for identifying other proteins that are locally regulated in HSD.

In the present study, we investigate the expression regulation and function of Proline-rich 7/Transmembrane Adapter Protein 3 (Prr7) in the context of HSD induced by chronic activity. Prr7 is localized in neuronal dendrites of hippocampal neurons (Murata et al., 2005; Kravchick et al., 2016; Lee et al., 2018) and the postsynaptic density in rodent brains (Murata et al., 2005; Jordan et al., 2004; Yoshimura et al., 2004), suggesting that it could play an important role in HSD. Functionally, exosomally secreted Prr7 induces synapse elimination in hippocampal neurons (Lee et al. 2018), whereas NMDA-receptor mediated induction of excitotoxicity is accompanied by a translocation of Prr7 from the synapse to the nucleus, followed by a triggering of Jun-dependent apoptotic pathway (Kravchick et al., 2016). However, whether synaptically localized Prr7 is involved in activity-dependent forms of synaptic plasticity, e.g. HSD, is unknown.

Here, we report that the downregulation of Prr7 at both RNA and protein level is required for dendritic spine elimination during HSD induced by chronic activity increase, and that the dendritic reduction of Prr7 is regulated post-transcriptionally by miR-329 and miR-495. Furthermore, our results suggest that the miR-329/495/Prr7 interaction ties in with the previously described SPAR/CDK5 pathway involved in homeostatic plasticity.

## **Results**

### *Prr7 mRNA and protein are downregulated locally in processes by chronic activity*

Prr7 has previously been identified as a synaptic protein and implicated in the control of excitatory synapse formation, but its role in synaptic plasticity, e.g. HSD is unknown. Specifically, whether the subcellular expression of Prr7 changes during HSD has not been investigated. To determine if Prr7 expression is regulated in HSD, we first examined Prr7 mRNA expression levels in mature (DIV21)

primary rat hippocampal cells treated with either Mock (Ethanol) or the GABA-A receptor antagonist Picrotoxin (PTX) for 48h. This is a well established experimental paradigm to induce HSD *in vitro*, as demonstrated by expected changes in spike frequency, EPSC amplitude, and expression of the GluA1 subunit of AMPARs (Fiore et al., 2014, Rajman et al., 2017; Seeburg et al., 2008; Bateup et al., 2013; Evers et al., 2010; Ibata et al., 2008). Using qPCR, we observed a decrease in Prr7 mRNA levels in whole cell extracts of PTX- compared to Mock treated hippocampal neurons (Fig. 1a), which was similar in magnitude to GluA1 mRNA which was previously shown to be downregulated during HSD.

Previous studies indicate that, in addition to neuron-wide changes, local alterations in gene expression in the synapto-dendritic compartment might also be involved in homeostatic plasticity (Colameo et al., 2021; Sutton et al., 2007). To determine local expression changes, we utilized a compartmentalized culture system as previously described (Bicker et al., 2013), which allowed separate measurements of Prr7 RNA expression in Mock vs. PTX-treated cells in cell bodies and processes (which are mainly represented by dendrites), respectively. Thereby we observed a significant decrease in Prr7 mRNA levels in the process compartment upon PTX treatment (Fig. 1b). Prr7 levels in the cell body compartment were more variable, but also trended downward by PTX, consistent with our observations in whole cell extracts.

We further probed for Prr7 protein expression by immunoblotting whole cell and compartmentalized protein extracts from PTX and Mock-treated hippocampal neurons. Whereas there was a general downward trend in Prr7 protein levels upon PTX treatment, the effect was most pronounced and statistically significant in dendrites, providing further support for an important contribution of local regulatory mechanism engaged in the control of Prr7 expression during HSD (Fig. 1c-f).

To further corroborate the observed subcellular differences in Prr7 regulation in neurons, we additionally analyzed Prr7 protein levels through Prr7 immunostaining of GFP-transfected hippocampal neurons which were either Mock- or PTX-treated. Therefore, we used a commercial Prr7 antibody whose specificity was validated by the presence of reduced signal intensity in Prr7 knockdown cells (Supplemental Fig. 1). We measured the average Prr7 puncta intensities within whole cell, cell body, and dendrite (whole cell with cell body removed) selections using GFP as a mask. Consistent with the Western blot data, reduction in Prr7 puncta intensity upon PTX was most robustly observed in neuronal dendrites, whereas analysis of cell bodies only revealed a non-significant reduction of the Prr7 signal (Fig. 1g-h). This decrease was homogenous along the dendrites since no difference in Prr7 downregulation was detected between proximal vs. distal dendrites (Supplemental Fig. 2).

Notably, no significant differences in either Prr7 mRNA or protein levels between the cell body and dendritic compartments were observed in Mock-treated neurons at baseline (Supplemental Fig. 3), indicating that mechanisms leading to Prr7 downregulation are specifically engaged during HSD.

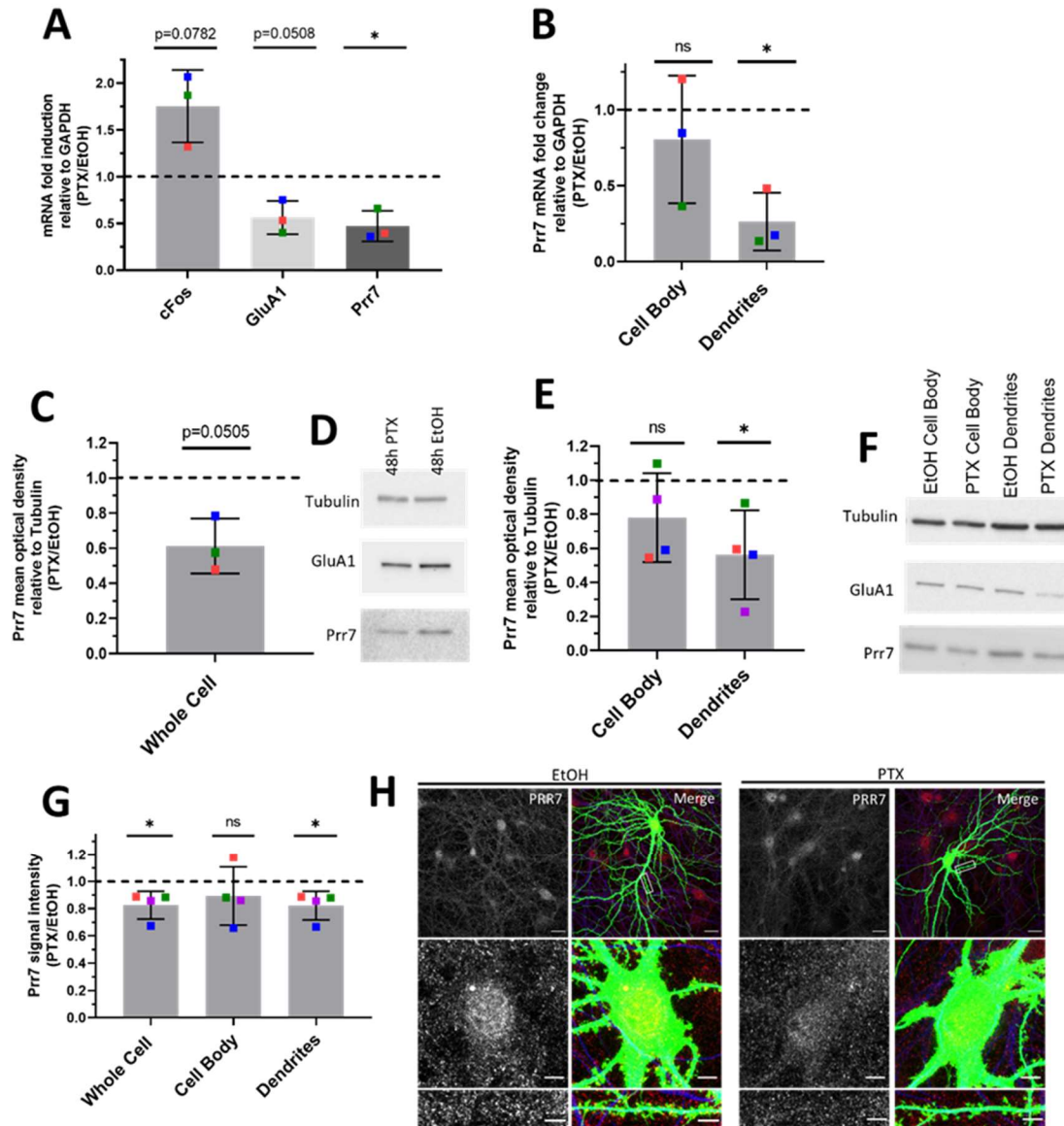
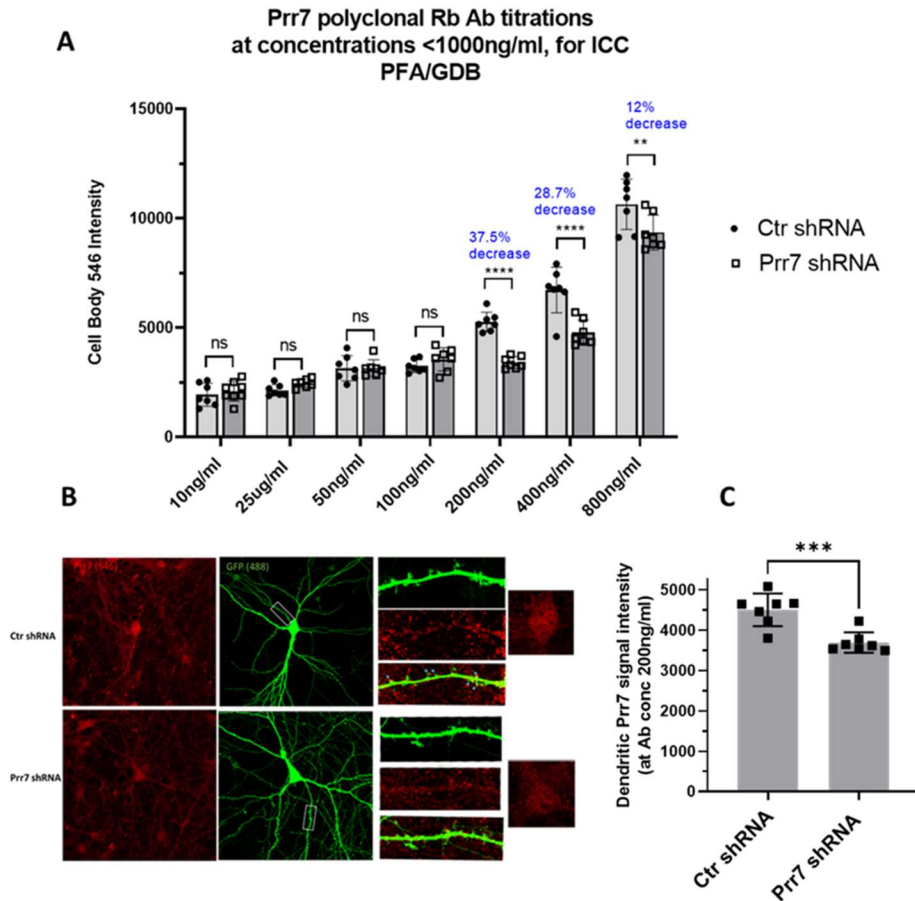
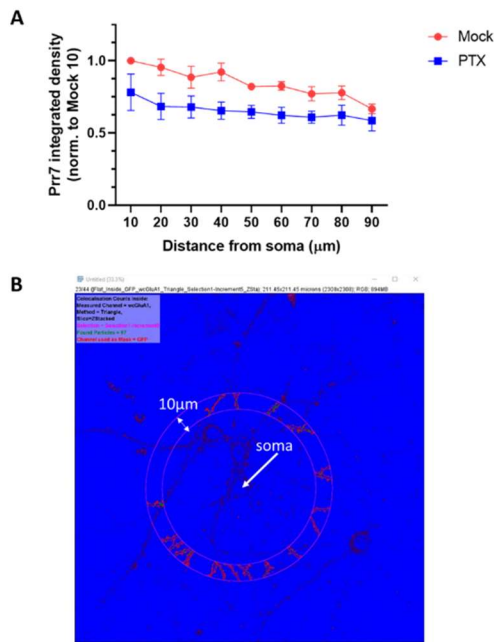


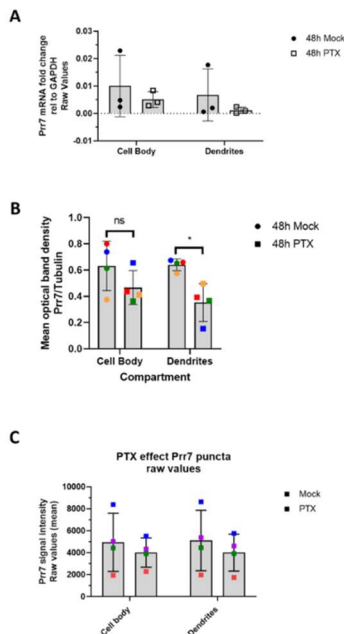
**Figure 1 Global and local Prr7 downregulation at both RNA and protein levels by chronic activity.** (a) Prr7 mRNA levels relative to GAPDH in hippocampal rat neurons treated with 100µM PTX or EtOH (1:500 volume) at DIV17 for 48h and lysed for RNA extraction on DIV19. \* p=0.0303. (b) Prr7 mRNA levels in compartmentalized hippocampal cell samples treated at DIV19 with 100µM PTX or EtOH (1:500 volume) for 48h (ns p=0.5059, \* p=0.0216). Prr7 protein levels as measured by mean optical band density relative to Tubulin in (c-d) whole cell hippocampal cell samples, and (e-f) compartmentalized hippocampal rat cultures treated at DIV19 with 100µM PTX or EtOH (1:500 volume) for 48h (ns p=0.1910, \* p=0.0441). All replicate blots are shown in Supplemental Data. (g) Average Prr7 punctum intensity in GFP-transfected (150ng) cell body or dendrites selection of hippocampal rat neurons treated with PTX or EtOH on DIV19 for 48h. Each point represents the grand average for the 7-9 cells imaged in a single experiment (\* p=0.0417 (whole cell), ns p=0.3988 (cell body), \* p=0.0427 (dendrites)). (h) Representative whole cell, cell body, and dendrite images showing Prr7 expression (grey-scale, left panels) and merged Prr7 (red), GFP (green), Map2 (blue) signals (right panels) in GFP-transfected hippocampal neurons treated with EtOH or PTX for 48h. Scale bars = 20µm (whole cell images) and 5µm (cell body and dendrite closeups). For all bar graphs, data = mean normalized to EtOH condition ± S.D., n=3-4, \*p<0.05, one-sample t-test with hypothetical mean set to 1. Colors of points represent data from the same independent experiment.



**Supplemental Figure 1 Prr7 polyclonal antibody validation for immunostaining.** (a) Titration series testing concentrations 10-800ng/ml of antibody by quantifying cell body Prr7 signal intensity in 7 neurons transfected with Ctr vs. Prr7 shRNA. DIV12 rat hippocampal cells were transfected with 150ng GFP-Amp plasmid, 7.5ng pSUPER control or Prr7 shRNA vector with pcDNA added up to 1 $\mu$ g total per well. On DIV18 cells were fixed 15min with 4% PFA/4% sucrose/PBS, blocked in 1xGDB for 15min, and immunostained for Prr7 (PA5-61266 Thermo at given concentrations) in GDB overnight at 4C. The following day coverslips were washed, secondary (546 anti-Rb for Prr7, 1:2000) added and 7-9 neurons imaged. \*\*  $p < 0.01$ , \*\*\*  $p < 0.001$ , \*\*\*\*  $p < 0.0001$ , 2-way ANOVA with Tukey's post-hoc HSD test. (b) Representative images of Ctr and Prr7 shRNA-transfected neurons stained for Prr7 using 200ng/ml antibody, with close-ups of dendrites and cell bodies. Arrows indicate that some, but not all, of dendritic spines colocalize with Prr7 puncta. (c) Results of average Prr7 punctum intensity in processes (cell body puncta subtracted) of imaged cells (\*\*\*)  $p=0.0007$ , unpaired Student's t-test).



**Supplemental Figure 2 Segmentation analysis of cells treated with EtOH or PTX for 48h and immunostained for Prr7.** (a) The same EtOH and PTX-treated cells as those analyzed for whole cell, cell body, dendrite Prr7 levels in Figure 1g-h were re-visited to measure Prr7 immunofluorescence with respect to distance from the soma. Through an automated method, concentric circles increasing in 10µm steps were drawn around the soma, and dendritic segments within each increasing step were selected using GFP as a mask. Subsequently the average Prr7 puncta intensity in the detected dendritic segments (as measured by integrated density) were obtained, and a grand average across the 7-9 cells imaged per condition was calculated for one experiment. Shown is the mean Prr7 immunofluorescence data across 3 independent experiments, normalized to the Mock 10µm point,  $\pm$  SEM. (b) A sample image showing dendritic segments selection and Prr7 puncta detected at 50µm from the soma through the automated analysis.



**Supplemental Figure 3 Raw pre-normalized Prr7 mRNA and protein data from compartmentalized experiments.** The same data from Fig. 1b, e, g are shown, but before normalization to the EtOH-treated conditions. Namely, (a) represents Prr7 mRNA levels in compartmentalized hippocampal cell samples treated at DIV19 with 100µM PTX or EtOH (1:500 volume) for 48h. (b) Prr7 protein levels as measured by mean optical band density relative to Tubulin in compartmentalized hippocampal rat cultures treated at DIV19 with PTX or EtOH for 48h. Mock Cell Body vs. PTX Cell Body: ns  $p=0.3612$ ; Mock Dendrites vs. PTX Dendrites: \*  $p=0.0495$ ; 2-way ANOVA with Tukey's post-hoc test. (c) Average Prr7 punctum intensity in GFP-transfected (150ng) cell body or dendrites selection of hippocampal rat cultures treated with PTX or EtOH on DIV19 for 48h, then immunostained for Prr7. For all graphs, data = mean  $\pm$  S.D.,  $n=3-4$ .

*Downregulation of Prr7 is necessary and sufficient for spine density reduction during HSD*

Based on our finding that Prr7 is downregulated during HSD, we asked whether Prr7 knockdown is sufficient to induce HSD. Prr7 knockdown was achieved using transfection of a Prr7 shRNA expressing plasmid based on a previously published Prr7 targeting sequence (Kravchick et al., 2016) We confirmed efficient and specific knockdown of Prr7 using the generated construct (Supplemental Fig. 4). Prr7 knockdown did not adversely affect cell health based on unaltered cell morphology between control and Prr7 shRNA-transfected neurons (Supplemental Fig. 1b).

Using the validated shRNA construct, we found that Prr7 loss in hippocampal neurons led to a significant decrease in dendritic spine density, to levels comparable to those induced by PTX (Fig. 2a-b). To determine whether spine density reduction was specific to Prr7 knockdown and not caused by off-target effects of the shRNA used, we generated an shRNA-resistant Prr7 expression construct (validations shown in Supplemental Fig 5 and 6). The spine density reduction from Prr7 shRNA was rescued when the shRNA-resistant Prr7 expression construct was introduced (Fig. 2c-d). Moreover, a small (~34%) increase in spine density was observed upon Prr7 overexpression alone. Furthermore, overexpression of Prr7 in hippocampal neurons led to complete prevention of spine density reduction in the presence of PTX (Fig. 2e-f).

Since AMPAR degradation is a hallmark of HSD, we studied the effect of Prr7 knockdown on the protein levels of the GluA1 subunit of AMPARs. Knockdown of Prr7 in cortical neurons led to a reduction in total GluA1 protein levels as judged by immunoblotting (Fig. 2g-h). Additionally in hippocampal neurons, GluA1 whole cell puncta intensity and surface GluA1 puncta number were reduced in the Prr7 knockdown condition based on immunostaining (Fig. 2i-l). Together, these observations suggest that loss of Prr7 might be sufficient to induce a reduction in spine density and AMPA-type glutamate receptor subunits, both of which are commonly observed during HSD.

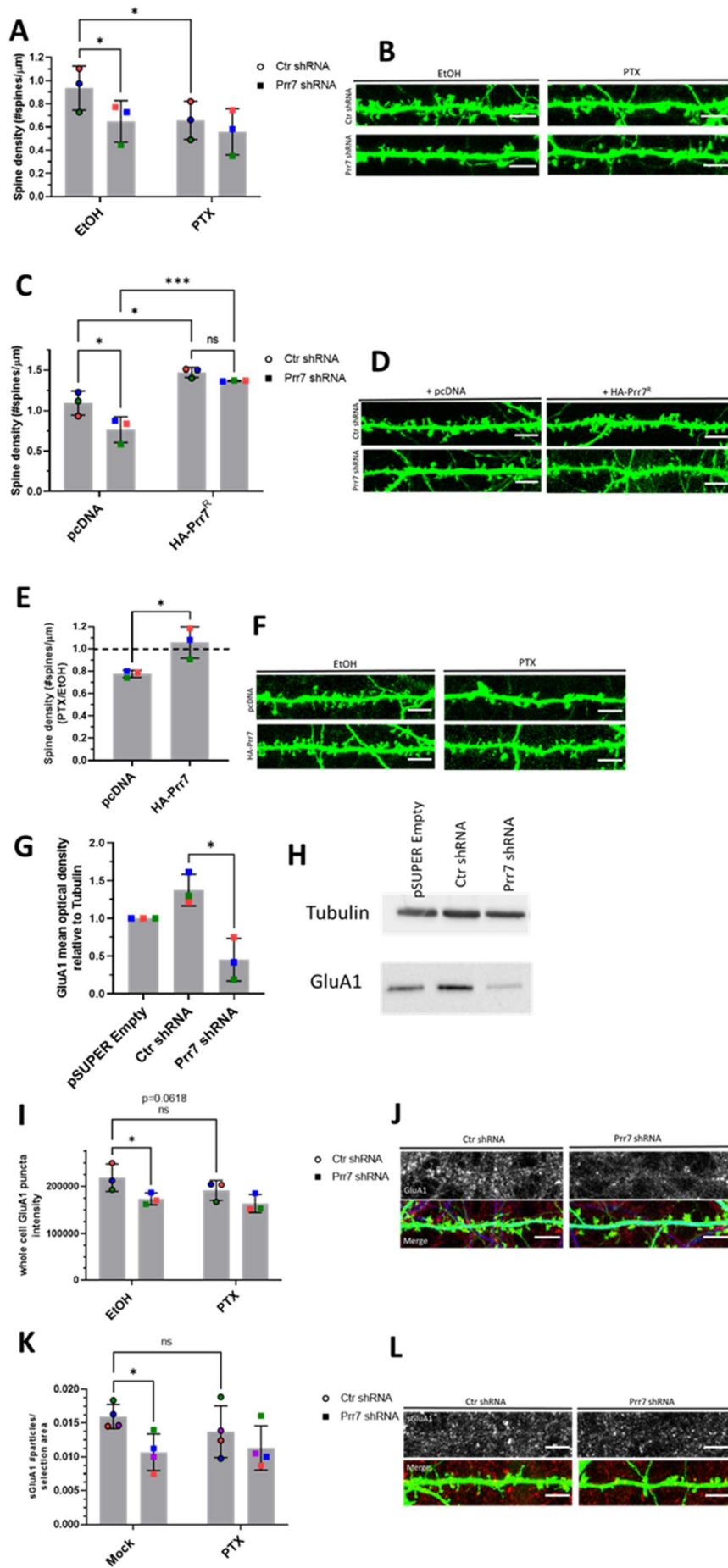
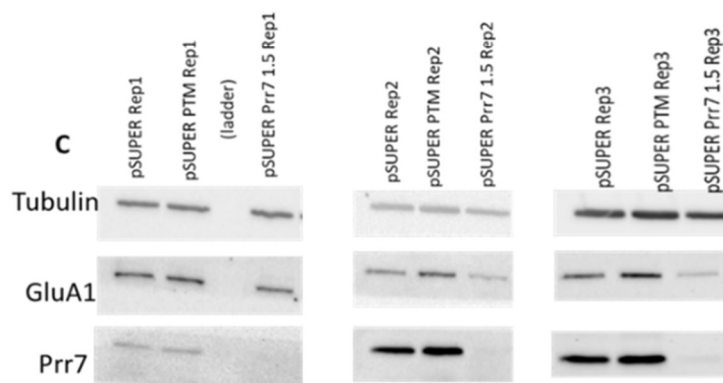
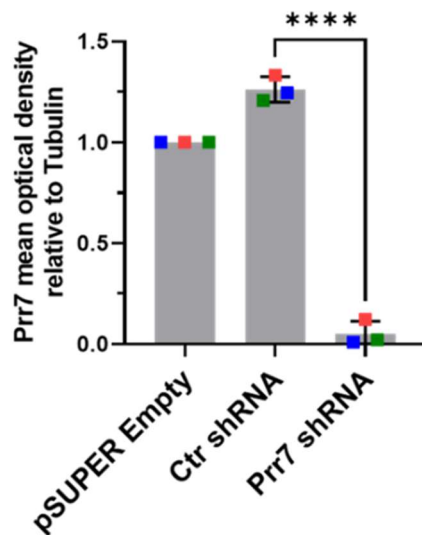
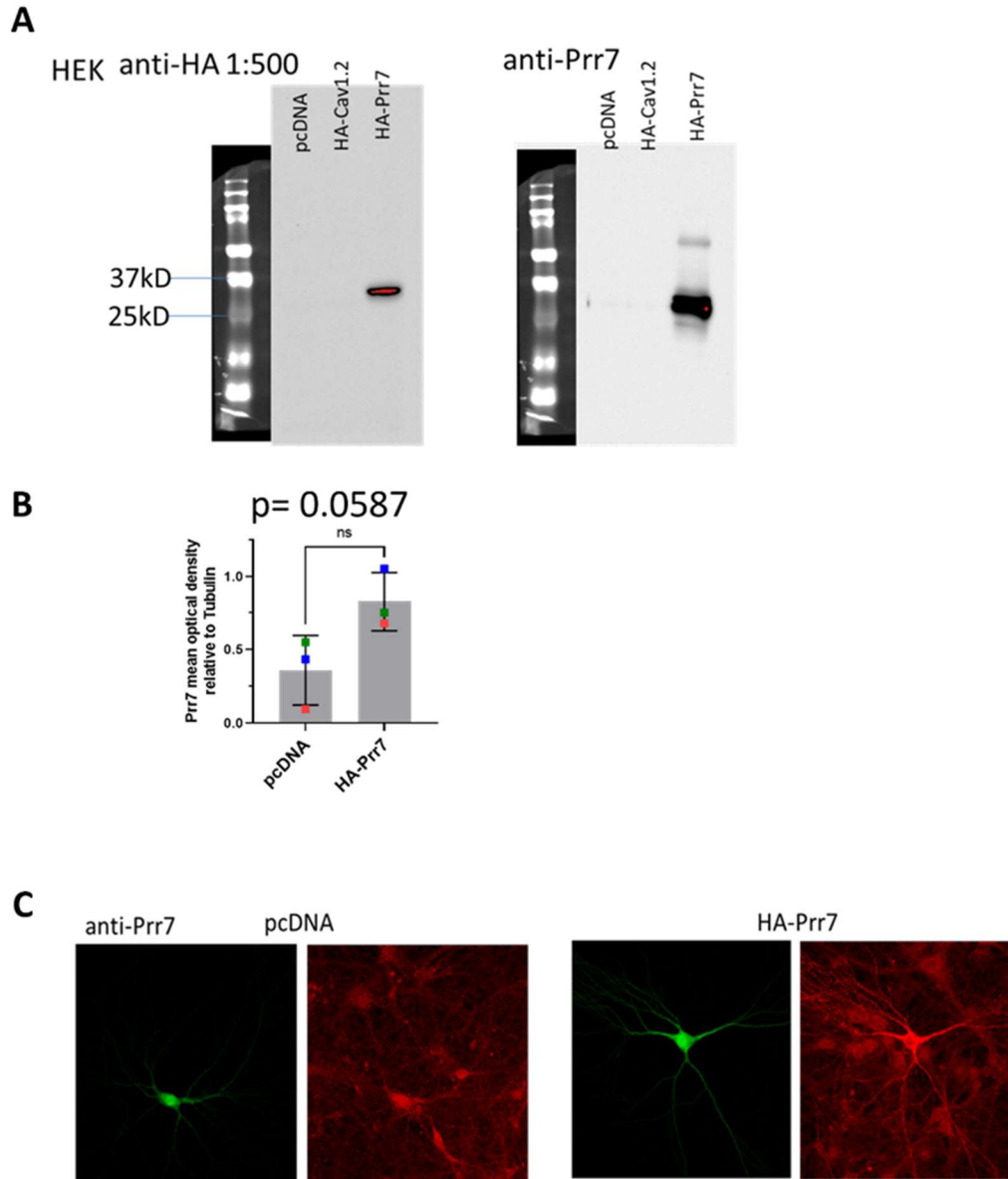


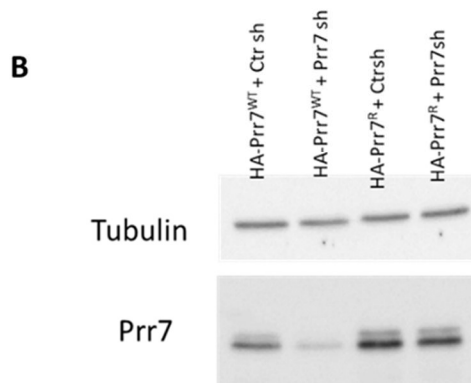
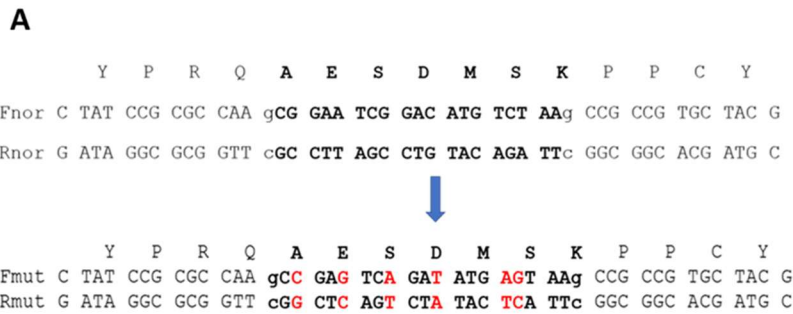
**Figure 2 Prr7 downregulation is necessary and sufficient for HSD.** (a-b) Spine densities of hippocampal rat neurons transfected with GFP (150ng) and either control or Prr7 shRNA vector (7.5ng pSUPER) on DIV13, treated at DIV19 with 100 $\mu$ M PTX or EtOH (1:500 volume) for 48h, with representative GFP images showing dendrites for each condition (Ctr EtOH vs. Prr7 EtOH:  $p=0.0175$ ; Ctr EtOH vs. Ctr PTX:  $p=0.0187$ ). (c-d) Spine densities of hippocampal neurons transfected with GFP (150ng), either control or Prr7 shRNA (7.5ng) and either pcDNA or shRNA-resistant Prr7 construct (400ng) on DIV13 and fixed on DIV20-21 (Ctr pcDNA vs. Prr7 pcDNA:  $p=0.0309$ ; Ctr pcDNA vs. Ctr HA-Prr7<sup>R</sup>:  $p=0.0146$ ; Prr7 pcDNA vs. Prr7 HA-Prr7<sup>R</sup>:  $p=0.0008$ ; Ctr HA-Prr7<sup>R</sup> vs. Prr7 HA-Prr7<sup>R</sup>:  $p=0.6899$ ). For these shRNA experiments, data = mean  $\pm$  S.D.,  $n=3$ , \* $p<0.05$ , \*\*\* $p<0.001$ , two-way ANOVA with Tukey's post-hoc HSD test. (e-f) Spine densities of hippocampal neurons transfected with GFP (150ng) and either pcDNA or HA-Prr7 construct (400ng) on DIV13 and treated at DIV19 with EtOH or PTX for 48h. Data = mean normalized to EtOH condition  $\pm$  S.D.,  $n=3$ , \* $p=0.0280$ , unpaired Student's t-test. (g-h) GluA1 protein levels as measured by mean optical band density relative to Tubulin in empty pSUPER, Ctr shRNA, and Prr7 shRNA-transfected cortical neuron whole cell extracts, with representative western blot images. Data = mean normalized to pSUPER empty condition  $\pm$  S.D.,  $n=3$ , \* $p=0.0105$ , unpaired Student's t-test. Full dataset of blots are shown in Supplemental Fig. 4. (i-j) Average whole cell GluA1 puncta intensity and (k-l) surface GluA1 puncta number for hippocampal neurons transfected with GFP, with either control or Prr7 shRNA, and treated with PTX or EtOH for 48h. Data = mean  $\pm$  S.D,  $n=3$ , 2-way ANOVA with Tukey's post-hoc HSD test. Whole cell GluA1: Ctr EtOH vs. Prr7 EtOH: \* $p=0.0228$ ; Ctr EtOH vs. Ctr PTX: ns  $p=0.0618$ . Surface GluA1: Ctr EtOH vs. Prr7 EtOH: \* $p=0.0121$ ; Ctr EtOH vs. Ctr PTX: ns  $p=0.1193$ . All scale bars shown = 5 $\mu$ m. Whole cell images from which dendrite segments were taken are shown in Supplemental Data.



**Supplemental Figure 4 Prr7 protein levels in Ctr shRNA and Prr7 shRNA-nucleofected cells (validation of Prr7 knockdown with pSUPER construct).** Prr7 protein levels as measured by mean optical band density relative to Tubulin in empty pSUPER, Ctr shRNA, and Prr7 shRNA (2 $\mu$ g)-nucleofected cortical neuron whole cell extracts, with corresponding western blot images (membranes were cut horizontally to probe for Prr7 (29kD), GluA1 (101kD), and Tubulin (50kD)). Protein extracts were loaded in the order of pSUPER empty  $\rightarrow$  Ctr shRNA  $\rightarrow$  Prr7 shRNA. The GluA1 data is presented in Fig. 2g-h. Data = mean normalized to pSUPER empty condition  $\pm$  S.D.,  $n=3$ , \*\*\*\* $p<0.0001$ , unpaired Student's t-test.



**Supplemental Figure 5 Validations of Prr7 overexpression with HA-Prr7 construct.** (a) HEK293 cells were transfected with pcDNA, HA-Cav1.2, or HA-Prr7 (HA-tag fused to N-terminus of Prr7 cDNA sequence) (all 2 $\mu$ g) and 1 $\mu$ g GFP (for visualization of transfection efficiency), then protein extracts from the cell lysate were immunoblotted for HA (left) and Prr7 (right) detection. Although the HA tag of the HA-Cav1.2 was not detected, this may be due to inadequate transfer given the large size of Cav1.2 (expect a band at 250kD). However, strong bands for HA and Prr7 were detected at the expected molecular weight of 29kD for the HA-Prr7 condition only, suggesting Prr7 overexpression in HEK cells which do not express endogenous Prr7. (b) Prr7 protein levels as measured by mean optical band density relative to Tubulin in 2 $\mu$ g pcDNA or HA-Prr7 with 1 $\mu$ g GFP-nucleofected cortical neuron protein extracts, with corresponding western blot images (membranes were cut horizontally to probe for for Prr7 (29kD), GluA1 (101kD), and Tubulin (50kD)). Data = mean  $\pm$  S.D., n=3, p=0.0587, unpaired Student's t-test. (c) Representative images of GFP (left) and Prr7 staining (right) in hippocampal rat neurons transfected with 400ng pcDNA or HA-Prr7 and 150ng GFP at DIV13, fixed at DIV18 and immunostained for Prr7. Importantly, the Prr7 overexpression appeared in not only the cell body but also in dendrites of HA-Prr7 transfected cells.



**Supplemental Figure 6 Validation of shRNA-resistant Prr7 expression construct. (a)** Position of 6 point mutations in Prr7 cDNA sequence to generate shRNA-resistant construct, using generated HA-Prr7 construct as a template. Prr7 shRNA targeting region is in bold text. The mutations introduced interfere with the recognition of Prr7 mRNA by shRNA, but the corresponding amino acid sequence of the resultant exogenous Prr7 protein (AESDMSK) remains unchanged. **(b)** HEK293 cells were transfected with 100ng of either HA-Prr7 wild type (HA-Prr7 wt) or shRNA-resistant mutant (HA-Prr7<sup>R</sup>), 1 $\mu$ g Ctr or Prr7 shRNA, and 1 $\mu$ g GFP (for assessing transfection efficiency). Protein extracts were obtained and immunoblotted for Prr7 and Tubulin expression. Prr7 knockdown due to Prr7 shRNA transfection is prevented in the presence of the mutant, but not the wild type expression construct.

### *miR-329 and miR-495 are required for Prr7 downregulation by PTX*

Next, we explored the mechanisms underlying PTX-dependent downregulation of Prr7. Following the observations that Prr7 expression is regulated at the RNA level upon PTX treatment, we hypothesized that it may be regulated post-transcriptionally by miRNAs. miRNAs already have strong implications toward activity-dependent synaptic plasticity mechanisms, including HSD (Fiore et al., 2014; Cohen et al., 2011; Rajman et al., 2017).

Upon analysis of the Prr7 3' UTR sequence using the Targetscan algorithm, we found four predicted miRNA binding sites, two of which overlap with one another (Fig. 3a). We examined the effect of inhibiting two of the four miRNA candidates, miR-329-3p and miR-495-3p, on Prr7 mRNA expression in the context of PTX treatment, through the use of a luciferase reporter with the Prr7 3' UTR cloned downstream of a firefly gene. We selected these two miRNAs for further studies since miR-495-3p is the most abundant of the four candidates, and miR-329-3p has been previously implicated in KCl-dependent dendritogenesis (Fiore et al., 2009). We observed a reduction in firefly luciferase activity upon PTX stimulation, which was prevented by a cocktail of miR-329-3p and miR-495-3p inhibitors (antisense locked nucleic acid inhibitors "pLNAs"). Importantly, this effect was not seen when a reporter

with mutated binding sites for these miRNAs on the Prr7 3' UTR was used (Fig. 3b), demonstrating that the effects were mediated by the miRNA binding sites present in the Prr7 3'UTR. The same effect was observed when transfecting miR-495-3p pLNA alone (Fig. 3c). A trend was observed for miR-329-3p pLNA alone, although the effect did not reach statistical significance (Fig. 3d). Taken together, these findings indicated that Prr7 is a direct target of miR-329-3p and miR-495-3p, with miR-495-3p contributing more to the downregulation, and that these interactions take place during HSD.

We then asked whether the miR-329-3p and miR-495-3p regulation of Prr7 during downscaling as suggested by luciferase could also be seen at the protein level for dendrite-localized Prr7. Decreases in Prr7 in dendrites upon PTX were prevented when cells were transfected with the cocktail of miR-329-3p and miR-495-3p pLNAs (Fig. 3e-f), but not for miR-329-3p or miR-495-3p pLNA alone, thereby confirming our results from luciferase assays and indicating an additive inhibitory role for miR-329-3p and miR-495-3p in Prr7 regulation.

Since miRNA inhibition appeared to upregulate Prr7 only in the context of PTX stimulation, we speculated that miR-329-3p and miR-495-3p themselves could be subject to PTX-dependent regulation. We examined endogenous miRNA activity in the Mock and PTX-stimulated hippocampal neurons through use of a single cell dual fluorescence assay ("sensor assay"), as previously described (Fiore et al., 2009). Specifically, the assay utilizes polycistronic vectors expressing both GFP and dsRed, whereby dsRed expression is post-transcriptionally controlled by the presence of two perfectly complementary binding sites for the miRNA of interest within the dsRed 3' UTR (Fig. 3g). If miRNAs of interest are active within a given cell, they would bind to the dsRed 3'UTR and downregulate dsRed expression. Thus, cells expressing only GFP without dsRed were counted as "miRNA positive", and those expressing dsRed were counted as "miRNA negative". Hippocampal neurons were transfected either with a control sensor (containing a sequence non-specific to any known miRNAs), a miR-329-3p or a miR-495-3p sensor. Subsequently, "miRNA positive" vs. "miRNA negative" cells were manually scored over the entirety of each coverslip for all conditions (Supplemental Fig. 7). The proportion of miRNA-positive neurons increased upon PTX treatment for both the miR-329-3p and miR-495-3p sensor transfections. This induction was not seen when a pLNA against the respective miRNA was co-transfected with the sensor, indicating that the sensor could reliably detect endogenous miRNA activity. In conclusion, PTX treatment increased the proportion of neurons displaying active miR-329-3p and miR-495-3p (Fig. 3h).

Next, we wanted to test whether the observed PTX-dependent increase in miR-329/495 activity was due to an upregulation of miRNA expression. qPCR analysis of these two miRNAs in RNA extracts obtained from compartmentalized neuron cultures indicated a non-significant PTX-dependent upregulation in mature miRNA levels for both miR-329-3p and miR-495-3p in the cell body upon PTX treatment (Fig. 3i). In the process compartment, mature miR-495-3p, but not miR-329-3p levels were significantly

increased by PTX. These findings suggest that in the case of miR-495-3p, PTX-dependent activity increase might involve a local upregulation of miR-495-3p expression in the dendritic compartment.

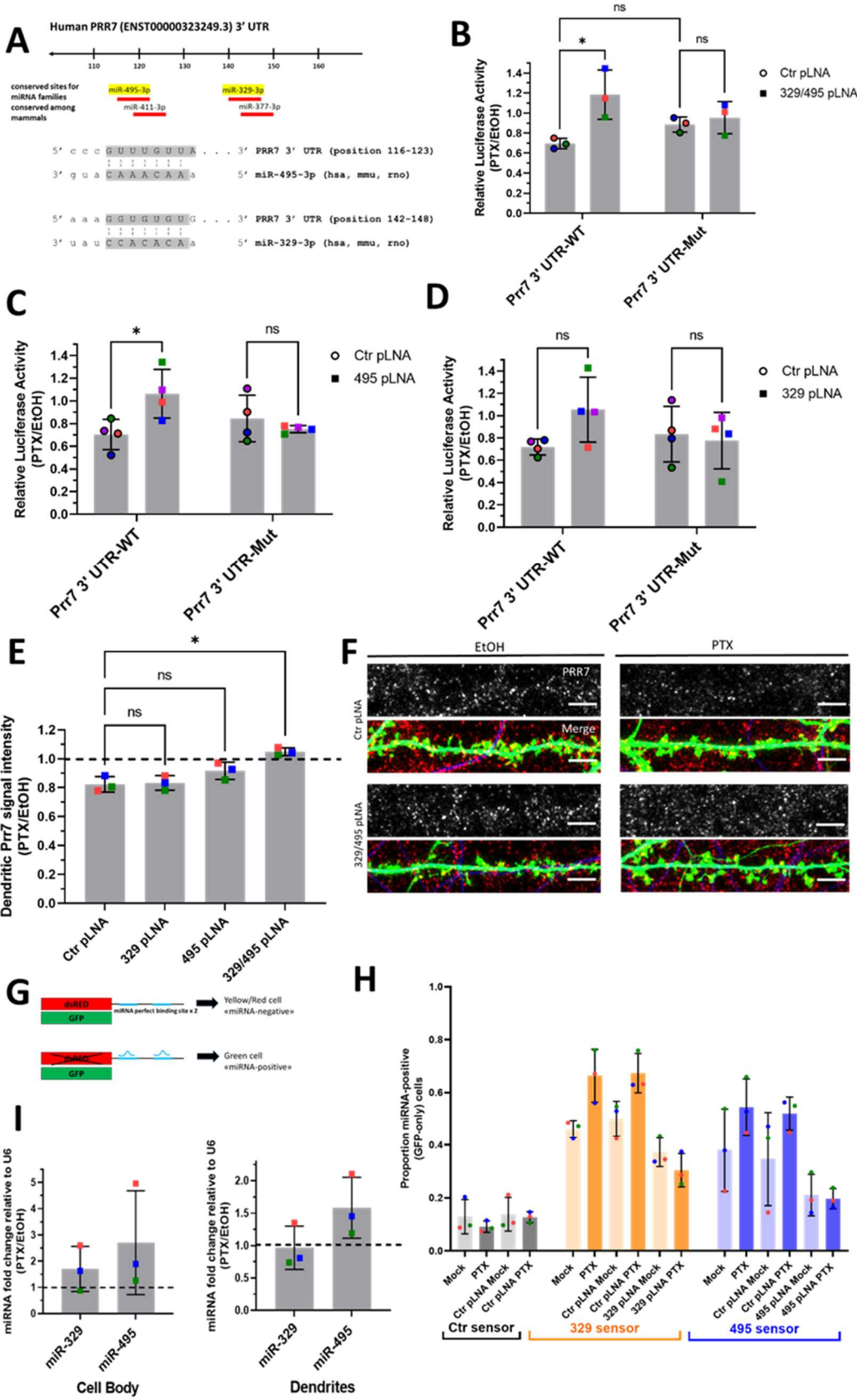
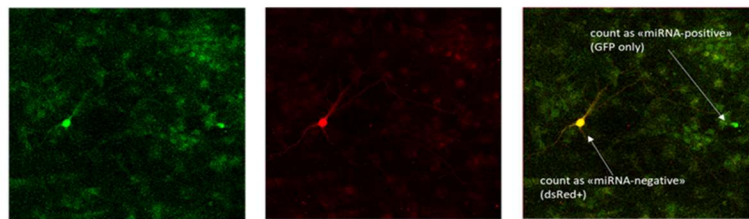
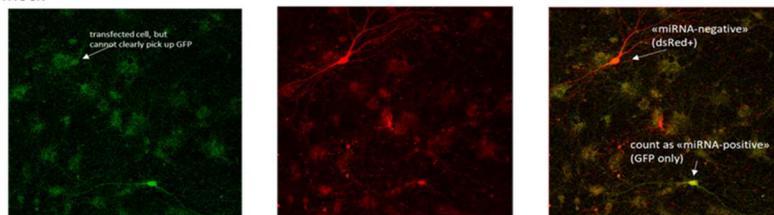


**Figure 3 miR-329 and miR-495 are required for Prr7 downregulation by PTX.** (a) Predicted miRNA binding sites for human Prr7 3' UTR, and seed matches for miR-329 and miR-495 from Target Scan (<http://www.targetscan.org/>). (b-d) Rat hippocampal neurons were co-transfected at DIV13 with either pmirGLO Prr7 WT or Mut 3' UTR plasmids (50ng), and control pLNA, 329 pLNA, 495 pLNA (20pmol) or miR-329/495 pLNA mix (10pmol each), and treated with either EtOH or 100 $\mu$ M PTX at DIV18. Cells were lysed at DIV20 and firefly/renilla luciferase activity ratios measured. Data = mean normalized to EtOH condition  $\pm$  S.D, n=3-4, 2-way ANOVA with Tukey's post-hoc HSD test. 329/495 pLNA data: Ctr WT vs. 329/495 WT: \* p=0.0194; Ctr WT vs. Ctr Mut: ns p=0.4724; Ctr Mut vs. 329/495 Mut: ns p=0.9452. 495 pLNA data: Ctr WT vs. 495 WT: \* p=0.0397; Ctr Mut vs. 495 Mut: ns p=0.8484. 329 pLNA data: Ctr WT vs. 329 WT: ns p=0.2275; Ctr Mut vs. 329 Mut: ns p=0.9841. (e) Average Prr7 punctum intensity in hippocampal cells transfected with GFP (150ng) and control, miR-329, miR-495 pLNA (20pmol), or miR-329/495 pLNA mix (10pmol each) at DIV13 and treated with PTX or EtOH on DIV19 for 48h. Data = mean normalized to EtOH condition  $\pm$  S.D., n = 3, one-way ANOVA with Tukey's post-hoc HSD test. Ctr vs. 329: ns p=0.9946; Ctr vs. 495: ns p=0.1739; Ctr vs. 329/495: \* p=0.0023. (f) Representative dendrite images showing Prr7 expression (grey-scale, top panels) and merged Prr7 (red), GFP (green), Map2 (blue) signals (bottom panels) in Ctr or 329/495 pLNA-transfected hippocampal neurons treated with 48h EtOH or PTX. Scale bars = 5 $\mu$ m. Whole cell images from which dendrite segments were taken are shown in Supplemental Data. (g-h) Schematic of single-cell dual-fluorescence miRNA sensor assay, and measurement of endogenous miR-329 and miR-495 activity upon PTX treatment in hippocampal neurons. Cells were transfected with miR-329, miR-495, or control sensor (125ng), with or without Ctr, miR-329, or miR-495 pLNA (5pmol) at DIV13, treated with 100 $\mu$ M PTX or EtOH at DIV19, and fixed at DIV21. The number of neurons expressing GFP only without dsRed vs. those expressing dsRed were counted. Data = mean proportion of GFP+ cells/total cell count  $\pm$  S.D, n=3. (i) Mature miR-329 and miR-495 levels in cell body and dendrite compartments of hippocampal neurons treated with either EtOH or PTX for 48h. Data = mean normalized to EtOH condition  $\pm$  S.D., n = 3.

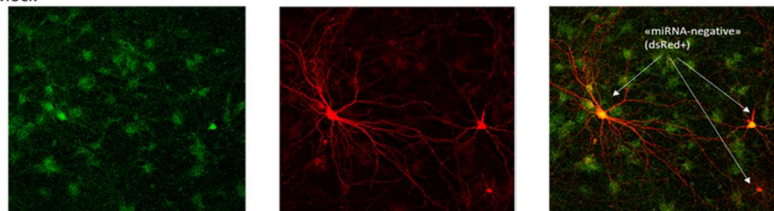
from 329 sensor PTX coverslip



495 sensor Mock



Ctr sensor Mock



**Supplemental Figure 7 Sample images from miRNA sensor assay.** Representative images of miR-329, miR-495, Control sensor-transfected hippocampal neurons (DIV13 transfection, DIV19 EtOH or PTX treatment, DIV21 fixation). GFP (left), dsRed (middle), and merged (right) images are shown. Cells that appear red or yellow in the merged channel were counted as “miRNA-negative” and those that appear green were counted as “miRNA-positive”.

*miR-329-3p and miR-495-3p are required for synaptic depression induced by PTX and Prr7 knockdown*

We next asked whether miR-329-3p and miR-495-3p were functionally involved in HSD. Therefore, we measured spine density in cells transfected with miR-329-3p and miR-495-3p pLNAs in the presence or absence of PTX treatment (48h). We found that both miR-329-3p and miR-495-3p inhibition, separately and together, rescued PTX-mediated spine density reduction (Fig. 4a-b). The rescue effect was most pronounced when using a miR-329/495 pLNA cocktail, consistent with our results from Prr7 regulation (Fig. 3b, e).

To corroborate Prr7 as an important downstream target in miR329/495-mediated HSD, we further asked whether the impaired HSD induced by the pLNA cocktail could be reinstated by lowering Prr7 levels through co-transfection of Prr7 shRNA. Consistent with this idea, transfection of Prr7 shRNA, but not control shRNA, restored the PTX-induced spine density reduction in the presence of miR-329 and miR-495 pLNAs (Fig. 4c-d). This result demonstrates that Prr7 is a key target of miR-329/-495 in PTX-mediated HSD.

We went on to test whether increasing levels of miR-329 and -495 was sufficient to induce spine elimination in the absence of PTX, thereby mimicking HSD. Towards this end, we constructed chimeric miR-329 and -495 overexpressing plasmids using a previously described strategy (Christensen et al. 2010; hairpin diagram Supplemental Fig. 8) which allows for efficient miRNA overexpression. Roughly 2-fold overexpression of the miRNA of interest relative to control (Supplemental Fig. 8) was observed, accompanied by consistently downward trends of Prr7 in dendrites (Supplemental Fig. 9). Despite the moderate effects on miRNA overexpression and Prr7 reduction achieved with this approach, stable overexpression of miR-329 and miR-495 was in both cases sufficient to induce a significant reduction in spine density (Fig. 4e-f). Thus, miR-329/495 overexpression mimics PTX-induced miR-329/495 expression followed by spine elimination in transfected hippocampal neurons.

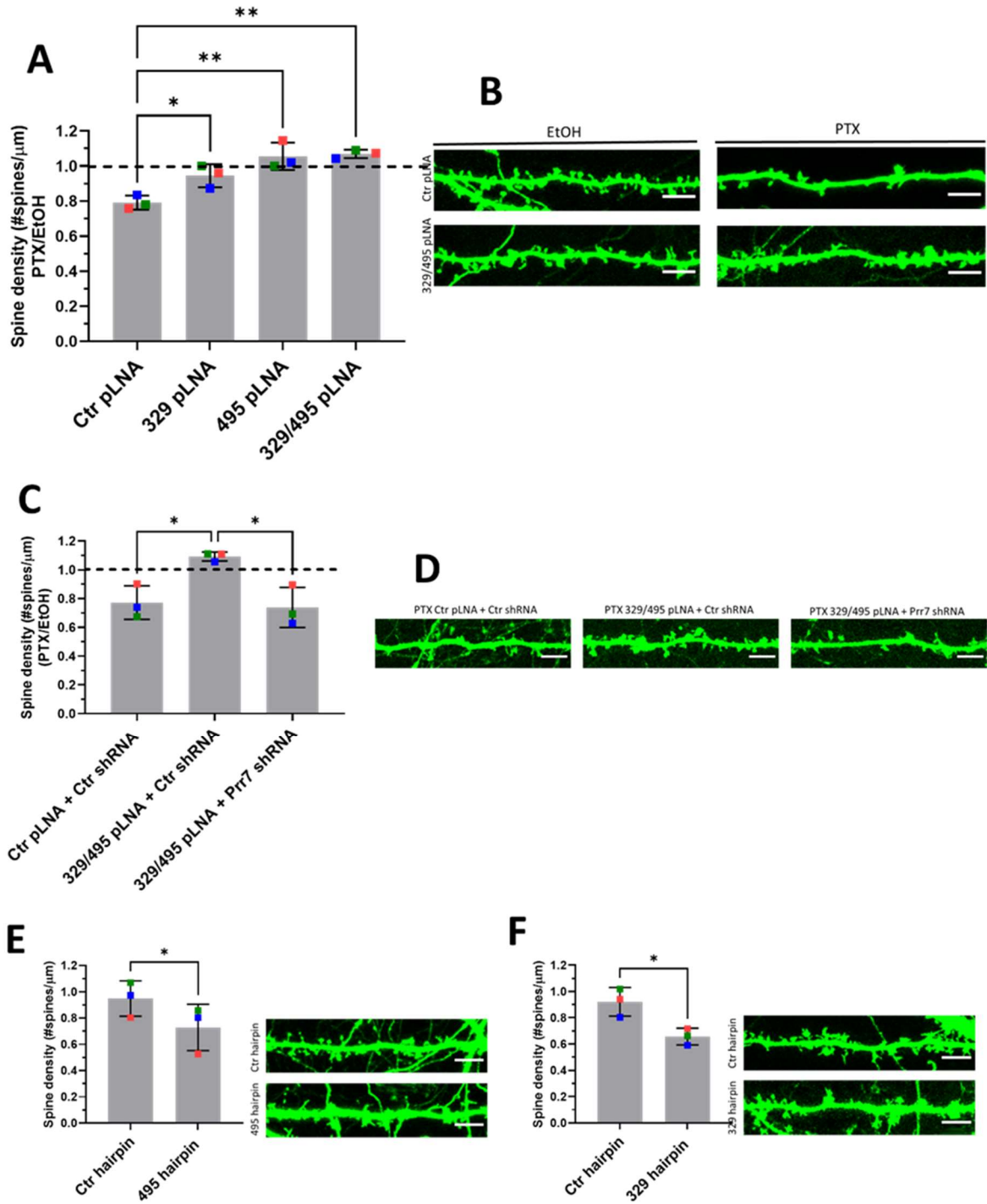
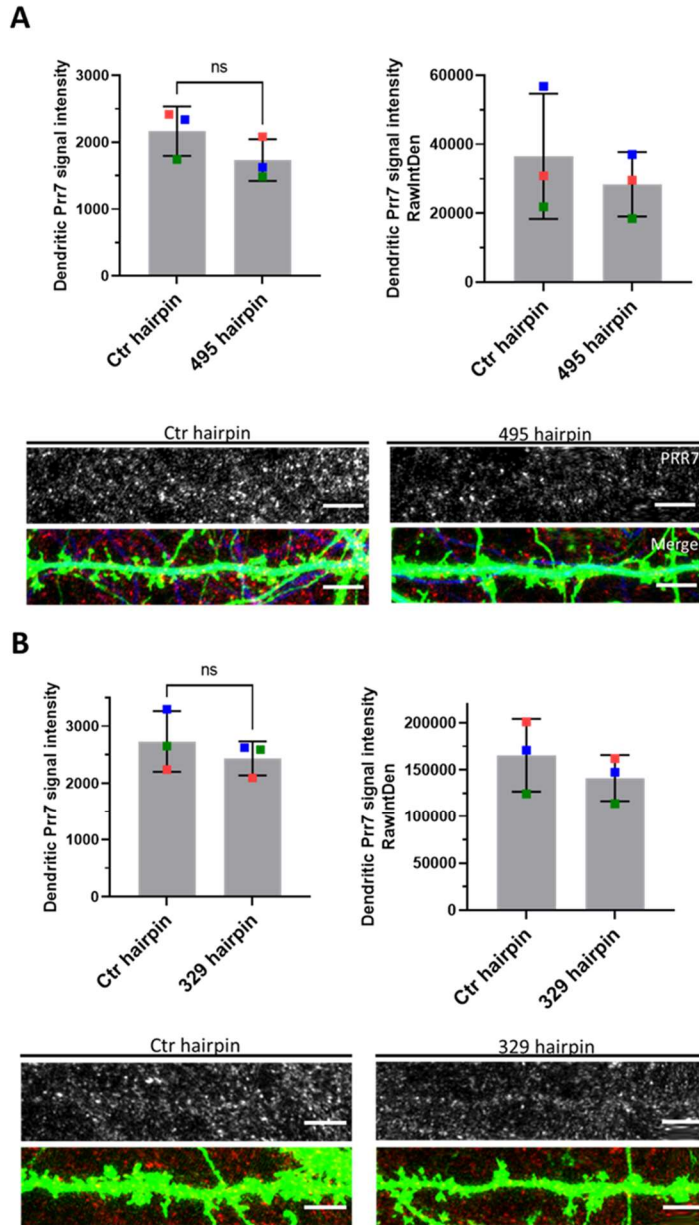


**Figure 4 miR-329 and miR-495-mediated Prr7 downregulation are required for synaptic depression induced by PTX.** (a-b) Spine densities of hippocampal cells transfected with GFP (150ng) and control, miR-329, miR-495 pLNA (20pmol) or miR-329/495 pLNA mix (10pmol each) on DIV13, treated with EtOH or 100μM PTX on DIV19 for 48h. Representative GFP images showing dendrites for each condition are shown. Ctr vs. 329: \* p=0.0400; Ctr vs. 495: \*\* p=0.0018; Ctr vs. 329/495: \*\* p=0.0013. (c-d) Spine densities of hippocampal cells transfected with GFP (150ng), control pLNA (20pmol) or miR-329/495 pLNA mix (10pmol each), and control or Prr7 shRNA (2.5ng pSUPER) on DIV13, treated with EtOH or PTX on DIV19 for 48h (Ctr + Ctrsh vs. 329/495 + Ctrsh: \* p=0.0240; 329/495 + Ctrsh vs. 329/495 + Prr7sh: \* p=0.0155). For these pLNA data, data = mean normalized to EtOH condition ± S.D., n=3, one-way ANOVA with Tukey's post-hoc HSD test. Spine densities of hippocampal cells transfected with control or (e) miR30a-495 chimeric hairpin (500ng), (f) miR30a-329 chimeric hairpin (500ng) on DIV13 and fixed on DIV18-19 (329hp) or DIV21 (495hp). Data = mean ± S.D., n=3, paired Student's t-test (Ctr vs. 495: \* p=0.0195; Ctr vs. 329: \* p=0.0285). Representative GFP images showing dendrites for each condition are shown. Whole cell images from which dendrite segments were taken are shown in Supplemental Data.





**Supplemental Figure 9 Dendritic Prr7 protein levels show decreasing trends in miR-495 and miR-329 hairpin transfected hippocampal neurons.** Average Prr7 punctum intensity in dendrite selections of (a) miR-495 hairpin and (b) miR-329 hairpin-transfected (500ng hairpin, DIV13) hippocampal rat neurons, which were fixed on either DIV21 (miR-495) or DIV18/19 (miR-329). Puncta intensity was measured by either mean value (left bar graphs) or integrated density (right bar graphs). Data = mean  $\pm$  S.D., n=3, paired Student's t-test. 495 hairpin: p= 0.0922 (left), p=0.2987 (right). 329 hairpin: p=0.2610 (left), p=0.0996 (right). Scale bars = 5 $\mu$ m.

*SPAR/CDK5 pathway is downstream of miR-329/miR-495/Prr7 in HSD*

We further explored the pathway downstream of miR329/495/Prr7 which mediates the effects on spine density. One attractive candidate is the Plk2/SPAR pathway which has previously been implicated in HSD (Pak and Sheng, 2003). Specifically, Plk2-mediated phosphorylation of SPAR is followed by proteasome-dependent SPAR degradation, leading to excitatory synapse weakening and spine loss. Intriguingly, both SPAR and Prr7 have been shown to interact with PSD-95, an important scaffold protein required for the integrity of the post-synaptic density. We therefore speculated that Prr7 might protect SPAR from Plk2-mediated degradation, possibly in conjunction with PSD-95. Thus, we tested whether reducing Prr7 levels affected SPAR expression in a way consistent with a role in HSD. We found a reduction in SPAR levels in cortical neurons nucleofected with Prr7 shRNA through western blotting (Fig. 5a-b). Moreover, dendrite-localized SPAR protein was reduced in Prr7 shRNA-transfected hippocampal neurons (Fig. 5c-d; Supplemental Fig. 11). SPAR reduction was also seen upon PTX treatment as previously reported (Pak and Sheng, 2003). Therefore, Prr7 may stabilize SPAR at basal levels of network activity.

CDK5 kinase-mediated SPAR phosphorylation primes SPAR for targeting by Plk2 (Seeburg et al., 2008). To determine whether Prr7 serves to stabilize SPAR by interfering with CDK5 activity, we treated Prr7 shRNA-transfected cells with 10 $\mu$ M Roscovitine, a CDK5 inhibitor, and quantified SPAR puncta intensity in dendrites. We found that a reduction in SPAR protein levels was no longer seen in Prr7 shRNA-transfected cells treated with Roscovitine relative to DMSO (Fig. 5e, g). Moreover, Roscovitine treatment rescued the spine density reduction in the Prr7 knockdown condition (Fig. 5f-g). These findings suggest that Prr7 functions upstream of CDK5, potentially stabilizing dendritic spines through protecting SPAR from CDK5-mediated priming phosphorylation, which in turn is required for SPAR phosphorylation by Plk2 and subsequent proteasome-dependent degradation.

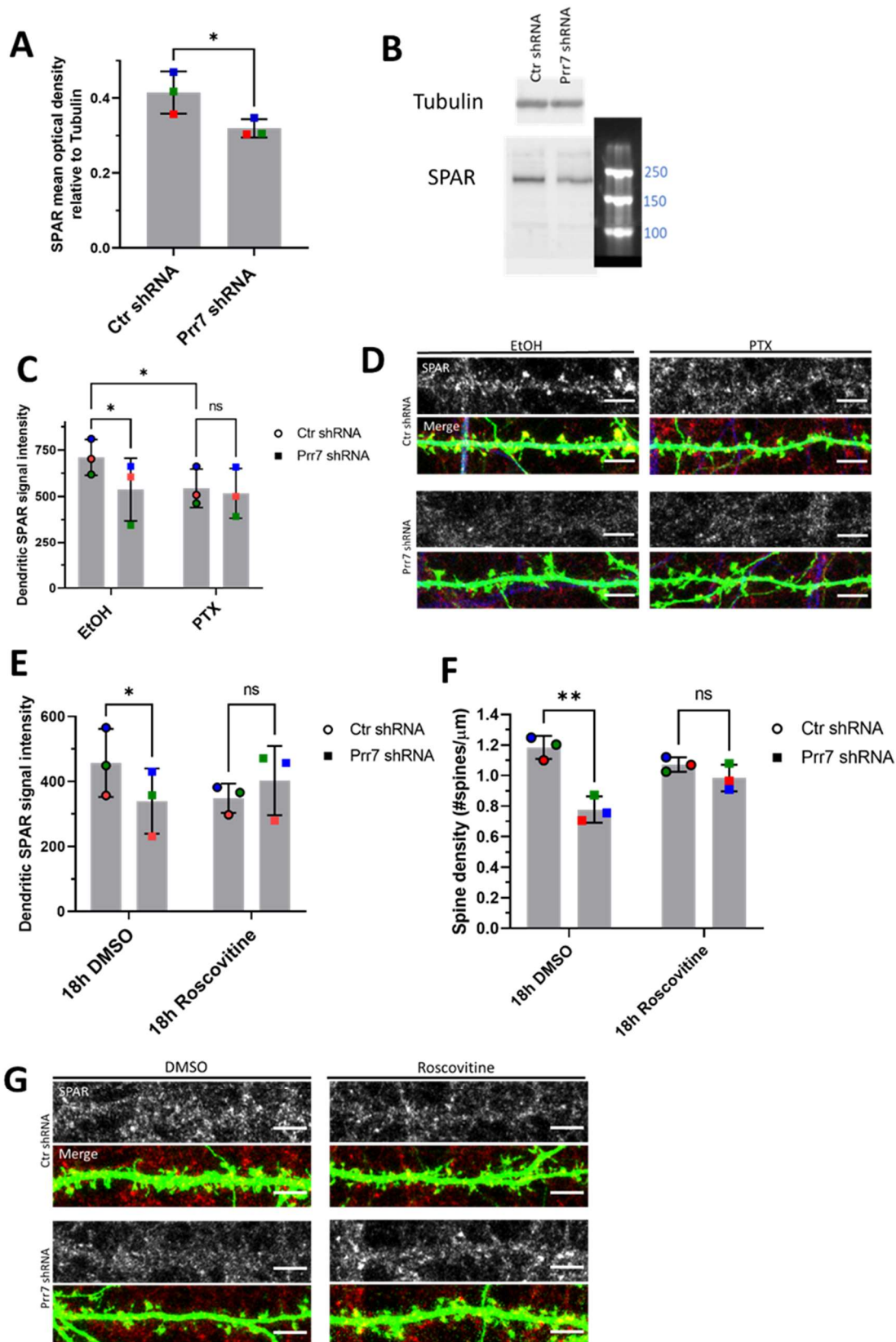
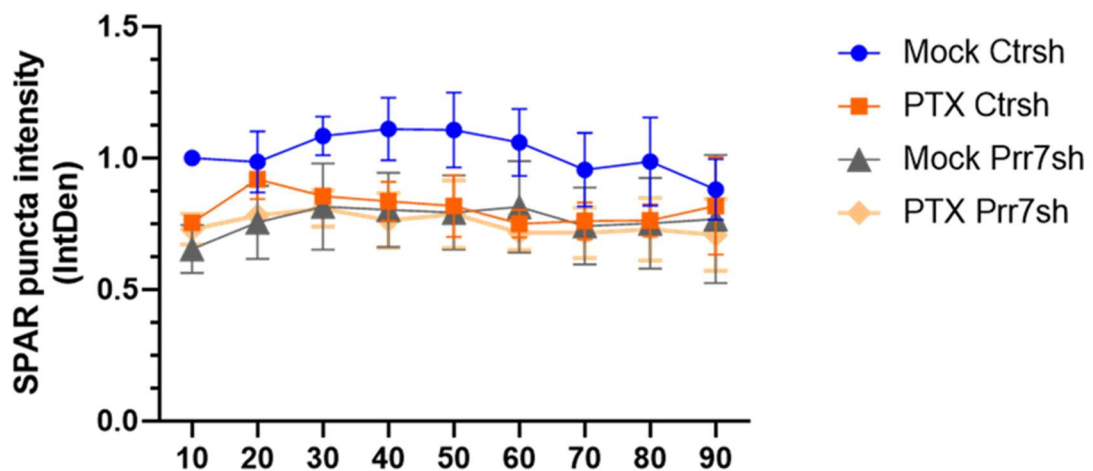


**Figure 5** SPAR/CDK5 pathway is downstream of miR-329/495/Prr7 regulation in HSD. (a-b) SPAR protein levels relative to Tubulin in rat cortical neurons nucleofected with control or Prr7 shRNA (2 $\mu\text{g}$ ) on day of dissociation (E18) and harvested for protein extraction 5 days later, with representative western blot (all replicate blots are shown in Supplemental Data). Data = mean  $\pm$  S.D., n=3, \* p=0.0462, paired Student's t-test. (c) Average SPAR punctum intensity in dendrite selection in rat hippocampal cells transfected with GFP (150ng), control or Prr7 shRNA (7.5ng pSUPER) at DIV13, treated with either EtOH (1:500 volume) or 100 $\mu\text{M}$  PTX at DIV19 for 48h, then immunostained for SPAR. Data = mean  $\pm$  S.D., where each point

represents grand average in dendrites for the 7-10 cells imaged in a single experiment.  $n=3$ , 2-way ANOVA with Tukey's HSD post-hoc test. Ctr EtOH vs. Prr7 EtOH: \*  $p=0.0429$ ; Ctr EtOH vs. Ctr PTX: \*  $p=0.0462$ ; Ctr PTX vs. Prr7 PTX: ns  $p=0.6932$ . **(d)** Representative dendrite images showing SPAR expression (grey-scale, top panels) and merged SPAR (red), GFP (green), Map2 (blue) signals (bottom panels) in Ctr or Prr7 shRNA-transfected hippocampal neurons treated with 48h EtOH or PTX. **(e)** Average dendrite SPAR punctum intensity in rat hippocampal cells transfected with GFP (150ng) and either control or Prr7 shRNA (7.5ng) at DIV13, treated with either DMSO (1:1000 volume) or Roscovitine (10 $\mu$ M) at DIV19 for 18h, then immunostained for SPAR. Data = mean  $\pm$  S.D., where each point represents grand average in dendrites for the 8-12 cells imaged in a single experiment.  $n=3$ . Ctr DMSO vs. Prr7 DMSO: \*  $p=0.0266$ ; Ctr Ros vs. Prr7 Ros: ns  $p=0.2328$ . **(f)** Spine densities for these same cells were measured. Ctr DMSO vs. Prr7 DMSO: \*\*  $p=0.0064$ ; Ctr Ros vs. Prr7 Ros: ns  $p=0.4288$ . For these Roscovitine data, data = mean  $\pm$  S.D., 2-way ANOVA with Tukey's HSD post-hoc test. **(g)** Representative dendrite images showing SPAR expression (grey-scale, top panels) and merged SPAR (red) and GFP (green) signals (bottom panels) in Ctr or Prr7 shRNA-transfected hippocampal neurons treated with 18h DMSO or Roscovitine. Scale bars = 5 $\mu$ m. Whole cell images from which dendrite segments were taken are shown in Supplemental Data.



**Supplemental Figure 11 Segmentation analysis of cells transfected with Control or Prr7 shRNA, treated with EtOH or PTX, and immunostained for SPAR.** The same cells as those analyzed for dendrite SPAR levels in Figure 5c were re-visited to measure SPAR immunofluorescence with respect to distance from the soma. Through an automated method, concentric circles increasing in 10 $\mu$ m steps were drawn around the soma, and dendritic segments within each increasing step were selected using GFP as a mask. Subsequently the average SPAR puncta intensity in the detected dendritic segments (as measured by integrated density) were obtained, and a grand average across the 7-10 cells imaged per condition was calculated for one experiment. Shown is the mean SPAR immunofluorescence data across 3 independent experiments, normalized to the Mock 10 $\mu$ m point,  $\pm$  SEM.

## Discussion

### Summary

Our study demonstrates the requirement of miR-329 and miR-495-mediated downregulation of Prr7 underlying dendritic spine elimination in HSD. From our results, we present the following model (Fig. 6). Under basal conditions, Prr7 mRNA is actively translated, as the targeting of the Prr7 3' UTR by miRNAs is inhibited by a yet unknown mechanism. Prr7 protein is required for the stabilization of SPAR through inhibiting the activity of CDK5, thereby maintaining the integrity of the post-synaptic density, including the stabilization of GluA1-containing AMPARs at the surface.

In contrast, following chronic activity, miR-329 and miR-495 are activated, and miR-495 expression is increased in dendrites. These miRNAs repress translation of Prr7 mRNA. In the absence of Prr7 protein, CDK5 phosphorylates SPAR, leading to an association between SPAR and Plk2, and subsequent

proteasomal SPAR degradation. The loss of SPAR results in the destabilization of PSD-95 complexes and GluA1 degradation, ultimately resulting in spine elimination.

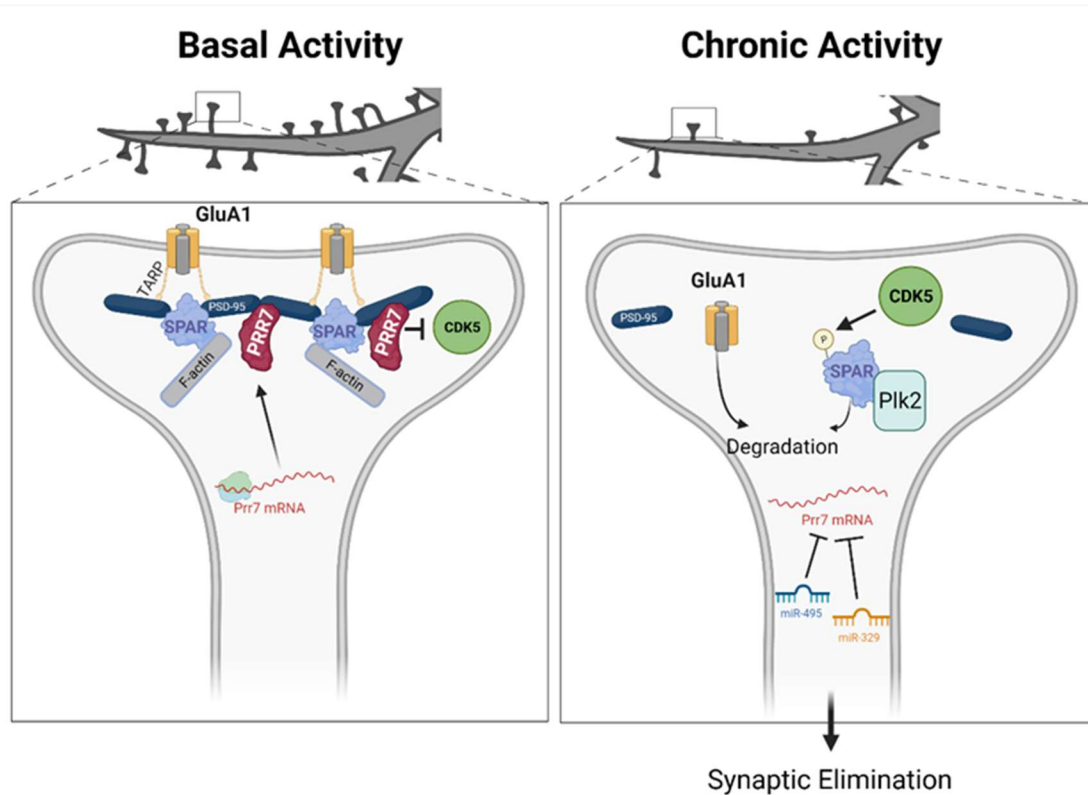


**Figure 6 Model of miRNA-mediated Prr7 downregulation and downstream effects on SPAR during HSD. Left panel:** under basal conditions, Prr7 mRNA is actively translated, as the miR-329 and miR-495 activity are inhibited (by a yet unknown mechanism). Prr7 protein stabilizes SPAR through inhibiting CDK5 activity and preventing SPAR phosphorylation. Thereby, the integrity of the post-synaptic density is maintained. **Right panel:** following chronic activity, miR-329 and miR-495 are activated, and miR-495 expression specifically is increased in dendrites. These miRNAs inhibit Prr7 mRNA, and thus Prr7 protein is lost. CDK5 phosphorylates SPAR, leading to targeting of SPAR by Plk2, and subsequent proteasomal degradation. As a result of SPAR loss, PSD-95 complexes are destabilized and GluA1 is degraded, leading to elimination of mature spines. (Figure generated with BioRender).

### *Role of Prr7 in synaptogenesis and plasticity*

Through Prr7 knockdown studies, we have revealed that Prr7 reduction leads to a decrease in spine number (Fig. 2a) as well as GluA1 protein levels (Fig. 2h-k), recapitulating two hallmarks of HSD. Although Prr7 was not found to associate with AMPARs in a previous study through immunoprecipitations (Kravchick et al., 2016), it is still possible that Prr7 influences AMPAR dynamics indirectly through interaction with other PSD components, e.g. the AMPAR auxiliary subunit Stargazin, which binds to both AMPARs and PSD-95 (Bats et al., 2007). Nevertheless, the current results are in agreement with the previously presented idea that Prr7 reduction serves a neuroprotective function against over-excitation (Kravchick et al., 2016), as well as Prr7 forms part of the post synaptic density core to promote neuronal maturation (Murata et al., 2005). The direct and indirect protein interactions

involving Prr7, and Prr7-associated complexes formed under basal vs. stimulated conditions need further clarification.

Our results using sparse transfection of hippocampal neuron cultures clearly indicate a cell-autonomous, postsynaptic function of Prr7. In contrast, a non-cell autonomous function of Prr7 through exosomal secretion and Wnt inhibition has previously been reported (Lee et al., 2018). In this study, treatment of exosomal Prr7-rich supernatant in hippocampal cultures led to a reduction of glutamatergic synapses, which is contrary to our observations. The differences in incubation time between treatment and imaging (fixation 18h vs. 8 days post-transfection) may account for this discrepancy. Namely, it is possible that upon acute (18h) Prr7 overexpression, spines are eliminated due to a rapid exosomal Prr7 secretion from the soma. In contrast, over a time scale of days, Prr7 might accumulate in the synapto-dendritic compartment where it promotes synaptogenesis to compensate for the initial spine loss. In addition, the observed increase in excitatory synapses upon Prr7 knockdown in Lee et al., was solely based on PSD-95 puncta number, and effects on spines were not addressed.

We further elucidated a mechanism in which CDK5/SPAR is controlled downstream of Prr7 activity (Fig. 5a-g). It is interesting to consider this new pathway linking miR-329/495/Prr7 to SPAR in relation to a study describing miR-134-dependent SPAR regulation via Pum2 downregulation and Plk2 function (Fiore et al., 2014). It is known that upon chronic activity Plk2 is activated, and there is a bifurcation into two downstream branches (Seeburg and Sheng, 2008; Seeburg et al., 2008; Evers et al., 2010): 1) activated Plk2 phosphorylates SPAR, leading to GluA1/GluA2 internalization, and 2) activated Plk2 phosphorylates the GluA2-interacting protein NSF, promoting specifically GluA2 internalization. Intriguingly, in Fiore et al. it was found that the miR-134 pathway only affected GluA2 levels, and therefore it was suggested to connect only to the second branch. Considering Prr7 knockdown affected GluA1 expression (Fig. 2h-i), it would be plausible that conversely miR-329/495/Prr7 feeds into specifically the first branch via influencing CDK5.

#### *Role of miRNAs in local activity-dependent regulation of Prr7 during HSD*

We have demonstrated that Prr7 expression at both RNA and protein levels is consistently reduced in the dendritic compartment in response to chronic activity (Fig 1b, e, g). The decrease in Prr7 mRNA in dendrites of PTX-treated neurons was also observed from RNA-seq analyses (Colameo et al., 2021). These observations support the idea that there is local regulation of Prr7 in the synapto-dendritic compartment during HSD. In this regard, local homeostatic mechanisms at the level of individual dendritic domains (Ju et al., 2004; Sutton et al., 2006) and at individual synapses (Hou et al., 2008) have been previously demonstrated. The exact mechanism by which local downregulation of Prr7 occurs is yet to be uncovered and will need the employment of techniques that allow the visualization of newly synthesized proteins. These include for example puromycin labeling with proximity ligation assay

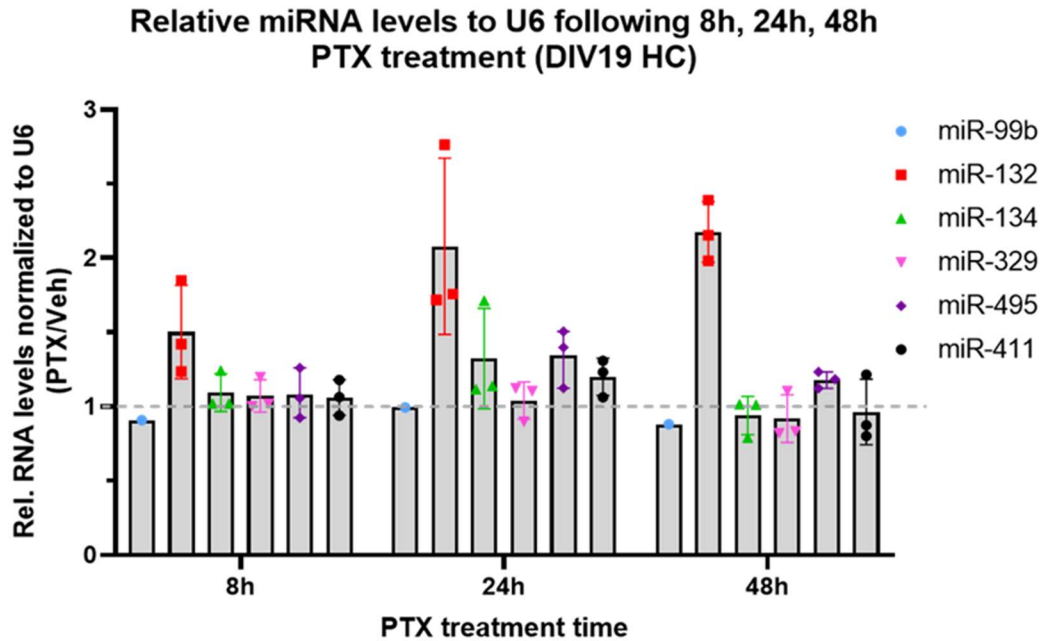
(puro-PLA) (tom Dieck et al., 2015) or single-molecule imaging of nascent peptides combined with single-molecule FISH, as performed in hippocampal dendrites (Wu et al., 2016).

We have shown that miR-329 and miR-495 activity and subsequent targeting of the Prr7 3' UTR are required for Prr7 reduction in dendrites during HSD. Our findings from pLNA experiments are most consistent with an additive repressive effect of these two miRNAs on Prr7 mRNA translation. Such additive effects of multiple miRNAs binding to the same target have been demonstrated previously, for example with N-cadherin (Rago et al., 2014).

The activity-dependency of the miRNA-Prr7 interaction is evidenced by the induction of sensor activity for both miRNAs upon PTX treatment (Fig. 3h), as well as the pLNAs showing effects exclusively under stimulated conditions. However, the mechanisms leading to miR-329 and miR-495 induction appear to be different. In the case of miR-495, mature levels increase, pointing to a PTX-dependent regulation of miR-495 expression (Fig. 3i; Supplemental Fig. 10). Since this increase is preferentially observed in dendrites, it might involve increased local miRNA processing, miR-495 transport into dendrites and/or the local inhibition of miRNA degradation.

With respect to miR-329, the lack of a clear induction in mature miRNA levels suggests mechanisms at the level of the miR-329 RISC, e.g. interference of miR-329 RISC binding to the Prr7 3'UTR by an RNA-binding protein which is removed upon PTX treatment. Examples for activity-dependent miRNA-RBP interplay have been previously reported (Rajman et al., 2017; Edbauer et al., 2010; Tominaga et al., 2011; Kedde et al., 2007).

Additionally, the understanding that miR-134, miR-329 and miR-495 activity all lead to SPAR downregulation in HSD is intriguing, given that these three miRNAs are derived from the same genomic region, termed the miR-379-410 cluster located within the imprinted DLK1-DIO3 region on chromosome 14q32 in humans (da Rocha et al., 2008). Another cluster member, miR-485, also plays a role in homeostatic plasticity through expression regulation of presynaptic synaptic vesicle protein (SV2A) (Cohen et al., 2011). This shared origin of cluster miRNAs not only further support the functional significance of miR-379-410 members in activity-dependent synaptic plasticity mechanisms as previously described (Fiore et al., 2009), but also would point toward an interesting idea that individual cluster members act in distinct yet converging pathways in HSD.



**Supplemental Figure 10 Whole Cell expression levels of mature miRNAs of interest in 8, 24, 48h PTX-treated hippocampal cells.** Hippocampal neurons were treated with 100 $\mu$ M PTX or equivalent volume of ethanol at DIV17 for 48h time point for three wells respectively, then at the same time of day on DIV18, these treatments were repeated for another three wells for the 24h time point. In the morning of DIV19, the 8h time point treatments were added, and in the evening of DIV19, cells were lysed and assessed by qPCR for mature miRNA levels. miR-99b and miR-132 were used as negative and positive controls respectively. Data = mean normalized to EtOH condition  $\pm$  S.D., n = 3.

*(Patho)physiological impact of the miR329/495/Prr7 pathway*

A previous study (Lackinger et al., 2019) revealed that mice with a constitutive functional deletion of miR-379-410 exhibited heightened sociability and anxiety, along with increased excitatory transmission in hippocampal excitatory neurons, as well as upregulation of Prr7. These findings not only are consistent with the proposed role of Prr7 in excitatory synaptogenesis, but also point toward the connection of miRNA/Prr7 interactions to social or anxiety behavior. In other words, our current results would prompt behavioral studies examining miR-329/495/Prr7 excitatory synapse regulation in vivo. Prr7 knockout mice have been generated in previous studies with no lethal effects in the context of immune regulation (Hrdinka et al., 2016), making the study of hippocampal excitatory transmission and behavior in these mice in the context of miRNA manipulation possible.

Together with the reported involvement of Prr7 in apoptosis (Kravchick et al., 2016), our results may also suggest the importance of miRNA-dependent Prr7 downregulation in synaptic homeostasis and neuronal survival in the face of excitotoxic insult. Namely, Prr7 knockdown was shown to attenuate the excitotoxic response in hippocampal neurons following NMDAR stimulation by glutamate in a c-Jun dependent manner (Kravchick et al., 2016). Consistent with this idea, we have shown that Prr7 reduction is necessary for excitatory synapse depression upon chronic stimulation. Given our findings of miR-329 and -495-mediated Prr7 inhibition by PTX, it would therefore be reasonable to ask if these same miRNAs are activated upon glutamate stimulation, and if such activation may have neuroprotective

effects against excitotoxicity. Taken together, a possible model emerges in which excessive NMDAR stimulation activates miRNAs that target Prr7, thereby reducing synapse-localized Prr7, as well as preventing Prr7 translocation to the nucleus. Consequently, the absence of dendritic Prr7 leads to spine elimination via SPAR degradation for the purpose of homeostasis, while the inhibition of nuclear Prr7 accumulation leads to c-Jun degradation for the purpose of neuronal survival.

More broadly, this idea may be tested in an *in vivo* context with possible future applications toward neuroprotection following status epilepticus or ischemic stroke, as NMDAR overstimulation is implicated in these conditions (McDonough and Shih, 1997). Additionally, dendritic spine loss has been observed in epilepsy (Swann et al., 2000) and after stroke (Brown et al., 2007), which could indeed suggest the initiation of HSD (in addition to other neuroprotective mechanisms) to counter excitotoxicity. The therapeutic effect of miR-329/-495 administration, or Prr7 inhibition in the context of these conditions is yet to be uncovered.

## **Materials and methods**

### *DNA constructs*

All primer sequences used for cloning are indicated in Supplemental Methods.

miR-30a-chimeric hairpins for miR-329 and miR-495 stable overexpression were generated via polynucleotide cloning into the 3' UTR of eGFP in pAAV-hSyn-EGFP vector (Addgene Plasmid #114213) using BsrGI and HindIII sites, as described previously (Christensen et al., 2010).

Control and Prr7 shRNA vectors were constructed using the pSUPER RNAi System (OligoEngine). Custom primers were designed for polynucleotide cloning into the pSUPER basic vector (VEC-PBS-0001/0002) using BglII/HindIII sites, to generate an shRNA targeting a 19-nucleotide sequence unique to rat Prr7 coding region (cggaatcggacatgtctaa).

For the Prr7 expression construct, full-length rat Prr7 coding sequence (NM\_001109116.1) was amplified from hippocampal rat cDNA, then subcloned into the CMV-pcDNA3 vector using BamHI/XbaI sites. Subsequently, a start codon (atg) with HA-tag (tacccatcagcagctcccagactacgct) was inserted at the HindIII site upstream of Prr7 by polynucleotide cloning. To generate the shRNA-resistant construct, 6 point mutations in the Prr7 coding region were introduced, such that Prr7 shRNA could no longer recognize the mRNA product, yet the amino acid sequence of the resultant exogenous Prr7 protein (AESDMSK) would remain unchanged. Mutagenesis was performed using Phusion-site directed mutagenesis kit (Thermo Fisher).

Bi-cistronic reporter constructs for miRNA activity were described previously (Fiore et al., 2009). Two perfectly complementary binding sites for either miR-329 and miR-495, separated by a 2-nucleotide

linker, were inserted into the dsRED 3' UTR of the pTracer-CMV-dsRED vector, using XbaI/NotI sites by polynucleotide cloning.

Wild type and mutant Prr7 3' UTR luciferase constructs were described and generated previously (Lackinger et al., 2018), wherein the 3' UTR of Prr7 (NM\_0010302964) was amplified from mouse DNA and cloned into the pmiRGLO dual-luciferase expression vector (Promega). Mutations in miRNA binding sites conserved across mammals were introduced by site-directed mutagenesis using Pfu Plus! DNA Polymerase (Roboklon).

### *Cell culture*

Primary cortical and hippocampal neuronal cultures were prepared from embryonic day 18 (E18) male and female Sprague-Dawley rats (Janvier Laboratories) as previously described (Schratt et al., 2006). Dissociated cortical neurons were directly seeded on 6-well plates coated with poly-L-ornithine (used for nucleofections), whereas hippocampal neurons were seeded on poly-L-lysine/laminin-coated coverslips in 24-well plates.

For compartmentalized cell cultures, dissociated hippocampal cells were plated onto 1- $\mu$ m pore and 30-mm diameter polyethylene tetra-phthalate (PET) membrane filter inserts (Millipore) that were matrix-coated with poly-L-lysine (Sigma-Aldrich) and Laminin (BD Biosciences) on the top and bottom, also as described previously (Bicker et al., 2013; Poon et al., 2006). All neuron cultures were maintained in Neurobasal media supplemented with 2% B27, 2mM GlutaMax, 100  $\mu$ g/ml streptomycin and 100U/ml penicillin (Gibco, Invitrogen) in an incubator with 5% CO<sub>2</sub> at 37 °C.

HEK293T cells (Sigma) were maintained in 6 cm dishes in DMEM media containing 10% fetal bovine serum, 1mM glutamine, 100U/ml penicillin, and 100  $\mu$ g/ml streptomycin ("HEK media") in an incubator with 5% CO<sub>2</sub> at 37 °C.

### *Transfections and Nucleofections*

All transfections of hippocampal cells were performed using Lipofectamine 2000 (Invitrogen), in triplicate wells on DIV13. 1  $\mu$ g of total DNA was transfected per well in a 24-well plate, where an empty pcDNA3 vector was used to make up the total amount of DNA. Neurons were transfected in culture media in the absence of streptomycin and penicillin for 2h, replaced with neuron culture media containing ApV (1:1000) for 45min, which was washed out and replaced with conditioning media.

Nucleofections were done on cortical neurons using the P3 Primary Cell 4D-Nucleofector X Kit (Lonza, LZ-V4XP-3024), on the day of preparation and dissociation (DIV 0). 4 million dissociated cortical cells were electroporated with 3  $\mu$ g total DNA per condition using the program DC-104, seeded in 6-well plates in DMEM/Glutamax supplemented with 5% FBS and incubated for 4h, then replaced with neuron

culture media and incubated at 37°C until harvesting. The following amounts of DNA were used for the relevant nucleofections: 2µg chimeric miR30a-miR329 and 495 hairpins for miRNA overexpression validation; 2µg pSUPER and 1µg GFP for protein quantifications upon Prr7 knockdown; 2µg HA-Prr7 and 1µg GFP for validation of Prr7 overexpression.

HEK293T cells were transfected in HEK media supplemented with HEPES (25mM) at 1.9 million cells seeded in 6cm dishes per condition, by combining DNA with polyethylenimine (PEI) and Optimem for 15min, then adding the mixture dropwise onto cells. Cells were incubated at 37°C for 2 days until harvesting. For HA-Prr7 validation, cells were transfected with 2µg pcDNA, HA-Cav1.2, or HA-Prr7, and 1µg GFP. For shRNA-resistant mutant validation, cells were transfected with 100ng HA-Prr7 constructs, 1µg pSUPER, and 1µg GFP.

### *Stimulation*

To examine downscaling processes, DIV18 or DIV19 hippocampal cells were stimulated with either picrotoxin (100µM, Sigma) or equivalent volume (1:500) of ethanol absolute for 48h. For the PTX time course experiment, the picrotoxin or ethanol treatment was added in triplicate wells at DIV17 for “48h” time point, on DIV18 for “24h”, on DIV19 for “8h”, and all cells lysed together for RNA extraction 8h following the final treatment.

For investigating CDK5 inhibition, DIV19 hippocampal cells were stimulated with either Roscovitine (10µM, Sigma R7772) or equivalent volume (1:1000) of DMSO for 18h.

### *Luciferase reporter assay*

DIV13 primary rat hippocampal neurons were transfected in triplicate with 20pmol pLNAs (10pmol for 329/495 mix) and 50ng Prr7 3' UTR pmiRGLO constructs per well. Cells were treated with PTX or ethanol on DIV18 or DIV19 for 48h, then lysed in Passive Lysis Buffer (diluted to 1x, Promega) for 15min, and dual-luciferase assay performed using homemade reagents (as described in Baker et al., 2014) on the GloMax Discover GM3000 (Promega).

pLNAs used were: Control pLNA (miRCURY LNA miRNA Power Inhibitor Negative control A, Qiagen #339135 YI00199006-DCA), miR-329 pLNA (miRCURY LNA miRNA Power Inhibitor RNO-MIR-329-3P, Qiagen # 339130 YI04101481-DCA), miR-495 pLNA (miRCURY LNA miRNA Power Inhibitor HSA-MIR-495-3P, Qiagen #339130 YI04101229-DCA).

### *Bicistronic reporter (dual color) assay/single cell fluorescent sensor assay*

For single cell fluorescent assay, DIV13 or DIV14 hippocampal cells were transfected in triplicate wells with 125ng of control, miR-329, or miR495 bicistronic sensor, and 5pmol control, miR-329, or miR-

495 pLNA (where applicable). On DIV19, cells were treated with PTX or ethanol for 48h, then fixed for 15min in 4% paraformaldehyde/4% sucrose/PBS, washed in PBS and directly mounted onto slides for imaging. To determine miRNA activity, dsRED-positive (red or yellow) vs. GFP-only (green) cells were manually counted at 20x objective with both 488 and 561 channels open for all coverslips, and the proportion of GFP-only cells over the total count was taken. Approximately 100-200 cells were counted per coverslip (300-600 total per experimental condition).

#### *Immunocytochemistry, spine density and image analysis*

For all imaging experiments, hippocampal cells were transfected on DIV13 in either duplicate or triplicate wells. The following amounts of DNA/RNA were used for the relevant experiments: 150ng GFP-amp, 20pmol pLNAs (10pmol for 329/495 mix), 500ng miR30a- hairpins, 7.5ng pSUPER constructs (with the exception of spine rescue experiment with pLNAs, for which 2.5ng was used), 400ng HA-Prr7 or HA-Prr7R. Where applicable, the transfected cells were further treated on DIV19 with picrotoxin/ethanol or roscovitine/DMSO.

For all experiments, cells were fixed for 15min with 4% paraformaldehyde/4% sucrose/PBS and washed with PBS. In cases where cells were only analyzed for spine morphology, coverslips were directly mounted onto microscope slides.

For immunostaining, following fixation coverslips were transferred to a humidified chamber protected from light. For Prr7 and whole cell GluA1 immunostaining, cells were permeabilized with 0.1% Triton/PBS for 5min. For Prr7 immunostaining, blocking for 30min in 1xGDB buffer (0.02% gelatin/0.5% Triton X-100/PBS) was followed by overnight incubation with primary antibody in GDB at 4°C. Secondary antibodies in GDB were applied for 45min. For whole cell GluA1 staining, blocking was performed for 10min in 0.1% Triton/10% NGS/PBS solution, then coverslips were incubated overnight with primary antibody in Triton/NGS/PBS solution at 4°C. Coverslips were washed with PBS before and after fixation, and application of each antibody, and briefly in MilliQ before slide mounting. For GluA1 surface staining, cells were treated with primary antibody at 37°C for 3h. After washing the cells four times with fresh cell media, cells were fixed for 15min with 4% paraformaldehyde/4% sucrose/PBS and washed with PBS. Coverslips were then transferred to a humidified chamber at room temperature, incubated in secondary antibody in GDB for 1h, washed with PBS, rinsed briefly with MilliQ water, and mounted onto glass slides for imaging. The following primary antibodies were used: Rabbit polyclonal anti-Prr7 (200ng/ml, PA5-61266, Invitrogen), Chicken monoclonal anti-Map2 (1:5000 dilution, PA1-16751, Thermo Fisher), rabbit polyclonal anti-SPAR (1:1500 dilution, kind gift of D.T. Pak), and rabbit polyclonal anti-GluA1 (PC246 Calbiochem EMD Biosciences, or ABN241 Sigma-Aldrich at final concentrations 1µg/ml for whole cell staining, 2µg/ml for surface staining). Alexa-546 and -647-conjugated secondary antibodies (1:2000 dilution) were used for detection.

All images were acquired with confocal laser-scanning microscope (Zeiss LSM) using a 40x/1.3 oil DIC UV-IR M27 objective. Z-stack images were obtained for 7-11 GFP-positive neurons with pyramidal morphology for each condition. Settings were: Opt sampling (1.0x Nyquist), Zoom factor 1.0, Pixel Dwell 0.90 $\mu$ s, Speed fps 0.23, Scan time 4.32s, Speed 6, Digital Gain 1.0, Pinhole 384 $\mu$ m. Z stacks were kept at 0.45 $\mu$ m and 9-11 slices obtained. Laser settings were kept constant between conditions. Images were processed by Airyscan processing at 6.0 strength 3D, and maximum intensity projections of the Z-stacks were used for signal quantification.

Prr7 and SPAR puncta intensities were analyzed with a custom-made Python-script developed by D. Colameo and can be added as a Plugin on Fiji (<https://github.com/dcolam/Cluster-Analysis-Plugin>). Whole cell, cell body, and dendrites (whole cell selection with cell body subtracted) were defined using GFP as a mask.

Spine density was measured manually using Fiji. For each cell analyzed, first a primary dendrite and one secondary dendrite branching off it was selected, and the total length of the selected segment obtained. Using the “cell counter” tool, the total spine number along the selected segment was counted (without discrimination of spine shape), and the count was divided by the total length to obtain #spines/ $\mu$ m. A second dendritic segment was selected, and the process repeated. The average of the two spine density readings was calculated per cell.

#### *Preparation of protein extracts and western blotting*

Protein extracts were prepared by first scraping and lysing cells in RIPA buffer (150mM NaCl, 1% Triton X-100, 0.5% Sodium Deoxycholate, 1mM EDTA, 1mM EGTA, 0.05% SDS, 50mM Tris pH 8.0, 1x complete protease inhibitor cocktail (Roche)), spinning down the lysate at maximum speed at 4°C for 15min, and collecting the supernatant. Protein concentration was measured using the Pierce BCA Protein Assay Kit (Thermo Fisher). Equal amounts of protein were diluted in Laemmli sample buffer supplemented with BME, boiled at 95°C for 5min and loaded onto SDS-PAGE gels (10% polyacrylamide for Prr7 probe, 8% for SPAR). For Prr7 western, proteins were transferred onto Trans-Blot Turbo 0.2 $\mu$ m nitrocellulose membranes (Biorad) using the Trans-Blot Turbo semi-dry transfer system (Biorad). For SPAR western, proteins were blotted onto 0.45 $\mu$ m PVDF membranes (Immobilon) soaked in transfer buffer (25mM Tris-HCl pH 8.3, 192mM Glycine, 20% MeOH) via wet transfer for 15-16h at 25V. For all experiments, blocking was done in 5% milk in 1xTBS-0.1% Tween20 (TBST) for 1.5-2h at room temperature, followed by overnight primary antibody incubation at 4°C. Following washes in milk, horse radish peroxidase (HRP)-conjugated secondary antibodies were applied onto the membranes for 1h at room temperature. Membranes were washed in TBST and visualized with the Clarity Western ECL Substrate (Biorad) on the ChemiDoc Imaging System (Biorad). The following primary antibodies were used: Rabbit anti-GluA1 (1:1000 dilution, PA1 37776, Thermo Fisher), Mouse monoclonal anti-Prr7 (1:250 dilution, MA1-10448, Thermo Fisher), Rabbit monoclonal anti-alpha

Tubulin (1:2000 dilution, 11H10 lot 112125S, Cell signaling). HRP-conjugated secondary antibodies Rabbit anti-Ms IgG H&L (402335 lot D00160409, Calbiochem), Goat anti-Rb IgG H&L (lot 2625715, Calbiochem) were used at 1:20,000 dilution.

#### *RNA extraction and Quantitative real-time PCR*

RNA was isolated using TriFast RNA extraction kit (30-2030, VWR) or RNA-Solv reagent (Omega Bio-tek). Genomic DNA was removed with TURBO DNase enzyme (Thermo Fisher). Reverse transcription was performed using either the Taqman MicroRNA Reverse Transcription Kit (Thermo Fisher) for miRNA detection, or iScript cDNA synthesis kit (Biorad) for mRNA detection. qPCR was performed using either Taqman Universal PCR Master Mix (Thermo Fisher) for microRNA detection, or the iTaq SYBR Green Supermix with ROX (Biorad), and plates were read on the CFX384 Real-Time System (Biorad). Data was analyzed via  $\Delta\Delta C_t$  method, and normalized to either U6 (for miRNAs) or GAPDH (for mRNAs). mRNA primer information is indicated in supplemental methods.

Taqman primers used were (all from Thermo Fisher): U6 snRNA (Assay ID: 001973), mmu-miR-495 (4427975, Assay ID: 001663), mmu-miR-329 (4427975, Assay ID: 00192), mmu-miR-134 (4427975, Assay ID: 001186), hsa-miR-132 (4427975, Assay ID: 000457), hsa-miR-99b-5p (4427975, Assay ID: 000436).

#### *Statistics*

Statistical tests were performed using GraphPad Prism version 9.2.0. For all datasets, three to four independent experiments were performed. Given the small sample size, normality was assumed for all datasets, and therefore one or two sample Student's t-test (two-sided), or one-way or two-way ANOVA followed by post-hoc Tukey test were performed. \*  $P < 0.05$ ; \*\*  $P < 0.01$ ; \*\*\*  $P < 0.001$ .

#### **Acknowledgements**

We would like to thank D. T. Pak and M. Sheng for generously providing the SPAR antibody. We thank M. Soutschek, R. Fiore, S. Bicker, C. Gilardi for cloning the pmiRGLO, miR-329/control sensors, Control pSUPER, and miR30a-Ctr hairpin constructs respectively. We thank the excellent technical assistance of T. Wüst and Cristina Furler. This work was supported by a grant from the Swiss National Foundation (SNF 310030\_205064) to G.S.

#### **Conflict of Interest**

The authors declare no competing interests.

## Author Contributions

MOI performed all experiments and analyses except for compartmentalized cell culture (plasmid cloning, transfections, luciferase assays, immunocytochemistry, western blotting, imaging, RT-qPCR), and wrote the manuscript. DC performed compartmentalized RNA/protein extractions and wrote the Python script for puncta analysis. IA contributed qPCR data. GS conceptualized and supervised the project, and wrote the manuscript.

## Supplemental Methods

### *Primer sequences (all 5' to 3')*

miR-329 hairpin:

Oligo A-329-BsrGI for: GTACAGCTGTTGACAGTGAGCGACAACACACCC

Oligo A-329-BsrGI rev: AGGTTAGCTGGGTGTGTTGTCGCTCACTGTCAACAGCT

Oligo B-329 for: AGCTAACCTTTTTTGTGAAGCCACAGATGGAAAAAGGT

Oligo B-329 rev: CCCAGAACCTTTTTCCATCTGTGGCTTCACAAAAA

Oligo C-329-HindIII for: TCTGGGTGTGTTGCTGCCTACTGCCTCGGAA

Oligo C-329-HindIII rev: AGCTTTCCGAGGCAGTAGGCAGCAACACA

miR-495 hairpin:

Oligo A-495-BsrGI for: GTACAGCTGTTGACAGTGAGCGACAAACAAACA

Oligo A-495-BsrGI rev: AGTGCACCATGTTTGTGTTGTCGCTCACTGTCAACAGCT

Oligo B-495 for: TGGTGCACCTTCTTTGTGAAGCCACAGATGGAAGAAGTG

Oligo B-495 rev: ACATGGCACTTCTTCCATCTGTGGCTTCACAAAGA

Oligo C-495-HindIII for: CCATGTTTGTGTTGCTGCCTACTGCCTCGGAA

Oligo C-495-HindIII rev: AGCTTTCCGAGGCAGTAGGCAGCAAACAA

Control hairpin:

Oligo A-Ctr-BsrGI for: TGTACAGCTGTTGACAGTGAGCGACAACCTTGTG

Oligo A-Ctr-BsrGI rev: AAGGACCACAAGGTTGTCGCTCACTGTCAACAGC

Oligo B-Ctr for: GTCCTTAGGTGCGTGTGAAGCCACAGATGGCGC

Oligo B-Ctr rev: GGTTTAGGTGCGCCATCTGTGGCTTCACACGCACCT

Oligo C-Ctr-HindIII for: ACCTAAACCACAAGGTTGCTGCCTACTGCCTCGGA

Oligo C-Ctr-HindIII rev: AAGCTTTCCGAGGCAGTAGGCAGCAACCTTG

pSUPER:

Prr7 shRNA targeting rat (and mouse) Prr7 coding region cggaatcggacatgtctaa:

siPrr7\_for 1: GATCCCC CGG AAU CGG ACA UGU CUA A TTCAAGAGA

siPrr7\_rev 1: AGCTTAAAAA CGG AAU CGG ACA UGU CUA A TCTCTTGAA

siPrr7\_for 2: UUA GAC AUG UCC GAU UCC G TTTTTA

siPrr7\_rev 2: UUA GAC AUG UCC GAU UCC G GGG

Control shRNA:

siCtr\_for1: GATCCCCAAACCTTGTGGTCCTTAGGTTCAAGAGA

siCtr\_rev1: AGCTTAAAAAAAACCTTGTGGTCCTTAGGTCTCTTGAA

siCtr\_for2: CCTAAGGACCACAAGGTTTTTTTTTA

siCtr\_rev2: CCTAAGGACCACAAGGTTTGGG

HA-Prr7:

Amplification of rat Prr7 coding sequence with BamHI and XbaI sites:

For: TATAGGATCCGTGATGTCCCAGGGCA

Rev: TCACTCTAGACTATACGGCTGTAGTCCTCCC

Start codon and HA-tag insertion using HindIII site:

For: AGCTT ATG TACCCATACGACGTCCCAGACTACGCT A

Rev: AGCTT AGCGTAGTCTGGGACGTCGTATGGGTA CAT A

shRNA-resistant HA-Prr7:

For: CGG CCC TGG AGC TAT CCG CGC CAA gCC GAG TCA GAT ATG AGT AA<sub>g</sub> CCG CCG  
TGC TAC GAG GAG GCG GTG

Rev: CAC CGC CTC CTC GTA GCA CGG CGG cTT ACT CAT ATC TGA CTC GG<sub>c</sub> TTG GCG  
CGG ATA GCT CCA GGG CCG

miRNA sensor:

miR-495 mature sequence: AAACAAACAUGGUGCACUUCUU

miR-495 for: GGCCGC aagaagtgcaccatgtttgttt ca aagaagtgcaccatgtttgttt T

miR-495 rev: CTAGA aaacaacatggtgcacttctt tg aaacaacatggtgcacttctt GC

(used in Fiore et al., 2009)

miR-329 mature sequence: aacacaccagcuaaccuuuuu

miR-329 for : ggccgc-aaaaaggttagctgggtgtgtt-AC-aaaaaggttagctgggtgtgtt-T

miR-329 rev : ctaga-aacacaccagctaacctttt-GT-aacacaccagctaacctttt-gc

miR-Ctr for :

GGCCGCAAGGGATTCTGATGTTGGTCACACTACAAGGGATTCTGATGTTGGTCACACTT

miR-Ctr rev :

CTAGAAGTGTGACCAACATCAGAATCCCTTGTAGTGTGACCAACATCAGAATCCCTTGC

(used in Lackinger et al., 2018)

Prr7 3' UTR luciferase reporter

Prr7 3' UTR for: AA ACTCGAGAGGACTACAGCCGTATAGAGG

Prr7 3' UTR rev: TTTGTGACGTACCAAAGCAGATCACACACC

Prr7 3' UTR mutagenesis was performed for each miRNA binding site sequentially.

Prr7 3' UTR mut1 for: TACCCTGTTGAATTCATTTTGAGGATAATAAAGG

Prr7 3' UTR mut1 rev: TCCTCAAAATGAATTCAACAGGGTAAGAAATCC

Prr7 3' UTR mut2 for: ATAATAAAGGTCTAGAATCTGCTTTGGTACGtCG

Prr7 3' UTR mut2 rev: ACCAAAGCAGATTCTAGACCTTTATTATCCTCAAAATG

*qPCR primers*

GAPDH for: GCCTTCTCTTGTGACAAAGTGGA

GAPDH rev: CCGTGGGTAGAGTCATACTGGAA

Prr7 for: GTCACGCCCTTTCTGAGC

Prr7 rev: ATGCAGCGCCGAGGTATA

GluA1 for: CGAGTTCTGCTACAAATCCCG

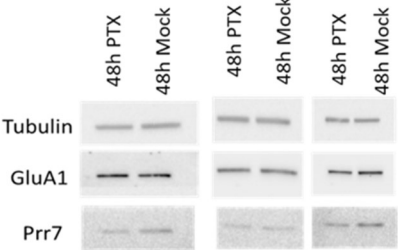
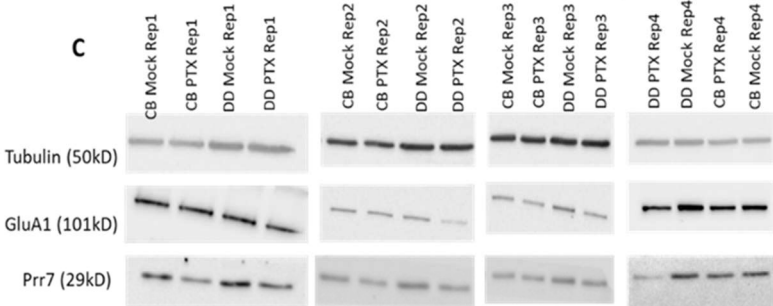
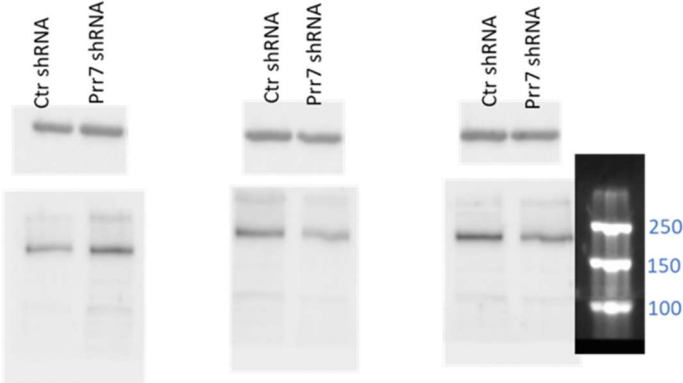
GluA1 rev: TGTCCGTATGGCTTCATTGATG

cFos for: CATCATCTAGGCCAGTGGC

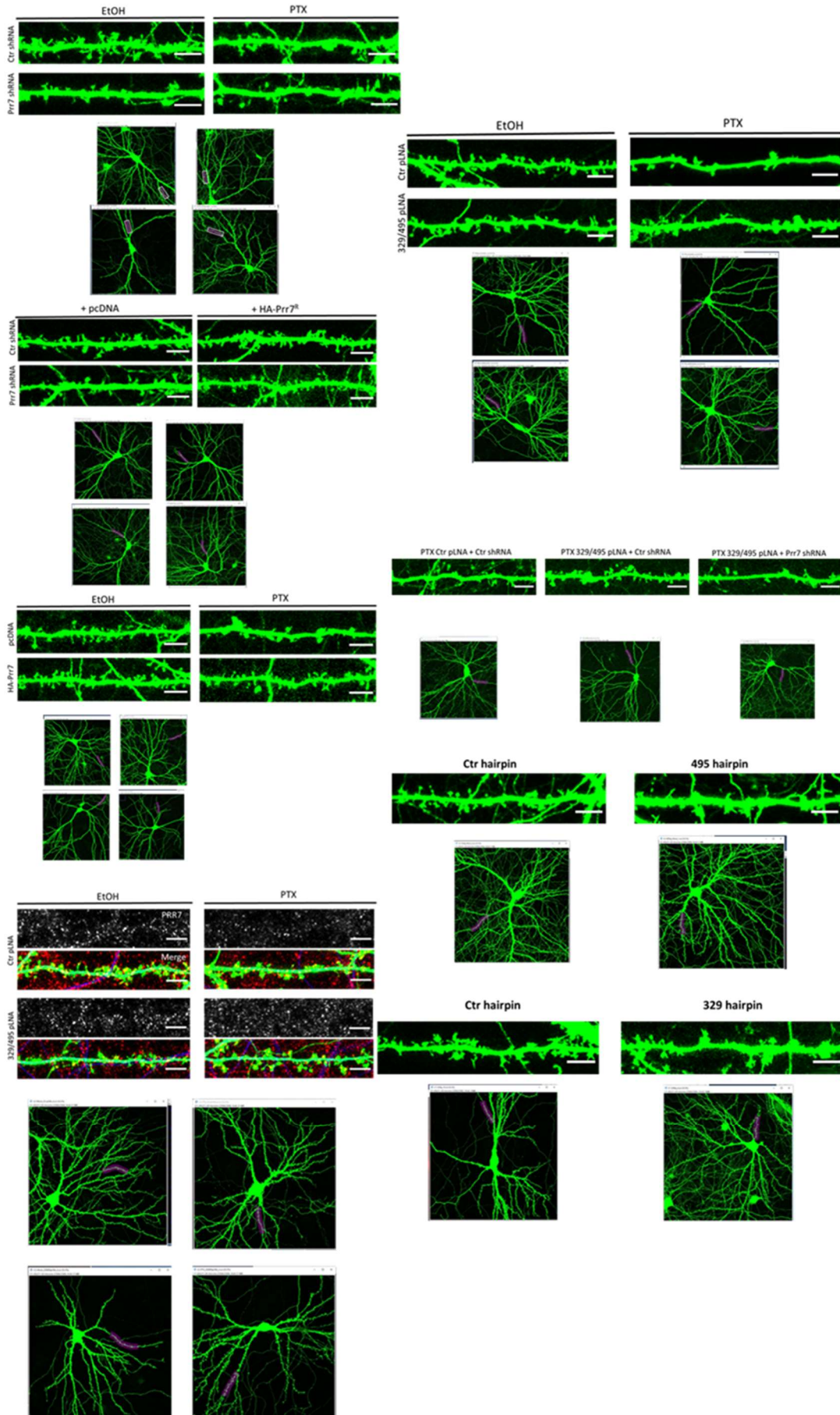
cFos rev: AGGAACCAGACAGGTCCACATCT

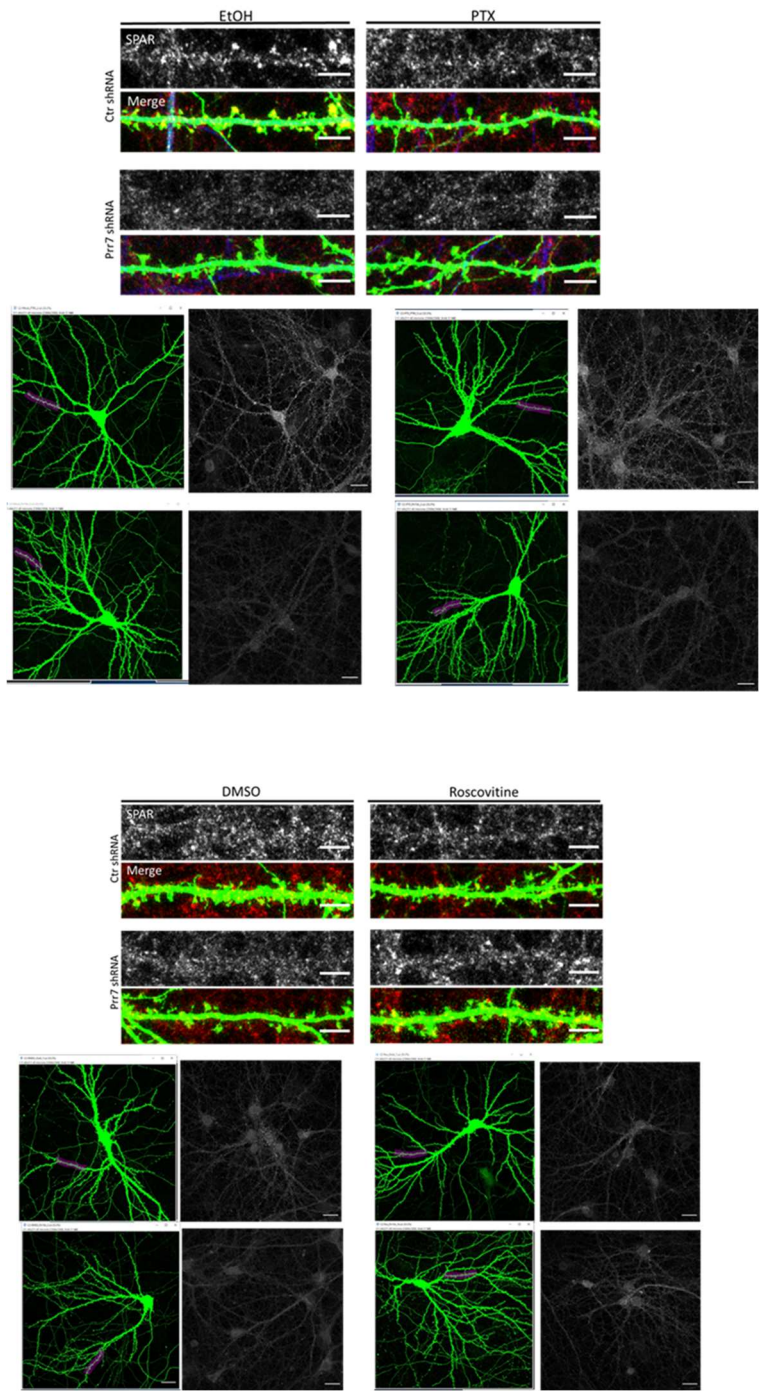
**Supplemental Data**

**GluA1 and SPAR western blots- all replicates**



# Cell segments used for dendrite closeups





## DISCUSSION

In this thesis, I primarily sought to determine whether Prr7 inhibition by miR379-410 cluster members is necessary for HSD. In addressing this main aim, I found that 1) miR-329 and miR-495 members of the cluster regulate Prr7 locally, and that this interaction is required for spine elimination during HSD; 2) Prr7 loss leads to SPAR degradation in a CDK5-dependent manner. The following section will discuss some of the additional questions that arise from these findings. Furthermore, given that the mechanism described is cell-autonomous, I will discuss how these results can have implications in broader contexts, namely at the level of intercellular interactions and neuronal circuits.

### *miR-329-3p and miR-495-3p target Prr7 locally in dendrites*

My findings indicate that upon chronic elevation of network activity, cluster members miR-329 and miR-495 are induced and inhibit Prr7 locally, which is a requirement for HSD to occur. A crucial question that still remains unanswered, however, is the mechanism of miR-329 and miR-495 induction by chronic activity. Both miR-329 and miR-495 are activated in a PTX-dependent manner based on the dual sensor assay (Fig. 3h), yet only miR-495 showed increases in expression levels upon PTX (Fig. 3i, Supplemental Fig. 10). I discuss possible mechanisms for miR-495 and miR-329 separately below.

#### miR-495 and TDMD

With respect to a mechanism for miR-495 upregulation by PTX, the involvement of Target-directed miRNA degradation (TDMD) is a possibility under consideration. TDMD is a phenomenon where RNA transcripts promote miRNA decay, and thus is essentially a reverse of the recognized roles of miRNAs and target mRNAs (Krützfeldt et al., 2005; Krützfeldt et al., 2007; Ameres et al., 2010; Baccarini et al., 2011). One of the identified examples of TDMD is the degradation of miR-7 triggered by the noncoding RNA Cyranol (Kleaveland et al., 2018). Further study of the interaction led to the finding that the miRNA decay is mediated by the E3 ligase ZSWIM8 (Shi et al., 2021), as evidenced by a significant upregulation of miR-7 following ZSWIM8 knockdown in induced differentiated neurons from mouse embryonic stem cells. Intriguingly, upon screening for other significantly increased miRNAs in the ZSWIM8 knockdown condition, the authors also identified miR-495. This observation leads to a possible model where under basal conditions, certain target mRNAs may be promoting ZSWIM8-facilitated miR-495 destruction. In contrast, under PTX-stimulated conditions, this inhibition is released, potentially through decreased expression of ZSWIM8. Preliminary experiments using a Prr7 3' UTR luciferase reporter showed decreased luciferase activity in ZSWIM8 shRNA-transfected cells, perhaps due to inhibition of miR-495 degradation, but similar decreases were observed in an empty luciferase reporter condition, leaving the results currently inconclusive (preliminary unpublished data).

### Local miR-495 Processing

Furthermore, the increases in miR-495 found in the dendritic compartment of PTX-treated cells (Fig. 3i) is interesting, as it suggests increased miR-495 local processing, and/or transport into dendrites by activity. Indeed, miRNA transport to dendrites and local miRNA processing have been suggested from observations such as pri-miRNA enrichment in RNA transport granules (Lugli et al., 2012), transport of pre-miRNAs to dendrites (Bicker et al., 2013; Lugli et al., 2008; Sambandan et al., 2017), and localization of Dicer to dendritic spines (Lugli et al., 2005). How miRNA processing and/or transport machinery are triggered by PTX stimulation is still unclear. BDNF-stimulated accumulation of pre-miR-134 into dendrites occurs in an NMDAR-dependent manner, followed by processing to form mature miRNAs (Zampa et al., 2018). Furthermore, dendritic ER has been identified as a regulator of local pre-miRNA processing, and the interactions among dendritic ER, Dicer, and TRBP are calcium-dependent, which was found also in the context of BDNF stimulation. Considering that NMDAR activation and L-type Voltage Gated Calcium Channel opening followed by calcium influx does occur during HSD, it may be that processing of pre-miR-495 to produce mature miR-495 is promoted through a shift in dendritic ER-Dicer-TRBP associations. It would also seem that Dicer itself is sensitive to neuronal activity. The regulation of Dicer activity by post-translational modification (e.g. phosphorylation (Aryal et al., 2018), SUMOylation (Gross et al., 2014) has been reported. Additionally, rapid Dicer-dependent cleavage of pre-miR-181a in spines and dendrites upon local stimulation via glutamate uncaging was visualized through a fluorescent sensor (Sambandan et al., 2017). Thus, local pre-miR-495 processing may be occurring under PTX-stimulation through the activation of Dicer.

### miR-329 and CELF4 Competition

As for miR-329, the fact that mature levels are unchanged by chronic excitation, yet miRNA activity is induced, indicates that regulation of miR-329 occurs post-processing. For example, miR-329 activity may be regulated through competition with an RNA binding protein that also targets the Prr7 3' UTR at the same site. A possibility that was explored was the regulation of miR-329 activity by CELF4 (Ammann, 2020). CELF4 is an excitatory neuron-specific RNA binding protein that has been shown to target mRNA 3' UTRs (St. Louis and Sagarsky, 2018). Bioinformatic predictions based on the miR-329-3p seed sequence and CELF4 binding sequence led to the hypothesis that miR-329 and CELF4 are in competition to bind to the same site on the 3' UTR of Prr7 mRNA. More specifically, the idea was that under basal conditions, CELF4 would prevent miR-329-3p binding to Prr7 mRNA, but under PTX-stimulated conditions CELF4 downregulation would occur, leading to increased miR-329 binding. CELF4 was found to be reduced by PTX (Ammann, 2020). A reduction in Prr7 with CELF4 knockdown was suggested by luciferase experiments (Ammann, 2020), however whether this downregulation could be attributed to induced miR-329 activity due to removal of CELF4 competition was inconclusive (due to apparent toxic effects of the miRNA inhibitors used).

### *Prr7 loss leads to SPAR degradation in a CDK5-dependent manner*

My experiments examining the effect of Prr7 knockdown on SPAR suggest that Prr7 acts to maintain the integrity of the postsynaptic density through SPAR stabilization (Fig. 5). Further, based on roscovitine studies, the suggestion would be that Prr7 maintains SPAR through inhibiting CDK5. The mechanism by which CDK5 inhibition occurs is yet to be clarified. In excitotoxic contexts, Prr7 acts as an inhibitor of the E3 ligase FBW7 in the nucleus (Kravchick et al., 2016). In this case, Prr7 blocks the ubiquitination of c-Jun by forming a complex with un-ubiquitinated c-Jun and FBW7. This ternary complex formation is said to govern the specific protection of c-Jun from FBW7, as Prr7 was not found to affect other targets of FBW7. One may ask if a similar complex among Prr7, CDK5, and SPAR exists, making Prr7 a CDK5 inhibitor specific to SPAR, or rather if Prr7 is a general CDK5 inhibitor.

To determine whether Prr7 is a general CDK5 inhibitor, perhaps it would be useful to probe for GKAP, another postsynaptic scaffold protein that is phosphorylated by CDK5 (Roselli et al., 2011). Much like the mechanism of SPAR, upon phosphorylation GKAP is degraded, which leads to synapse loss (Roselli et al., 2011). If Prr7 is indeed a general CDK5 inhibitor, then CDK5-mediated GKAP loss likely also contributes to the large reduction in dendritic spines observed in the Prr7 knockdown condition. Additionally, if characterization of Prr7 as a general CDK5 inhibitor is indeed true, such a result would have quite profound implications, as *in vivo* studies on CDK5 have revealed a central role of CDK5 in hippocampal learning and memory (Hawasli et al., 2007; Fischer et al., 2002).

### *Prr7 loss leads to GluA1 reduction*

In addition to SPAR stabilization, Prr7 knockdown also led to reduced expression of GluA1 (Fig. 2i-l). Given a previously described mechanism of SPAR loss leading to GluA1 and GluA2 downregulation (via separate pathways) in HSD (Seeburg et al., 2008; Pak and Sheng, 2003; Evers et al., 2010), one can infer that the reduced GluA1 protein levels upon Prr7 knockdown is a downstream consequence of SPAR degradation. Indeed, GluA1 RNA levels were unaffected by Prr7 knockdown (unpublished data), which would indicate that Prr7-mediated GluA1 regulation occurs at the protein level.

In an experiment not included in the manuscript, I found that GluA1 protein reduction upon Prr7 knockdown was rescued through treatment with the lysosomal inhibitor leupeptin (unpublished data). Indeed, GluA1 degradation is understood to occur following ubiquitination by the E3 ligase Nedd4-1 and subsequent trafficking to the lysosome (Schwarz et al., 2010). The leupeptin-mediated rescue would suggest that Prr7 inhibits the trafficking of GluA1 to the lysosome for degradation, but whether it is via SPAR stabilization or direct inhibition of Nedd4-1, is not yet clear. It would perhaps be worthwhile to ask if SPAR overexpression in conditions of Prr7 knockdown also restores GluA1 levels. Such an experiment would address whether Prr7-GluA1 regulation occurs independently of SPAR.

### *miRNA regulation in the context of NF-κB-mediated HSD endpoint*

In my studies, I only examined the 48h time point after PTX treatment, and therefore have only taken a “snapshot” of the neuron’s compensatory response to chronic excitation. One may expect at a later timepoint, that the HSD mechanism would be terminated, in order to prevent overcompensation. Thus, just as one might ask how PTX-mediated miRNA induction occurs, conversely: once enough compensatory depression has been performed, how is the miRNA induction stopped? A study reporting the activation of Nuclear Factor κ B (NF-κB) following Plk2 induction to serve as an endpoint to HSD (Mihalas et al., 2013) may help to answer this question. Intriguingly, the authors of the study found that the NF-κB activation is tied to a restoration of SPAR. Interferon activation, which is partly facilitated by NF-κB, has been shown to impair microprocessor activity in the context of viral infection in HEK and Hela cells (Witteveldt et al., 2018). Therefore, a possible mechanism could be that NF-κB activation connects to the cessation of miRNA induction via Drosha inhibition to signal the end of HSD, which thereby restores Prr7 and SPAR levels.

### *HSD in proximal vs. distal dendrites*

A discrepancy worth addressing, which exists between my present SPAR immunostaining results and previous studies on SPAR, concerns the reported proximal-distal gradient in SPAR loss during HSD. Namely, a pronounced reduction in SPAR protein levels in proximal dendrites (~10-30μm from the soma) in response to chronic excitation by PTX has been reported (Pak and Sheng 2003). In contrast, the segmentation analysis performed on the SPAR immunostaining images in my study (Supplemental Fig. 11) indicated uniform loss of SPAR across the entire dendritic length by PTX and Prr7 knockdown. The discrepancy may be due to a difference in treatment length, in that the gradient was observed at 24h post-PTX in previous studies, whereas in the present study the 48h time point was tested. This difference is interesting, as it could imply that spine elimination in HSD occurs in a sequential manner starting from the dendrites closest to the soma and progressing outward to more distal processes.

The authors observed that the SPAR gradient was in alignment with a Plk2 gradient, in which the sites where Plk2 was most induced corresponded to the greatest SPAR loss (Pak and Sheng 2003). It may be worthwhile to ask how other regulators of SPAR, such as miR-329, miR-495, and Prr7, may behave in a spatial context over the course of HSD, and what exactly is driving the spatial specificity.

Undoubtedly, a key player in the initiation of HSD is Ca<sup>2+</sup>, as the cascade of CaMKK/CaMKIV is triggered by the influx of calcium through L-type voltage gated channels and NMDARs. Interestingly, although the total calcium channel density is observed to be rather uniform across dendrites in CA1 hippocampal neurons, L-type (and N-type) calcium channels predominate in more proximal regions (as defined as <100μm from the soma) (Magee et al., 1998). In the same study, on the other hand the distribution of K<sup>+</sup> channels was found to be more dense at distal regions with greater than 5-fold increase in number compared to proximal regions. Therefore, in considering the relative ratio of inward Ca<sup>2+</sup>

current vs. outward  $K^+$  current, the conclusion drawn was that the more proximal regions are more excitable than the distal regions.

Thus, one could perhaps visualize an influx of  $Ca^{2+}$  through L-type voltage gated channel opening where  $Ca^{2+}$  concentrations are particularly high in proximal dendrites due to the higher density of L-type channels. Over time, it could be that the  $Ca^{2+}$  diffuses to the distal regions. In light of studies indicating pre-miRNA processing can be regulated in a  $Ca^{2+}$ -dependent manner (Antoniou et al., 2018), it may be that the production of mature miRNAs follows the direction of  $Ca^{2+}$  diffusion, resulting in a sequential “spreading out” of Prr7 and SPAR loss from the proximal to distal direction. Perhaps the 24h time point post-PTX treatment marks only the beginning of this process. Indeed, slower  $Ca^{2+}$  decay kinetics in proximal regions (50-100 $\mu$ m from the soma) have been reported in comparison to distal dendrites (>150 $\mu$ m from the soma) (Holthoff et al., 2002), which would support the idea that beginning of the diffusion process at the proximal dendrites is rather slow, creating a marked gradient, which over time progressively increases in diffusion rate.

With this model, it can be predicted that there would be a Prr7 gradient consistent with the SPAR gradient over the course of HSD, and that there would also be sequential proximal-distal directionality in spine elimination.

#### *Prr7 as a switch governing excitotoxicity*

An important question to ask considering Prr7's established role in excitotoxicity (Kravchick et al., 2016) is: what is the “switch” that triggers Prr7-mediated cell apoptosis, and can our knowledge of miRNA-mediated Prr7 downregulation somehow help in strategizing ways to counter this mechanism? Excitotoxicity is associated with NMDAR overstimulation (Barker-Haliski and White, 2015), which reinforces the importance of  $Ca^{2+}$  in processes that regulate excitability.  $Ca^{2+}$  accumulation and abnormal  $Ca^+$  load are tied to cell death, in the context of ischemia (Cross et al., 2010) and seizure-induced brain damage (McDonough and Shih, 1997). In fact, excitotoxicity could perhaps be interpreted as deregulation of intracellular calcium homeostasis (Cross et al., 2010). Dendritic spines act as compartments that limit diffusion of  $Ca^{2+}$  between neighboring spines and parent dendrites, thereby strongly concentrating the  $Ca^{2+}$  that flows into the postsynaptic membrane (Holmes 1990; Koch and Zador 1993; Svoboda et al., 1996). Therefore, perhaps it could be imagined that excessive  $Ca^{2+}$  accumulation occurs at the level of individual spines. Prr7 is localized at synapses, and its translocation to the nucleus is what results in cell apoptosis (Kravchick et al., 2016). Therefore, a speculation could be that Prr7 is sensitive to levels of synaptic  $Ca^{2+}$  accumulation, such that when synaptic  $Ca^{2+}$  concentration goes beyond a certain threshold, Prr7 is modified (e.g. phosphorylated) and immediately transported to the nucleus to carry out apoptosis.

Thus, the solution to prevent Prr7 translocation could be to find ways to lower the synaptic  $\text{Ca}^{2+}$  accumulation even in conditions of NMDAR overstimulation. As described, spines themselves act as compartments and limit the diffusion of  $\text{Ca}^{2+}$ . Thus, in excitotoxic conditions, overexpression of miR-329 and miR-495 may help to counter excitotoxicity by targeting synaptic Prr7 before it has the chance to translocate. Synaptic Prr7 loss would result in spine elimination, thereby helping to diffuse out the  $\text{Ca}^{2+}$  accumulated within the compartment and depressing the excitability of the cell. Furthermore, the prevention of Prr7 translocation would protect against cell apoptosis.

#### *Exosome-mediated Prr7 signaling in homeostatic plasticity*

So far, I have focused on cell-autonomous processes, however it would be necessary to find the significance of miRNA-Prr7 interactions in broader contexts, such as in cell-cell communication, to gain a better understanding of how Prr7 regulation elicits changes at the circuit level.

The discovery of Prr7 in exosomes (Lee et al., 2018) is interesting, as it reveals a potential role of Prr7 as a signaling molecule that facilitates intercellular communication. Exosome-mediated secretion of Prr7 was reported to be NMDAR activity-dependent, which could suggest that at the beginning of the HSD mechanism, there would also be some triggering of exosomal Prr7 release. In an *in vitro* study examining exosome release from primary cortical neurons onto dissociated hippocampal cells (Chivet et al. 2014), exosomes were found to be released postsynaptically from the somato-dendritic compartment of the cortical neurons in an NMDAR-dependent manner. Additionally, it was observed that the released exosomes bound mainly to the presynaptic compartments of the recipient hippocampal cells. The NMDAR-dependent release of exosomes from the somato-dendritic compartment of cultured cortical neurons was observed and thereby supported by another study (Lachenal et al., 2011).

Thus, in the case of exosome-mediated release of Prr7, it would seem reasonable to expect that the Prr7 release occurs from the postsynaptic compartment to presynaptic compartments of contacting or neighboring neurons. Subsequently, exosome-enclosed Prr7 uptake would occur into the presynaptic membrane, either through fusion with the plasma membrane or internalization (Théry et al., 2009). Intriguingly, CDK5 is present within presynaptic membranes of hippocampal neurons and is known to phosphorylate Synapsin1, leading to enhanced Synapsin1 binding to F-actin, thereby preventing synaptic vesicle trafficking to the active zone and inhibiting neurotransmitter release (Verstegen et al., 2014). Upon uptake of Prr7 into the presynaptic compartment, Prr7 may act to prevent Synapsin1 phosphorylation by inhibiting CDK5, and help to strengthen presynaptic activity. With this model, due to exosome-mediated loss of Prr7 from the postsynaptic membrane, the “releasing cell” would exhibit spine elimination (which in this regard, is consistent with the results of Lee et al. 2018), while the “receiving cell”, upon uptake of Prr7 in the presynaptic membrane, would exhibit increased presynaptic activity.

Going further, perhaps such a pathway of Prr7 signaling from postsynaptic to presynaptic membranes, could underlie a phenomenon recognized as “retrograde compensation” (Frank et al., 2006), a form of homeostatic plasticity between cells. Namely, in this process, there is a compensatory increase in presynaptic activity in response to blockade of postsynaptic glutamate receptors.

*Further considerations to apply findings to circuit, regional, and behavioral -levels*

Furthermore, studies on Prr7 have all focused on Prr7 expressed in excitatory neurons, but the possibility of Prr7 expression in inhibitory neurons has not been fully clarified. In order to better understand how Prr7 dysregulation could lead to changes at the circuit level, it would be necessary to consider the interplay between homeostatic responses of excitatory neurons relative to inhibitory neurons. Nevertheless, it seems Prr7 is neuron-specific (Lee et al., 2018), which could give reason to give more attention to the role of Prr7 on neuron-neuron interactions than to neuron-glia interactions to further explore the function of Prr7 in homeostatic plasticity at the circuit-level.

Going further, it would be important to think about implications at the regional level. I have studied the role of Prr7 in homeostatic mechanisms in the hippocampus, which is reasonable given the enrichment of Prr7 in hippocampal and neocortical regions (Lee et al., 2018), and the existing literature on HSD has almost entirely been in the context of the hippocampus. However, it is important to recognize that homeostatic plasticity mechanisms can be highly region specific, as mechanisms can be different even between hippocampal layers (Kim and Tsien 2008). Therefore, whether the role of miRNA-mediated Prr7 regulation holds throughout the hippocampus (e.g. between dorsal and ventral hippocampus), as well as in other connected brain regions (e.g. amygdala, hypothalamus, prefrontal cortex), would need to be investigated.

Examination of identified genetic disorders where the miR379-410 cluster, and Prr7 are aberrantly expressed could give an idea as to how interference of the miR-329 and miR-495-mediated regulation of Prr7 manifests in terms of neurological phenotype. Kagami-Ogata Syndrome (KOS; reviewed in Ogata and Kagami, 2016; Sakaria et al., 2021) and Temple Syndrome (TS; Kagami et al., 2017) are two imprinting disorders that lead to altered expression of the miR379-410 cluster (thus including miR-329 and miR-495), in opposite directions. Specifically, KOS is principally caused by paternal disomy of the 14q32 region, resulting in inheritance of two paternal alleles and in principle would correspond to complete miRNA cluster silencing. Conversely, TS is tied to uniparental disomy for the maternal allele, essentially resulting in overexpression of the miRNA cluster. However, it is important to recognize that dysregulation of cluster expression in these patients is not due to disomy in all cases; other mechanisms that affect the cis-acting regulatory elements upstream of the cluster-encoding region may also result in altered expression. For example, deletion of the MEG3 promoter, abnormal methylation or deletion in the MEG3-DMR (differentially methylated region) or IG-DMR (which controls methylation pattern of

MEG3-DMR and MEG3 promoter activity) are also understood to lead to these conditions (Prasasya et al., 2020).

Despite the different ways in which the cluster expression can be altered (through epimutations and mutations), there is a general observation of intellectual disability associated with these syndromes, which is suggested to persist into adulthood (Prasasya et al., 2020). This persistence is in contrast to other non-neurological symptoms that are present at infancy for these patients but progressively disappear over the course of development. Specifically, early in development, patients for both syndromes exhibit multiple developmental features that require early intervention (e.g. abdominal wall defect and feeding difficulties in KOS, metabolic symptoms in TS), which are noted to improve significantly over time, resulting in patients becoming eventually free from treatments for these symptoms (e.g. KOS patients eventually no longer require tracheostomy or tube feeding).

Yet, limited clinical reports of adult cases for these conditions make it difficult to gain an understanding of how neurological symptoms persist and manifest in adulthood. However, there is some suggestion of a phenotype overlap with ASD, with sociability being affected, following a report on an adult case of TS (Kimura et al., 2018). Indeed, cluster-deficient mice exhibit hypersocial behaviors (Lackinger et al., 2019), which points toward a connection between cluster members and sociability regulation.

In terms of *Prr7*, there are no diseases that draw a direct connection to *Prr7* to date. However, a condition called Sotos Syndrome is recognized to be caused by a mutation in the *NSD1* (nuclear receptor binding SET domain protein 1) gene (Tatton-Brown et al., 2005). Intriguingly the *Prr7* gene locus is in close proximity to *NSD1*, with both genes being located at the 5q35.2-3 region, which could suggest that in some cases of Sotos *Prr7* is deleted. Sotos Syndrome patients also present with ASD-like symptoms (Lane et al., 2017), which further draws a correlation between *Prr7* and sociability.

Taken together, perhaps future studies may be directed toward understanding the function of miRNA-mediated regulation of *Prr7* toward sociability, as well as toward better determining how sociability difficulty may manifest in adult patients of Sotos, KOS, and TS.

## REFERENCES

- Abbott LF, Nelson SB. Synaptic plasticity: taming the beast. *Nat Neurosci.* 2000 Nov;3 Suppl:1178-83.
- Ameres SL, Horwich MD, Hung JH, Xu J, Ghildiyal M, Weng Z, Zamore PD. Target RNA-directed trimming and tailing of small silencing RNAs. *Science.* 2010 Jun 18;328(5985):1534-9. doi: 10.1126/science.1187058.
- Ammann, I. Competitive Regulation of gene expression by miRNAs and RBPs in rat neurons. Master's Thesis. ETH Zurich. 2020.
- Anggono V, Clem RL, Huganir RL. PICK1 loss of function occludes homeostatic synaptic scaling. *J Neurosci.* 2011 Feb 9;31(6):2188-96.
- Antoniou A, Khudayberdiev S, Idziak A, Bicker S, Jacob R, Schratt G. The dynamic recruitment of TRBP to neuronal membranes mediates dendritogenesis during development. *EMBO Rep.* 2018 Mar;19(3):e44853.
- Aoto J, Nam CI, Poon MM, Ting P, Chen L. Synaptic signaling by all-trans retinoic acid in homeostatic synaptic plasticity. *Neuron.* 2008 Oct 23;60(2):308-20. doi: 10.1016/j.neuron.2008.08.012.
- Aryal NK, Pant V, Wasylshen AR, Parker-Thornburg J, Baseler L, El-Naggar AK, Liu B, Kalia A, Lozano G, Arur S. Constitutive Dicer1 phosphorylation accelerates metabolism and aging in vivo. *Proc Natl Acad Sci U S A.* 2019 Jan 15;116(3):960-969.
- Baccarini A, Chauhan H, Gardner TJ, Jayaprakash AD, Sachidanandam R, Brown BD. Kinetic analysis reveals the fate of a microRNA following target regulation in mammalian cells. *Curr Biol.* 2011 Mar 8;21(5):369-76.
- Bagni C, Zukin RS. A Synaptic Perspective of Fragile X Syndrome and Autism Spectrum Disorders. *Neuron.* 2019 Mar 20;101(6):1070-1088.
- Baj G, Patrizio A, Montalbano A, Sciancalepore M, Tongiorgi E. Developmental and maintenance defects in Rett syndrome neurons identified by a new mouse staging system in vitro. *Front Cell Neurosci.* 2014;8:18.
- Barker-Haliski M, White HS. Glutamatergic Mechanisms Associated with Seizures and Epilepsy. *Cold Spring Harb Perspect Med.* 2015 Jun 22;5(8):a022863.
- Bartel DP. MicroRNAs: target recognition and regulatory functions. *Cell.* 2009 Jan 23;136(2):215-33.
- Bateup HS, Denefrio CL, Johnson CA, Saulnier JL, Sabatini BL. Temporal dynamics of a homeostatic pathway controlling neural network activity. *Front Mol Neurosci.* 2013 Sep 18;6:28. doi: 10.3389/fnmol.2013.00028.
- Bats C, Groc L, Choquet D. The interaction between Stargazin and PSD-95 regulates AMPA receptor surface trafficking. *Neuron.* 2007 Mar 1;53(5):719-34. doi: 10.1016/j.neuron.2007.01.030.
- Beattie EC, Stellwagen D, Morishita W, Bresnahan JC, Ha BK, Von Zastrow M, Beattie MS, Malenka RC. Control of synaptic strength by glial TNF $\alpha$ . *Science.* 2002 Mar 22;295(5563):2282-5.
- Besag FM. Epilepsy in patients with autism: links, risks and treatment challenges. *Neuropsychiatr Dis Treat.* 2017 Dec 18;14:1-10
- Bi GQ, Poo MM. Synaptic modifications in cultured hippocampal neurons: dependence on spike timing, synaptic strength, and postsynaptic cell type. *J Neurosci.* 1998 Dec 15;18(24):10464-72.
- Bicker S, Khudayberdiev S, Weiß K, Zocher K, Baumeister S, Schratt G. The DEAH-box helicase DHX36 mediates dendritic localization of the neuronal precursor-microRNA-134. *Genes Dev.* 2013 May 1;27(9):991-6. doi: 10.1101/gad.211243.112. Erratum in: *Genes Dev.* 2013 Jul 15;27(14):1633.
- Bliss TV, Lomo T. Long-lasting potentiation of synaptic transmission in the dentate area of the anaesthetized rabbit following stimulation of the perforant path. *J Physiol.* 1973 Jul;232(2):331-56.
- Brown CE, Wong C, Murphy TH. Rapid morphologic plasticity of peri-infarct dendritic spines after focal ischemic stroke. *Stroke.* 2008 Apr;39(4):1286-91. doi: 10.1161/STROKEAHA.107.498238.
- Bohnsack MT, Czaplinski K, Gorlich D. Exportin 5 is a RanGTP-dependent dsRNA-binding protein that mediates nuclear export of pre-miRNAs. *RNA.* 2004 Feb;10(2):185-91.

- Burrone J, O'Byrne M, Murthy VN. Multiple forms of synaptic plasticity triggered by selective suppression of activity in individual neurons. *Nature*. 2002 Nov 28;420(6914):414-8.
- Cannon WB. Organization for physiological homeostasis. *Physiological Reviews*, 1929 July 1;9(3):399-431.
- Cattanach BM, Rasberry C. Evidence of imprinting involving the distal region of Chr 12. *Mouse Genome* 1993; 91:858.
- Chao HT, Zoghbi HY, Rosenmund C. MeCP2 controls excitatory synaptic strength by regulating glutamatergic synapse number. *Neuron*. 2007 Oct 4;56(1):58-65. doi: 10.1016/j.neuron.2007.08.018.
- Chen K, Baram TZ, Soltesz I. Febrile seizures in the developing brain result in persistent modification of neuronal excitability in limbic circuits. *Nat Med*. 1999 Aug;5(8):888-94.
- Chendrimada TP, Gregory RI, Kumaraswamy E, Norman J, Cooch N, Nishikura K, Shiekhattar R. TRBP recruits the Dicer complex to Ago2 for microRNA processing and gene silencing. *Nature*. 2005 Aug 4;436(7051):740-4.
- Chivet M, Javalet C, Laulagnier K, Blot B, Hemming FJ, Sadoul R. Exosomes secreted by cortical neurons upon glutamatergic synapse activation specifically interact with neurons. *J Extracell Vesicles*. 2014 Nov 13;3:24722.
- Chowdhury D, Turner M, Patriarchi T, Hergarden AC, Anderson D, Zhang Y, Sun J, Chen CY, Ames JB, Hell JW. Ca<sup>2+</sup>/calmodulin binding to PSD-95 mediates homeostatic synaptic scaling down. *EMBO J*. 2018 Jan 4;37(1):122-138. doi: 10.15252/embj.201695829.
- Christensen M, Larsen LA, Kauppinen S, Schrott G. Recombinant Adeno-Associated Virus-Mediated microRNA Delivery into the Postnatal Mouse Brain Reveals a Role for miR-134 in Dendritogenesis in Vivo. *Front Neural Circuits*. 2010 Jan 12;3:16. doi: 10.3389/neuro.04.016.2009.
- Cohen JE, Lee PR, Chen S, Li W, Fields RD. MicroRNA regulation of homeostatic synaptic plasticity. *Proc Natl Acad Sci U S A*. 2011 Jul 12;108(28):11650-5. doi: 10.1073/pnas.1017576108.
- Colameo D, Rajman M, Soutschek M, Bicker S, von Ziegler L, Bohacek J, Winterer J, Germain PL, Dieterich C, Schrott G. Pervasive compartment-specific regulation of gene expression during homeostatic synaptic scaling. *EMBO Rep*. 2021 Oct 5;22(10):e52094. doi: 10.15252/embr.202052094.
- Cross JL, Meloni BP, Bakker AJ, Lee S, Knuckey NW. Modes of Neuronal Calcium Entry and Homeostasis following Cerebral Ischemia. *Stroke Res Treat*. 2010 Nov 1;2010:316862.
- Edbauer D, Neilson JR, Foster KA, Wang CF, Seeburg DP, Batterson MN, Tada T, Dolan BM, Sharp PA, Sheng M. Regulation of synaptic structure and function by FMRP-associated microRNAs miR-125b and miR-132. *Neuron*. 2010 Feb 11;65(3):373-84. doi: 10.1016/j.neuron.2010.01.005. Erratum in: *Neuron*. 2010 Oct 6;68(1):161.
- Evers DM, Matta JA, Hoe HS, Zarkowsky D, Lee SH, Isaac JT, Pak DT. Plk2 attachment to NSF induces homeostatic removal of GluA2 during chronic overexcitation. *Nat Neurosci*. 2010 Oct;13(10):1199-207. doi: 10.1038/nn.2624. Epub 2010 Aug 29.
- Farh KK, Grimson A, Jan C, Lewis BP, Johnston WK, Lim LP, Burge CB, Bartel DP. The widespread impact of mammalian MicroRNAs on mRNA repression and evolution. *Science*. 2005 Dec 16;310(5755):1817-21.
- Filipowicz W, Bhattacharyya SN, Sonenberg N. Mechanisms of post-transcriptional regulation by microRNAs: are the answers in sight? *Nat Rev Genet*. 2008 Feb;9(2):102-14.
- Fiore R, Khudayberdiev S, Christensen M, Siegel G, Flavell SW, Kim TK, Greenberg ME, Schrott G. Mef2-mediated transcription of the miR379-410 cluster regulates activity-dependent dendritogenesis by fine-tuning Pumilio2 protein levels. *EMBO J*. 2009 Mar 18;28(6):697-710. doi: 10.1038/emboj.2009.10.
- Fiore R, Rajman M, Schwale C, Bicker S, Antoniou A, Bruehl C, Draguhn A, Schrott G. MiR-134-dependent regulation of Pumilio-2 is necessary for homeostatic synaptic depression. *EMBO J*. 2014 Oct 1;33(19):2231-46. doi: 10.15252/embj.201487921.
- Fischer A, Sananbenesi F, Schrick C, Spiess J, Radulovic J. Cyclin-dependent kinase 5 is required for associative learning. *J Neurosci*. 2002 May 1;22(9):3700-7.

Frank CA, Kennedy MJ, Goold CP, Marek KW, Davis GW. Mechanisms underlying the rapid induction and sustained expression of synaptic homeostasis. *Neuron*. 2006 Nov 22;52(4):663-77. doi: 10.1016/j.neuron.2006.09.029.

Glantz LA, Lewis DA. Decreased dendritic spine density on prefrontal cortical pyramidal neurons in schizophrenia. *Arch Gen Psychiatry*. 2000 Jan;57(1):65-73. doi: 10.1001/archpsyc.57.1.65.

Glynn MW, Elmer BM, Garay PA, Liu XB, Needleman LA, El-Sabeawy F, McAllister AK. MHCI negatively regulates synapse density during the establishment of cortical connections. *Nat Neurosci*. 2011 Apr;14(4):442-51.

Goold CP, Nicoll RA. Single-cell optogenetic excitation drives homeostatic synaptic depression. *Neuron*. 2010 Nov 4;68(3):512-28. doi: 10.1016/j.neuron.2010.09.020.

Groc L, Choquet D. Linking glutamate receptor movements and synapse function. *Science*. 2020 Jun 12;368(6496):eaay4631. doi: 10.1126/science.aay4631.

Gross TJ, Powers LS, Boudreau RL, Brink B, Reissetter A, Goel K, Gerke AK, Hassan IH, Monick MM. A microRNA processing defect in smokers' macrophages is linked to SUMOylation of the endonuclease DICER. *J Biol Chem*. 2014 May 2;289(18):12823-34.

Hartman KN, Pal SK, Burrone J, Murthy VN. Activity-dependent regulation of inhibitory synaptic transmission in hippocampal neurons. *Nat Neurosci*. 2006 May;9(5):642-9. doi: 10.1038/nn1677.

Haase AD, Jaskiewicz L, Zhang H, Lainé S, Sack R, Gatignol A, Filipowicz W. TRBP, a regulator of cellular PKR and HIV-1 virus expression, interacts with Dicer and functions in RNA silencing. *EMBO Rep*. 2005 Oct;6(10):961-7.

Hawasli AH, Benavides DR, Nguyen C, Kansy JW, Hayashi K, Chambon P, Greengard P, Powell CM, Cooper DC, Bibb JA. Cyclin-dependent kinase 5 governs learning and synaptic plasticity via control of NMDAR degradation. *Nat Neurosci*. 2007 Jul;10(7):880-886.

Heyam A, Lagos D, Plevin M. Dissecting the roles of TRBP and PACT in double-stranded RNA recognition and processing of noncoding RNAs. *Wiley Interdiscip Rev RNA*. 2015 May-Jun;6(3):271-89.

Holmes WR. Is the function of dendritic spines to concentrate calcium? *Brain Res*. 1990 Jun 11;519(1-2):338-42.

Holthoff K, Tsay D, Yuste R. Calcium dynamics of spines depend on their dendritic location. *Neuron*. 2002 Jan 31;33(3):425-37.

Hou Q, Zhang D, Jarzylo L, Haganir RL, Man HY. Homeostatic regulation of AMPA receptor expression at single hippocampal synapses. *Proc Natl Acad Sci U S A*. 2008 Jan 15;105(2):775-80. doi: 10.1073/pnas.0706447105. Epub 2008 Jan 3. Erratum in: *Proc Natl Acad Sci U S A*. 2017 Mar 28;114(13):E2799.

Hrdinka M, Sudan K, Just S, Drobek A, Stepanek O, Schlüter D, Reinhold D, Jordan BA, Gintschel P, Schraven B, Kreutz MR. Normal Development and Function of T Cells in Proline Rich 7 (Prr7) Deficient Mice. *PLoS One*. 2016 Sep 22;11(9):e0162863. doi: 10.1371/journal.pone.0162863.

Hsieh H, Boehm J, Sato C, Iwatsubo T, Tomita T, Sisodia S, Malinow R. AMPAR removal underlies Abeta-induced synaptic depression and dendritic spine loss. *Neuron*. 2006 Dec 7;52(5):831-43.

Hutsler JJ, Zhang H. Increased dendritic spine densities on cortical projection neurons in autism spectrum disorders. *Brain Res*. 2010 Jan 14;1309:83-94. doi: 10.1016/j.brainres.2009.09.120.

Hutvagner G, McLachlan J, Pasquinelli AE, Bálint E, Tuschl T, Zamore PD. A cellular function for the RNA-interference enzyme Dicer in the maturation of the let-7 small temporal RNA. *Science*. 2001 Aug 3;293(5531):834-8.

Ibata K, Sun Q, Turrigiano GG. Rapid synaptic scaling induced by changes in postsynaptic firing. *Neuron*. 2008 Mar 27;57(6):819-26. doi: 10.1016/j.neuron.2008.02.031.

Isokawa M, Levesque M, Fried I, Engel J Jr. Glutamate currents in morphologically identified human dentate granule cells in temporal lobe epilepsy. *J Neurophysiol*. 1997 Jun;77(6):3355-69. doi: 10.1152/jn.1997.77.6.3355.

- Jawaid S, Kidd GJ, Wang J, Swetlik C, Dutta R, Trapp BD. Alterations in CA1 hippocampal synapses in a mouse model of fragile X syndrome. *Glia*. 2018 Apr;66(4):789-800. doi: 10.1002/glia.23284.
- Jonas S, Izaurralde E. Towards a molecular understanding of microRNA-mediated gene silencing. *Nat Rev Genet*. 2015 Jul;16(7):421-33.
- Jordan BA, Fernholz BD, Boussac M, Xu C, Grigorean G, Ziff EB, Neubert TA. Identification and verification of novel rodent postsynaptic density proteins. *Mol Cell Proteomics*. 2004 Sep;3(9):857-71. doi: 10.1074/mcp.M400045-MCP200.
- Ju W, Morishita W, Tsui J, Gaietta G, Deerinck TJ, Adams SR, Garner CC, Tsien RY, Ellisman MH, Malenka RC. Activity-dependent regulation of dendritic synthesis and trafficking of AMPA receptors. *Nat Neurosci*. 2004 Mar;7(3):244-53. doi: 10.1038/nn1189.
- Juraska JM, Drzewiecki CM. Cortical reorganization during adolescence: What the rat can tell us about the cellular basis. *Dev Cogn Neurosci*. 2020 Oct;45:100857. doi: 10.1016/j.den.2020.100857.
- Kagami M, Nagasaki K, Kosaki R, Horikawa R, Naiki Y, Saitoh S, Tajima T, Yorifuji T, Numakura C, Mizuno S, Nakamura A, Matsubara K, Fukami M, Ogata T. Temple syndrome: comprehensive molecular and clinical findings in 32 Japanese patients. *Genet Med*. 2017 Dec;19(12):1356-1366.
- Kamble N, Netravathi M, Nagaraju BC, Lenka A, Kumar K, Sowmya V, Jain S, Pal PK. Evaluation of Cognition and Cortical Excitability in Huntington's Disease. *Can J Neurol Sci*. 2018 Mar;45(2):176-181.
- Kawamata T, Tomari Y. Making RISC. *Trends Biochem Sci*. 2010 Jul;35(7):368-76.
- Kauselmann G, Weiler M, Wulff P, Jessberger S, Konietzko U, Scafidi J, Staubli U, Bereiter-Hahn J, Strebhardt K, Kuhl D. The polo-like protein kinases Fnk and Snk associate with a Ca(2+)- and integrin-binding protein and are regulated dynamically with synaptic plasticity. *EMBO J*. 1999 Oct 15;18(20):5528-39. doi: 10.1093/emboj/18.20.5528.
- Kedde M, Strasser MJ, Boldajipour B, Oude Vrielink JA, Slanchev K, le Sage C, Nagel R, Voorhoeve PM, van Duijse J, Ørom UA, Lund AH, Perrakis A, Raz E, Agami R. RNA-binding protein Dnd1 inhibits microRNA access to target mRNA. *Cell*. 2007 Dec 28;131(7):1273-86. doi: 10.1016/j.cell.2007.11.034.
- Kim J, Tsien RW. Synapse-specific adaptations to inactivity in hippocampal circuits achieve homeostatic gain control while dampening network reverberation. *Neuron*. 2008 Jun 26;58(6):925-37.
- Kimura T, Kagami M, Matsubara K, Yatsuga S, Mukasa R, Yatsuga C, Matsumoto T, Koga Y. Temple syndrome diagnosed in an adult patient with clinical autism spectrum disorder. *Clin Case Rep*. 2018 Nov 8;7(1):15-18.
- Kirov SA, Sorra KE, Harris KM. Slices have more synapses than perfusion-fixed hippocampus from both young and mature rats. *J Neurosci*. 1999 Apr 15;19(8):2876-86. doi: 10.1523/JNEUROSCI.19-08-02876.1999.
- Kleaveland B, Shi CY, Stefano J, Bartel DP. A Network of Noncoding Regulatory RNAs Acts in the Mammalian Brain. *Cell*. 2018 Jul 12;174(2):350-362.e17.
- Koch C, Zador A. The function of dendritic spines: devices subserving biochemical rather than electrical compartmentalization. *J Neurosci*. 1993 Feb;13(2):413-22.
- Koss WA, Belden CE, Hristov AD, Juraska JM. Dendritic remodeling in the adolescent medial prefrontal cortex and the basolateral amygdala of male and female rats. *Synapse*. 2014 Feb;68(2):61-72.
- Kovács RÁ, Vadász H, Bulyáki É, Török G, Tóth V, Mátyás D, Kun J, Hunyadi-Gulyás É, Fedor FZ, Csicsi Á, Medzihradszky K, Homolya L, Juhász G, Kékesi KA, Józsi M, Györfy BA, Kardos J. Identification of Neuronal Pentraxins as Synaptic Binding Partners of C1q and the Involvement of NPI in Synaptic Pruning in Adult Mice. *Front Immunol*. 2021 Feb 8;11:599771.
- Kravchick DO, Karpova A, Hrdinka M, Lopez-Rojas J, Iacobas S, Carbonell AU, Iacobas DA, Kreutz MR, Jordan BA. Synaptonuclear messenger PRR7 inhibits c-Jun ubiquitination and regulates NMDA-mediated excitotoxicity. *EMBO J*. 2016 Sep 1;35(17):1923-34. doi: 10.15252/embj.201593070.

- Krützfeldt J, Rajewsky N, Braich R, Rajeev KG, Tuschl T, Manoharan M, Stoffel M. Silencing of microRNAs in vivo with 'antagomirs'. *Nature*. 2005 Dec 1;438(7068):685-9. doi: 10.1038/nature04303. Epub 2005 Oct 30.
- Krützfeldt J, Kuwajima S, Braich R, Rajeev KG, Pena J, Tuschl T, Manoharan M, Stoffel M. Specificity, duplex degradation and subcellular localization of antagomirs. *Nucleic Acids Res*. 2007;35(9):2885-92. doi: 10.1093/nar/gkm024. Epub 2007 Apr 16. PMID: 17439965; PMCID: PMC1888827.
- Labialle S, Marty V, Bortolin-Cavaillé ML, Hoareau-Osman M, Pradère JP, Valet P, Martin PG, Cavaillé J. The miR-379/miR-410 cluster at the imprinted Dlk1-Dio3 domain controls neonatal metabolic adaptation. *EMBO J*. 2014 Oct 1;33(19):2216-30.
- Lachenal G, Pernet-Gallay K, Chivet M, Hemming FJ, Belly A, Bodon G, Blot B, Haase G, Goldberg Y, Sadoul R. Release of exosomes from differentiated neurons and its regulation by synaptic glutamatergic activity. *Mol Cell Neurosci*. 2011 Feb;46(2):409-18.
- Lackinger M, Sungur AÖ, Daswani R, Soutschek M, Bicker S, Stemmler L, Wüst T, Fiore R, Dieterich C, Schwarting RK, Wöhr M, Schratt G. A placental mammal-specific microRNA cluster acts as a natural brake for sociability in mice. *EMBO Rep*. 2019 Feb;20(2):e46429. doi: 10.15252/embr.201846429.
- Lane C, Milne E, Freeth M. Characteristics of Autism Spectrum Disorder in Sotos Syndrome. *J Autism Dev Disord*. 2017 Jan;47(1):135-143.
- Lee SH, Shin SM, Zhong P, Kim HT, Kim DI, Kim JM, Heo WD, Kim DW, Yeo CY, Kim CH, Liu QS. Reciprocal control of excitatory synapse numbers by Wnt and Wnt inhibitor PRR7 secreted on exosomes. *Nat Commun*. 2018 Aug 24;9(1):3434. doi: 10.1038/s41467-018-05858-2.
- Lee Y, Hur I, Park SY, Kim YK, Suh MR, Kim VN. The role of PACT in the RNA silencing pathway. *EMBO J*. 2006 Feb 8;25(3):522-32.
- Leite JP, Neder L, Arisi GM, Carlotti CG Jr, Assirati JA, Moreira JE. Plasticity, synaptic strength, and epilepsy: what can we learn from ultrastructural data? *Epilepsia*. 2005;46 Suppl 5:134-41.
- Letellier M, Elramah S, Mondin M, Soula A, Penn A, Choquet D, Landry M, Thoumine O, Favereaux A. miR-92a regulates expression of synaptic GluA1-containing AMPA receptors during homeostatic scaling. *Nat Neurosci*. 2014 Aug;17(8):1040-2. doi: 10.1038/nn.3762. Epub 2014 Jul 13. Erratum in: *Nat Neurosci*. 2014 Dec;17(12):1841.
- Lugli G, Larson J, Martone ME, Jones Y, Smalheiser NR. Dicer and eIF2c are enriched at postsynaptic densities in adult mouse brain and are modified by neuronal activity in a calpain-dependent manner. *J Neurochem*. 2005 Aug;94(4):896-905. doi: 10.1111/j.1471-4159.2005.03224.x.
- Lugli G, Torvik VI, Larson J, Smalheiser NR. Expression of microRNAs and their precursors in synaptic fractions of adult mouse forebrain. *J Neurochem*. 2008 Jul;106(2):650-61. doi: 10.1111/j.1471-4159.2008.05413.x. Epub 2008 Apr 12.
- Lugli G, Larson J, Demars MP, Smalheiser NR. Primary microRNA precursor transcripts are localized at post-synaptic densities in adult mouse forebrain. *J Neurochem*. 2012 Nov;123(4):459-66.
- Lund E, Güttinger S, Calado A, Dahlberg JE, Kutay U. Nuclear export of microRNA precursors. *Science*. 2004 Jan 2;303(5654):95-8.
- Lyles V, Zhao Y, Martin KC. Synapse formation and mRNA localization in cultured Aplysia neurons. *Neuron*. 2006 Feb 2;49(3):349-56. doi: 10.1016/j.neuron.2005.12.029.
- Maestú F, de Haan W, Busche MA, DeFelipe J. Neuronal excitation/inhibition imbalance: core element of a translational perspective on Alzheimer pathophysiology. *Ageing Res Rev*. 2021 Aug;69:101372.
- Magee J, Hoffman D, Colbert C, Johnston D. Electrical and calcium signaling in dendrites of hippocampal pyramidal neurons. *Annu Rev Physiol*. 1998;60:327-46.
- Malow BA. Sleep deprivation and epilepsy. *Epilepsy Curr*. 2004 Sep-Oct;4(5):193-5.

Marshall J, Dolan BM, Garcia EP, Sathe S, Tang X, Mao Z, Blair LA. Calcium channel and NMDA receptor activities differentially regulate nuclear C/EBP $\beta$  levels to control neuronal survival. *Neuron*. 2003 Aug 14;39(4):625-39. doi: 10.1016/s0896-6273(03)00496-3.

McDonough JH Jr, Shih TM. Neuropharmacological mechanisms of nerve agent-induced seizure and neuropathology. *Neurosci Biobehav Rev*. 1997 Sep;21(5):559-79. doi: 10.1016/s0149-7634(96)00050-4. PMID: 9353792.

Megías M, Emri Z, Freund TF, Gulyás AI. Total number and distribution of inhibitory and excitatory synapses on hippocampal CA1 pyramidal cells. *Neuroscience*. 2001;102(3):527-40. doi: 10.1016/s0306-4522(00)00496-6.

Meister G. Argonaute proteins: functional insights and emerging roles. *Nat Rev Genet*. 2013 Jul;14(7):447-59.

Mendez P, Stefanelli T, Flores CE, Muller D, Lüscher C. Homeostatic Plasticity in the Hippocampus Facilitates Memory Extinction. *Cell Rep*. 2018 Feb 6;22(6):1451-1461. doi: 10.1016/j.celrep.2018.01.025.

Mihalas AB, Araki Y, Huganir RL, Meffert MK. Opposing action of nuclear factor  $\kappa$ B and Polo-like kinases determines a homeostatic end point for excitatory synaptic adaptation. *J Neurosci*. 2013 Oct 16;33(42):16490-501.

Miller S, Yasuda M, Coats JK, Jones Y, Martone ME, Mayford M. Disruption of dendritic translation of CaMKII $\alpha$  impairs stabilization of synaptic plasticity and memory consolidation. *Neuron*. 2002 Oct 24;36(3):507-19. doi: 10.1016/s0896-6273(02)00978-9.

Moulin TC, Rayêe D, Schiöth HB. Dendritic spine density changes and homeostatic synaptic scaling: a meta-analysis of animal studies. *Neural Regen Res*. 2022 Jan;17(1):20-24.

Murata Y, Doi T, Taniguchi H, Fujiyoshi Y. Proteomic analysis revealed a novel synaptic proline-rich membrane protein (PRR7) associated with PSD-95 and NMDA receptor. *Biochem Biophys Res Commun*. 2005 Feb 4;327(1):183-91. doi: 10.1016/j.bbrc.2004.11.154.

Murthy VN, Schikorski T, Stevens CF, Zhu Y. Inactivity produces increases in neurotransmitter release and synapse size. *Neuron*. 2001 Nov 20;32(4):673-82.

Nakamura K, Moorhouse AJ, Cheung DL, Eto K, Takeda I, Rozenbroek PW, Nabekura J. Overexpression of neuronal K<sup>+</sup>-Cl<sup>-</sup> co-transporter enhances dendritic spine plasticity and motor learning. *J Physiol Sci*. 2019 May;69(3):453-463.

Nakayama AY, Harms MB, Luo L. Small GTPases Rac and Rho in the maintenance of dendritic spines and branches in hippocampal pyramidal neurons. *J Neurosci*. 2000 Jul 15;20(14):5329-38. doi: 10.1523/JNEUROSCI.20-14-05329.2000.

O'Brien RJ, Kamboj S, Ehlers MD, Rosen KR, Fischbach GD, Huganir RL. Activity-dependent modulation of synaptic AMPA receptor accumulation. *Neuron*. 1998 Nov;21(5):1067-78. doi: 10.1016/s0896-6273(00)80624-8. PMID: 9856462.

Ogata T, Kagami M. Kagami-Ogata syndrome: a clinically recognizable upd(14)pat and related disorder affecting the chromosome 14q32.2 imprinted region. *J Hum Genet*. 2016 Feb;61(2):87-94. doi: 10.1038/jhg.2015.113.

Pak DT, Sheng M. Targeted protein degradation and synapse remodeling by an inducible protein kinase. *Science*. 2003 Nov 21;302(5649):1368-73. doi: 10.1126/science.1082475. Epub 2003 Oct 23.

Pelkey KA, Chittajallu R, Craig MT, Tricoire L, Wester JC, McBain CJ. Hippocampal GABAergic Inhibitory Interneurons. *Physiol Rev*. 2017 Oct 1;97(4):1619-1747. doi: 10.1152/physrev.00007.2017.

Petersen CC, Malenka RC, Nicoll RA, Hopfield JJ. All-or-none potentiation at CA3-CA1 synapses. *Proc Natl Acad Sci USA*. 1998, 95 (8): 4732-4737. 10.1073/pnas.95.8.4732

Pielot R, Smalla KH, Müller A, Landgraf P, Lehmann AC, Eisenschmidt E, Haus UU, Weismantel R, Gundelfinger ED, Dieterich DC. SynProt: A Database for Proteins of Detergent-Resistant Synaptic Protein Preparations. *Front Synaptic Neurosci*. 2012 Jun 25;4:1. doi: 10.3389/fnsyn.2012.00001.

Pillai RS, Bhattacharyya SN, Artus CG, Zoller T, Cougot N, Basyuk E, Bertrand E, Filipowicz W. Inhibition of translational initiation by Let-7 MicroRNA in human cells. *Science*. 2005 Sep 2;309(5740):1573-6.

- Poon MM, Chen L. Retinoic acid-gated sequence-specific translational control by RAR $\alpha$ . *Proc Natl Acad Sci U S A*. 2008 Dec 23;105(51):20303-8. doi: 10.1073/pnas.0807740105. Epub 2008 Dec 10. Erratum in: *Proc Natl Acad Sci U S A*. 2009 May 5;106(18):7679.
- Prasasya R, Grotheer KV, Siracusa LD, Bartolomei MS. Temple syndrome and Kagami-Ogata syndrome: clinical presentations, genotypes, models and mechanisms. *Hum Mol Genet*. 2020 Sep 30;29(R1):R107-R116. doi: 10.1093/hmg/ddaa133.
- Quinn DP, Kolar A, Harris SA, Wigerius M, Fawcett JP, Krueger SR. The Stability of Glutamatergic Synapses Is Independent of Activity Level, but Predicted by Synapse Size. *Front Cell Neurosci*. 2019 Jun 27;13:291.
- Rabinowitch I, Segev I. The interplay between homeostatic synaptic plasticity and functional dendritic compartments. *J Neurophysiol*. 2006a Jul;96(1):276-83. doi: 10.1152/jn.00074.2006.
- Rabinowitch I, Segev I. The endurance and selectivity of spatial patterns of long-term potentiation/depression in dendrites under homeostatic synaptic plasticity. *J Neurosci*. 2006b Dec 27;26(52):13474-84. doi: 10.1523/JNEUROSCI.4333-06.2006.
- Rago L, Beattie R, Taylor V, Winter J. miR379-410 cluster miRNAs regulate neurogenesis and neuronal migration by fine-tuning N-cadherin. *EMBO J*. 2014 Apr 16;33(8):906-20. doi: 10.1002/embj.201386591.
- Rajman M, Metge F, Fiore R, Khudayberdiev S, Aksoy-Aksel A, Bicker S, Ruedell Reschke C, Raoof R, Brennan GP, Delanty N, Farrell MA, O'Brien DF, Bauer S, Norwood B, Veno MT, Krüger M, Braun T, Kjems J, Rosenow F, Henshall DC, Dieterich C, Schratt G. A microRNA-129-5p/Rbfox crosstalk coordinates homeostatic downscaling of excitatory synapses. *EMBO J*. 2017 Jun 14;36(12):1770-1787. doi: 10.15252/embj.201695748.
- Riccomagno MM, Kolodkin AL. Sculpting neural circuits by axon and dendrite pruning. *Annu Rev Cell Dev Biol*. 2015;31:779-805.
- da Rocha ST, Edwards CA, Ito M, Ogata T, Ferguson-Smith AC. Genomic imprinting at the mammalian Dlk1-Dio3 domain. *Trends Genet*. 2008 Jun;24(6):306-16. doi: 10.1016/j.tig.2008.03.011.
- Roselli F, Livrea P, Almeida OF. CDK5 is essential for soluble amyloid  $\beta$ -induced degradation of GKAP and remodeling of the synaptic actin cytoskeleton. *PLoS One*. 2011;6(7):e23097.
- Runge K, Cardoso C, de Chevigny A. Dendritic Spine Plasticity: Function and Mechanisms. *Front Synaptic Neurosci*. 2020 Aug 28;12:36. doi: 10.3389/fnsyn.2020.00036.
- Rothschild G, Eban E, Frank LM. A cortical-hippocampal-cortical loop of information processing during memory consolidation. *Nat Neurosci*. 2017 Feb;20(2):251-259.
- Rutherford LC, Nelson SB, Turrigiano GG. BDNF has opposite effects on the quantal amplitude of pyramidal neuron and interneuron excitatory synapses. *Neuron*. 1998 Sep;21(3):521-30.
- Sakaria RP, Mostafavi R, Miller S, Ward JC, Pivnick EK, Talati AJ. Kagami-Ogata Syndrome: Case Series and Review of Literature. *AJP Rep*. 2021 Mar;11(2):e65-e75.
- Sambandan S, Akbalik G, Kochen L, Rinne J, Kahlstatt J, Glock C, Tushev G, Alvarez-Castelao B, Heckel A, Schuman EM. Activity-dependent spatially localized miRNA maturation in neuronal dendrites. *Science*. 2017 Feb 10;355(6325):634-637.
- Schafer DP, Lehrman EK, Kautzman AG, Koyama R, Mardinly AR, Yamasaki R, Ransohoff RM, Greenberg ME, Barres BA, Stevens B. Microglia sculpt postnatal neural circuits in an activity and complement-dependent manner. *Neuron*. 2012 May 24;74(4):691-705. doi: 10.1016/j.neuron.2012.03.026.
- Schratt GM, Tuebing F, Nigh EA, Kane CG, Sabatini ME, Kiebler M, Greenberg ME. A brain-specific microRNA regulates dendritic spine development. *Nature*. 2006 Jan 19;439(7074):283-9. doi: 10.1038/nature04367. Erratum in: *Nature*. 2006 Jun 15;441(7095):902..
- Schwarz LA, Hall BJ, Patrick GN. Activity-dependent ubiquitination of GluA1 mediates a distinct AMPA receptor endocytosis and sorting pathway. *J Neurosci*. 2010 Dec 8;30(49):16718-29.

- Seeburg DP, Feliu-Mojer M, Gaiottino J, Pak DT, Sheng M. Critical role of CDK5 and Polo-like kinase 2 in homeostatic synaptic plasticity during elevated activity. *Neuron*. 2008 May 22;58(4):571-83. doi: 10.1016/j.neuron.2008.03.021.
- Seeburg DP, Sheng M. Activity-induced Polo-like kinase 2 is required for homeostatic plasticity of hippocampal neurons during epileptiform activity. *J Neurosci*. 2008 Jun 25;28(26):6583-91. doi: 10.1523/JNEUROSCI.1853-08.2008.
- Seitz H, Youngson N, Lin SP, Dalbert S, Paulsen M, Bachellerie JP, Ferguson-Smith AC, Cavaillé J. Imprinted microRNA genes transcribed antisense to a reciprocally imprinted retrotransposon-like gene. *Nat Genet*. 2003 Jul;34(3):261-2.
- Shi CY, Kingston ER, Kleaveland B, Lin DH, Stubna MW, Bartel DP. The ZSWIM8 ubiquitin ligase mediates target-directed microRNA degradation. *Science*. 2020 Dec 18;370(6523):eabc9359.
- Siegel G, Obernosterer G, Fiore R, Oehmen M, Bicker S, Christensen M, Khudayberdiev S, Leuschner PF, Busch CJ, Kane C, Hübel K, Dekker F, Hedberg C, Rengarajan B, Drepper C, Waldmann H, Kauppinen S, Greenberg ME, Draguhn A, Rehmsmeier M, Martinez J, Schrott GM. A functional screen implicates microRNA-138-dependent regulation of the depalmitoylation enzyme APT1 in dendritic spine morphogenesis. *Nat Cell Biol*. 2009 Jun;11(6):705-16.
- Sohal VS, Rubenstein JLR. Excitation-inhibition balance as a framework for investigating mechanisms in neuropsychiatric disorders. *Mol Psychiatry*. 2019 Sep;24(9):1248-1257.
- Soden ME, Chen L. Fragile X protein FMRP is required for homeostatic plasticity and regulation of synaptic strength by retinoic acid. *J Neurosci*. 2010 Dec 15;30(50):16910-21.
- Spano GM, Bannings SW, Marshall W, de Vivo L, Bellesi M, Loschky SS, Tononi G, Cirelli C. Sleep Deprivation by Exposure to Novel Objects Increases Synapse Density and Axon-Spine Interface in the Hippocampal CA1 Region of Adolescent Mice. *J Neurosci*. 2019 Aug 21;39(34):6613-6625.
- St. Louis IV and Sagarsky C. Ch.3: Mammalian Cis-Acting RNA Sequence Elements, Gene Expression and Regulation in Mammalian Cells: Transcription from General Aspects. 2018; 35-66.
- Sutton MA, Ito HT, Cressy P, Kempf C, Woo JC, Schuman EM. Miniature neurotransmission stabilizes synaptic function via tonic suppression of local dendritic protein synthesis. *Cell*. 2006 May 19;125(4):785-99. doi: 10.1016/j.cell.2006.03.040.
- Sutton MA, Taylor AM, Ito HT, Pham A, Schuman EM. Postsynaptic decoding of neural activity: eEF2 as a biochemical sensor coupling miniature synaptic transmission to local protein synthesis. *Neuron*. 2007 Aug 16;55(4):648-61. doi: 10.1016/j.neuron.2007.07.030.
- Svoboda K, Tank DW, Denk W. Direct measurement of coupling between dendritic spines and shafts. *Science*. 1996 May 3;272(5262):716-9.
- Swann JW, Al-Noori S, Jiang M, Lee CL. Spine loss and other dendritic abnormalities in epilepsy. *Hippocampus*. 2000;10(5):617-25. doi: 10.1002/1098-1063(2000)10:5<617::AID-HIPO13>3.0.CO;2-R.
- Swanwick CC, Murthy NR, Mtchedlishvili Z, Sieghart W, Kapur J. Development of gamma-aminobutyric acidergic synapses in cultured hippocampal neurons. *J Comp Neurol*. 2006
- Tatton-Brown K, Douglas J, Coleman K, Baujat G, Cole TR, Das S, Horn D, Hughes HE, Temple IK, Faravelli F, Waggoner D, Turkmen S, Cormier-Daire V, Irrthum A, Rahman N; Childhood Overgrowth Collaboration. Genotype-phenotype associations in Sotos syndrome: an analysis of 266 individuals with NSD1 aberrations. *Am J Hum Genet*. 2005 Aug;77(2):193-204. doi: 10.1086/432082.
- Théry C, Ostrowski M, Segura E. Membrane vesicles as conveyors of immune responses. *Nat Rev Immunol*. 2009 Aug;9(8):581-93. doi: 10.1038/nri2567.
- Thiagarajan TC, Lindskog M, Tsien RW. Adaptation to synaptic inactivity in hippocampal neurons. *Neuron*. 2005 Sep 1;47(5):725-37

Tierling S, Dalbert S, Schoppenhorst S, Tsai CE, Oligier S, Ferguson-Smith AC, Paulsen M, Walter J. High-resolution map and imprinting analysis of the Gtl2-Dnchc1 domain on mouse chromosome 12. *Genomics*. 2006 Feb;87(2):225-35.

tom Dieck S, Kochen L, Hanus C, Heumüller M, Bartnik I, Nassim-Assir B, Merk K, Mosler T, Garg S, Bunse S, Tirrell DA, Schuman EM. Direct visualization of newly synthesized target proteins in situ. *Nat Methods*. 2015 May;12(5):411-4. doi: 10.1038/nmeth.3319.

Tominaga K, Srikantan S, Lee EK, Subaran SS, Martindale JL, Abdelmohsen K, Gorospe M. Competitive regulation of nucleolin expression by HuR and miR-494. *Mol Cell Biol*. 2011 Oct;31(20):4219-31. doi: 10.1128/MCB.05955-11.

Turrigiano GG, Leslie KR, Desai NS, Rutherford LC, Nelson SB. Activity-dependent scaling of quantal amplitude in neocortical neurons. *Nature*. 1998 Feb 26;391(6670):892-6.

Turrigiano GG, Nelson SB. Homeostatic plasticity in the developing nervous system. *Nat Rev Neurosci*. 2004 Feb;5(2):97-107.

Turrigiano GG. The self-tuning neuron: synaptic scaling of excitatory synapses. *Cell*. 2008 Oct 31;135(3):422-35. doi: 10.1016/j.cell.2008.10.008.

Turrigiano G. Homeostatic synaptic plasticity: local and global mechanisms for stabilizing neuronal function. *Cold Spring Harb Perspect Biol*. 2012 Jan 1;4(1):a005736. doi: 10.1101/cshperspect.a005736.

Verstegen AM, Tagliatti E, Lignani G, Marte A, Stoloro T, Atias M, Corradi A, Valtorta F, Gitler D, Onofri F, Fassio A, Benfenati F. Phosphorylation of synapsin I by cyclin-dependent kinase-5 sets the ratio between the resting and recycling pools of synaptic vesicles at hippocampal synapses. *J Neurosci*. 2014 May 21;34(21):7266-80.

de Vivo L, Bellesi M, Marshall W, Bushong EA, Ellisman MH, Tononi G, Cirelli C. Ultrastructural evidence for synaptic scaling across the wake/sleep cycle. *Science*. 2017 Feb 3;355(6324):507-510.

V.-St., & Sagarsky, C. Mammalian Cis-Acting RNA Sequence Elements. In *Gene Expression and Regulation in Mammalian Cells - Transcription From General Aspects*. InTech. 2018.

Wang HW, Noland C, Siridechadilok B, Taylor DW, Ma E, Felderer K, Doudna JA, Nogales E. Structural insights into RNA processing by the human RISC-loading complex. *Nat Struct Mol Biol*. 2009 Nov;16(11):1148-53.

Wierenga CJ, Walsh MF, Turrigiano GG. Temporal regulation of the expression locus of homeostatic plasticity. *J Neurophysiol*. 2006 Oct;96(4):2127-33. doi: 10.1152/jn.00107.2006.

Wiesel, T.N. , Hubel, D.H. Effects of Visual Deprivation on Morphology and Physiology of Cells in the Cats Lateral Geniculate Body. *J Neurophysiol*. 1963a; 26: 978–93.

Winter J, Jung S, Keller S, Gregory RI, Diederichs S. Many roads to maturity: microRNA biogenesis pathways and their regulation. *Nat Cell Biol*. 2009 Mar;11(3):228-34.

Witteveldt J, Ivens A, Macias S. Inhibition of Microprocessor Function during the Activation of the Type I Interferon Response. *Cell Rep*. 2018 Jun 12;23(11):3275-3285.

Wu B, Eliscovich C, Yoon YJ, Singer RH. Translation dynamics of single mRNAs in live cells and neurons. *Science*. 2016 Jun 17;352(6292):1430-5. doi: 10.1126/science.aaf1084.

Yi R, Qin Y, Macara IG, Cullen BR. Exportin-5 mediates the nuclear export of pre-microRNAs and short hairpin RNAs. *Genes Dev*. 2003 Dec 15;17(24):3011-6.

Yoshimura Y, Yamauchi Y, Shinkawa T, Taoka M, Donai H, Takahashi N, Isobe T, Yamauchi T. Molecular constituents of the postsynaptic density fraction revealed by proteomic analysis using multidimensional liquid chromatography-tandem mass spectrometry. *J Neurochem*. 2004 Feb;88(3):759-68. doi: 10.1046/j.1471-4159.2003.02136.x.

Yu LM, Goda Y. Dendritic signalling and homeostatic adaptation. *Curr Opin Neurobiol*. 2009 Jun;19(3):327-35. doi: 10.1016/j.conb.2009.07.002.

Zampa F, Bicker S, Schratt G. Activity-Dependent Pre-miR-134 Dendritic Localization Is Required for Hippocampal Neuron Dendritogenesis. *Front Mol Neurosci*. 2018 Jun 11;11:171.